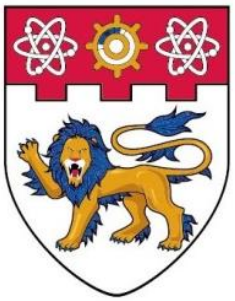

NANYANG TECHNOLOGICAL UNIVERSITY
SINGAPORE

SYNTHESIS OF REACTIVE MGO FROM REJECT BRINE

DONG HAOLIANG

School of Civil and Environmental Engineering

<2018>

SYNTHESIS OF REACTIVE MGO FROM REJECT BRINE

DONG HAOLIANG

School of Civil and Environmental Engineering

A thesis submitted to the Nanyang Technological University

in fulfilment of the requirements for the degree of

Doctor of Philosophy

<2018>

Acknowledgements

I would like to give sincere thanks to my supervisors Prof. Yang En-Hua and Dr. Cise Unluer for their helpful advice, valuable guidance and encouragement throughout my four-year Ph.D. study. They teach me the genuine of research and science.

I would like to thank all the colleagues in my group. Their advice and support on life and academic, allow me a wonderful experience in Singapore.

I would like to give my special thanks to Nanyang Technological University for the scholarship to support me to pursue a Ph.D. in Civil and Environmental Engineering. To all the technicians in the department, I feel so grateful for the trainings and help I received on XRD, FESEM, TGA and BET.

I would like to offer my genuine thanks to my parents for their understanding, support and care. It is with their love without reservation that I can overcome all the difficulties and challenges in my life.

Once again, thank all the people I met in Singapore. It is you who make my Ph.D. so meaningful.

Table of contents

Table of contents ii
Summary vi
List of publications vii
List of Tables viii
List of Figures ix
Chapter 1 Introduction 1
1.1. Background 1
1.2. Research objective 6
1.3. Methodology 6
1.4. Roadmap 8
1.5. Structures of the thesis 9
Chapter 2 Literature review 11
2.1. Introduction 11
2.2. Cement sustainability 11
2.2.1. Climate change and sustainable development 11
2.2.2. Concrete production and cement industry 12
2.3. Reactive MgO cements 13
2.3.1. Introduction on MgO cements 13
2.3.2. Applications, advantages and disadvantages of MgO cements 14
2.3.3. Global production of MgO cements 15
2.4. Production of reactive MgO from $MgCO_3$ 16
2.4.1. Mining and crushing 16
2.4.2. Pyro-processing 17
2.5. Production of reactive MgO from seawater/brine 18
2.5.1. Extraction 18
2.5.2. Raw materials pre-treatment 19
2.5.3. Processing 19
2.6. Production of reactive MgO from other magnesium-containing sources 24
2.7. Reject brine 27

2.8. A new idea to treat reject brine 28
2.9. Summary 30
Chapter 3 Synthesis of reactive MgO from reject brine via the addition of NH_4OH 34
3.1. Introduction 34
3.2. Materials and Methodology 39
3.2.1. Materials 39
3.2.2. Methodology 40
3.3. Results and Discussion 41
3.3.1. Reaction kinetics 41
3.3.2. Recovery of Mg^{2+} and Ca^{2+} from reject brine 42
3.3.3. Characterization of the synthesized $Mg(OH)_2$ 44
3.3.4. Characterization of the synthesized reactive MgO 49
3.4. Conclusions 52
Chapter 4 Recovery of reactive MgO from reject brine via the addition of NaOH 54
4.1. Introduction 54
4.2 Materials and Methodology 55
4.2.1 Materials 55
4.2.2 Methodology 55
4.3 Results and Discussion 57
4.3.1 Recovery of Mg^{2+} and Ca^{2+} from reject brine 57
4.3.2 Characterization of the synthesized $Mg(OH)_2$ 59
4.3.3 Characterization of the synthesized reactive MgO 64
4.4 Conclusions 71
Chapter 5 Characterization and comparison of MgO recovered from reject brine obtained from desalination plants 72
5.1. Introduction 72
5.2. Materials and Methodology 73
5.2.1. Materials 73
5.2.2. Methodology 73
5.3. Results and Discussions 74
5.3.1. Characterization of $Mg(OH)_2$ 74

5.3.2. Characterization of MgO 77
5.4. Conclusions 85
Chapter 6 Production of Mg-carbonates via the sequestration of CO_2 in $Mg(OH)_2$ slurries generated from reject brine 87
6.1. Introduction 87
6.2. Materials and Methodology 90
6.2.1. Materials 90
6.2.2. Methodology 91
6.3. Results and Discussion 92
6.3.1. Characterization of HMCs synthesized from $Mg(OH)_2$ slurry 92
6.3.2. Comparison of reject brine vs. $Mg(OH)_2$ slurry as a source for the synthesis of HMCs 99
6.4. Conclusions 103
Chapter 7 Recovery of ultra-high pure MgO from reject brine obtained from desalination plants 105
7.2. Materials and Methodology 108
7.2.1. Materials 108
7.2.2. Methodology 109
7.2.3. Equipment 110
7.3. Results and Discussions 110
7.3.1. Characterization of $MgC_2O_4•2H_2O$ 110
7.3.2. Characterization of MgO 115
7.4. Conclusions 119
Chapter 8 Comparative life cycle assessment of reactive MgO produced from local reject brine 120
8.1. Introduction 120
8.2. Materials and methods 124
8.2.1. Goal, functional unit and scope 124
8.2.2. Inventory 126
8.2.3. Impact assessment 129
8.3. Results and discussions 129
8.3.1 Production of raw materials 129

8.3.2 Calcination of $Mg(OH)_2$ from reject brine 130
8.3.3 CED and GHG emission of MgO calcined from $Mg(OH)_2$ 132
8.3.4 Carbonation of $Mg(OH)_2$ from reject brine 134
8.3.5 Calcination of $MgCO_3 \cdot 3H_2O$ from reject brine 135
8.4. Conclusions 137
Chapter 9 Conclusions and recommendations for future research 139
9.1. Conclusions 139
9.2. Recommendations for future research 141
References 143

Summary

Portland cement (PC) is the most common binder used in concrete and construction materials. The production of PC is estimated to be at 3 billion tonnes yearly at a global scale, being responsible for 5-7% of anthropogenic CO_2 emissions worldwide. Reactive magnesia (MgO) cement has received attention as an alternative binder due to the lower calcination temperatures (~700 ℃) used during its production, its ability to store CO_2 permanently while gaining strength, and complete recyclability at the end of use. However, the sustainable production of reactive MgO remains a challenge. Reject brine, which is a concentrated by-product with a high salt concentration obtained from treating brackish water or seawater in desalination plants, provides an ideal alternative to recover reactive MgO due to the high concentrations of Mg. This research focuses on identifying different routes to synthesize and characterize the precursors, i.e. $Mg(OH)_2$, hydrated magnesium carbonates (HMCs) and $MgC_2O_4 \cdot 2H_2O$ from reject brine, and to investigate the potential of the production of reactive MgO with high purity and reactivity. The relationships between the calcination conditions, e.g. calcination temperatures and durations, and reactivities of MgO have been explored. The phase change of HMCs and the carbon storage efficiency via the injection of CO_2 into $Mg(OH)_2$ slurries generated from reject brine are comprehensively studied. Finally the economic feasibility, energy consumption and carbon footprint of the production of reactive MgO from reject brine via different routes have been calculated and presented by means of life cycle assessment (LCA)

List of publications

Dong, H., C. Unluer, E.-H. Yang and A. Al-Tabbaa (2017). "Synthesis of reactive MgO from reject brine via the addition of NH_4OH." Hydrometallurgy 169: 165-172.

Dong, H., C. Unluer, E.-H. Yang and A. Al-Tabbaa (2018). "Recovery of reactive MgO from local reject brine via the addition of NaOH." Desalination 429: 88-95

Dong, H., C. Unluer, E.-H. Yang, Fei, J. and A. Al-Tabbaa (2018). "Investigation of the properties of MgO recovered from reject brine obtained from desalination plants." Journal of Cleaner Production 196:100-108

Dong, H., C. Unluer, E.-H. Yang and A. Al-Tabbaa (2017). "Production of Mg-carbonates via the sequestration of CO_2 in $Mg(OH)_2$ slurries generated from reject brine (Submitted).

List of Tables

Table 3.1 Chemical composition of the reject brine used in this study 39
Table 3.2 TG/DTA results of $Mg(OH)_2$ obtained from the reaction of 200 ml reject brine with different amounts of NH_4OH 48
Table 3.3 Chemical composition of the synthesized $Mg(OH)_2$ based on TG/DTA and ICP-OES results 49
Table 4.1 Chemical composition of the reject brine used in this study 55
Table 4.2 TG/DTA results of the decomposition of $Mg(OH)_2$ obtained from the reaction of reject brine with NaOH at different NaOH/Mg^{2+} ratios 63
Table 4.3 Composition of synthesized $Mg(OH)_2$ based on TG/DTA and ICP-OES results 63
Table 5.1 Chemical composition of reject brine used in this study 73
Table 5.2 Chemical composition, crystallite size, SSA and pore volume of $Mg(OH)_2$ obtained from the reaction of reject brine with NH_4OH and NaOH 76
Table 5.3 Crystallite size, primary size and pore volume of MgO produced under different calcination temperatures and durations 81
Table 6.1 Chemical composition of reject brine used in this study. 91
Table 6.2 Physical properties of two type of $Mg(OH)_2$ used in this research. 91
Table 6.3 Chemical composition of HMCs obtained from the $Mg(OH)_2$ slurry and reject brine at a $Mg(OH)_2$:CO_2 molar ratio of 1:1 under a pH of 8 103
Table 7.1 Chemical composition of reject brine used in this study. 108
Table 7.2 Concentrations of Ca^{2+} and Mg^{2+} in the residual brine 113
Table 7.3 Crystallite size, primary particle sizes and pore volumes of MgO produced under different calcination temperatures and durations 117
Table 8.1 Energy consumption of PC and MgO production via the dry-route (Hassan 2013). . 121
Table 8.2 Chemical composition of reject brine used in this study. 127
Table 8.3 Annual fuel mix for electricity generation by energy products (Energy Market Authority (EMA)) 128
Table 8.4 Inventory for the energy consumption of the production of raw materials (unit GJ/tonne) (Neelis, Worrell et al. 2009). 130
Table 8.5 Energy consumption of the calcination process to produce 1 tonne of reactive MgO via the decomposition of $Mg(OH)_2$. 131
Table 8.6 Global warming potential of the production of 1 tonne of reactive MgO via the decomposition of $Mg(OH)_2$ obtained from reject brine via different routes. 134
Table 8.7 Global warming potential of the production of 1 tonne of $MgCO_3$•$3H_2O$ via the direct carbonation of $Mg(OH)_2$ slurries obtained from reject brine via different routes. 134
Table 8.8 Energy consumption of the calcination process to produce 1 tonne of reactive MgO via the decomposition of $MgCO_3$•$3H_2O$. 135
Table 8.9 Global warming potential of the production of 1 tonne of reactive MgO via the decomposition of $MgCO_3$•$3H_2O$ obtained from reject brine via different routes 137

List of Figures

Figure 1.1 Methodology of the proposed research 7
Figure 1.2 Roadmap of the proposed research..... 9
Figure 2.1 Diagram of open-pit method in mining of $MgCO_3$ 17
Figure 2.2 (a) Titration of seawater with NaOH; (b) Titration of seawater with Na_2CO_3 (Irving 1926). 20
Figure 2.3 Stabcal simulation for oxalate precipitates showing the concentration of Ca^{2+} and Mg^{2+} profile versus pH (Tran, Van Luong et al. 2013). 23
Figure 2.4 (a) The percentage of precipitated Ca^{2+} at Oxalate/Ca molar ratio of 6.82:1 at pH 1. (b) Recovery of Mg at different pH (Tran, Van Luong et al. 2013).. 23
Figure 2.5 Morphology of $Mg(OH)_2$ precipitate under the condition of a) $MgCl_2$ + NaOH at 60 ℃ b) $MgCl_2$ + NH_3H_2O at 60 ℃ (Henrist, Mathieu et al. 2003). 25
Figure 2.6 XRD pattern of $Mg(OH)_2$ precipitates reacted (a) at 60 ℃ I_{001}/I_{110}= 0.51 and (b) at 25 ℃, I_{001}/I_{110} = 1.6 (Henrist, Mathieu et al. 2003).. 25
Figure 2.7 Chart of $Mg(OH)_2$ morphologies at different temperature and pH of the hydrothermal growth process (Yan, Xue et al. 2005). 26
Figure 2.8 SEM images of $Mg(OH)_2$nanoflowers synthesized at pH 9.5(Yan, Xue et al. 2005). 27
Figure 2.9 Kinetics of the carbonation reaction (Ferrini, De Vito et al. 2009).. 29
Figure 2.10 Images of synthesized nesquehonite under (a) optical microscopy; (b) under SEM at high magnification (Ferrini, De Vito et al. 2009). 29
Figure 2.11 Comparison of experimental and predicted results for brine carbonation versus pH (Soong, Goodman et al. 2004). 30
Figure 3.1 pH of the reaction of reject brine with different amounts of NH_4OH 42
Figure 3.2 Equilibrium time as a function of NH_4OH dosage 42
Figure 3.3 Percentage of Mg^{2+} and Ca^{2+} sequestrated from reject brine as a function of NH_4OH dosage 44
Figure 3.4 XRD diffractograms of $Mg(OH)_2$ obtained from the reaction of 200 ml reject brine with different amounts of NH_4OH 45
Figure 3.5 FESEM images of $Mg(OH)_2$ obtained from the reaction of 200 ml reject brine with (a) 2.12, (b) 4.24, (c) 6.36, (d) 8.48, (e) 10.6, (f) 12.72, (g) 14.84, (h) 16.96 and (i) 19.08 ml of NH_4OH as collected by filtration through a 45 μm membrane followed by vacuum drying and grinding to pass a 125 μm sieve 46
Figure 3.6 Typical TG/DTA curve of $Mg(OH)_2$ obtained from the reaction of 200 ml reject brine with 6.36 ml of NH_4OH 47
Figure 3.7 XRD diffractograms of the produced reactive MgO 50
Figure 3.8 FESEM images of the reactive MgO produced at 500 ℃ at different magnifications of (a) x14,000 and (b) x30,000 51
Figure 3.9 SSA of the synthesized reactive MgO (SRM) compared with 12 commercial MgO samples reported in (Jin and Al-Tabbaa 2014) 52
Figure 4.1 pH of the reaction between reject brine and NaOH at different NaOH/Mg^{2+} ratios ... 58

Figure 4.2 Percentage of Mg^{2+} and Ca^{2+} sequestrated from reject brine as a function of the $NaOH/Mg^{2+}$ molar ratio 59
Figure 4.3 XRD diffractograms of $Mg(OH)_2$ obtained from the reaction of reject brine with NaOH at different $NaOH/Mg^{2+}$ molar ratios 60
Figure 4.4 FESEM images of $Mg(OH)_2$ obtained from the reaction of reject brine with NaOH at different $NaOH/Mg^{2+}$ molar ratios of (a) 2, (b) 2.5, (c) 3 and (d) 4 61
Figure 4.5 A typical TG/DTA curve of $Mg(OH)_2$ obtained from the reaction of reject brine at a $NaOH/Mg^{2+}$ molar ratio of 2 62
Figure 4.6 SSA of MgO produced under different calcination temperatures and durations 65
Figure 4.7 Effect of calcination temperature and duration on the reactivity of MgO 66
Figure 4.8 Relationship between the SSA and the reactivity of MgO 66
Figure 4.9 XRD diffractograms of reactive MgO produced via the calcination of $Mg(OH)_2$ under different temperatures and durations 67
Figure 4.10 FESEM images of MgO obtained from the calcination of $Mg(OH)_2$ under different conditions: (a) 500 ℃-2h, (b) 500 ℃-6h, (c) 500 ℃-12h, (d) 600 ℃-2h, (e) 600 ℃-6h, (f) 600 ℃-12h, (g) 700 ℃-2h, (h) 700 ℃-6h and (i) 700 ℃-12h 68
Figure 4.11 Costs of the production of reactive MgO from reject brine via the addition of NaOH compared with NH_3 and CaO 70
Figure 5.1 XRD diffractograms of $Mg(OH)_2$ obtained from the reaction of reject brine with NH_4OH and NaOH 75
Figure 5.2 FESEM images of $Mg(OH)_2$ obtained from the reaction of reject brine with (a) NH_4OH and (b) NaOH 77
Figure 5.3 XRD diffractograms of reactive MgO obtained from the calcination of $Mg(OH)_2$ that was synthesized via the reaction of reject brine with (a) NH_4OH and (b) NaOH, under different calcination temperatures and durations 78
Figure 5.4 SSA of MgO produced under different calcination temperatures and durations 80
Figure 5.5 Effect of calcination temperature and duration on the neutralization time of reactive MgO 83
Figure 5.6 Relationship between the neutralization time and SSA of MgO 83
Figure 5.7 FESEM images of MgO obtained from the calcination of $Mg(OH)_2$ that was synthesized via the reaction of reject brine with NH_4OH under (a) 500 ℃-2h, (b) 600 ℃-2h, (c) 700 ℃-2h, (d) 700 ℃-6h and (e) 700 ℃-12h 85
Figure 5.8 FESEM images of MgO obtained from the calcination of $Mg(OH)_2$ that was synthesized via the reaction of reject brine with NaOH under (a) 500 ℃-2h and (b) 700 ℃-12h 85
Figure 6.1 FESEM images of HMCs obtained under a pH of 8 at different $Mg(OH)_2$:CO_2 molar ratios of (a) 1:1, (b) 1:2, (c) 1:3, (d) 1:4, (e) 1:5, (f) 1:6 and (g) 1:7 94
Figure 6.2 XRD diffractograms of HMCs obtained under a pH of 8 at different $Mg(OH)_2$:CO_2 molar ratios 95
Figure 6.3 FESEM images of HMCs obtained at a $Mg(OH)_2$:CO_2 molar ratio of 1:1 under different pH values of (a) 8, (b) 9, (c) 10 and (d) 11 96

Figure 6.4 XRD diffractograms of HMCs obtained at a $Mg(OH)_2$:CO_2 molar ratio of 1:1 under different pH values 97
Figure 6.5 Typical FESEM images of HMCs obtained at a $Mg(OH)_2$:CO_2 molar ratio of 1:2 under different pH values of (a) 8, (b) 9, (c) 10 and (d) 11 98
Figure 6.6 XRD diffractograms of HMCs obtained at a $Mg(OH)_2$:CO_2 molar ratio of 1:2 under different pH values 99
Figure 6.7 SEM images of HMCs obtained at a $Mg(OH)_2$:CO_2 molar ratio of 1:1 under a pH of 8, showing (a) $Mg(OH)_2$ slurry and (b) reject brine 100
Figure 6.8 XRD diffractograms of HMCs obtained from $Mg(OH)_2$ slurry and reject brine at a $Mg(OH)_2$:CO_2 molar ratio of 1:1 under a pH of 8 101
Figure 6.9 Typical TG/DTA curves of HMCs obtained from $Mg(OH)_2$ slurry and reject brine at a $Mg(OH)_2$:CO_2 molar ratio of 1:1 under a pH of 8 102
Figure 7.1 XRD diffractograms of precipitates obtained from the reaction of reject brine with $H_2C_2O_4$•$2H_2O$ from a two-step reaction 112
Figure 7.2 A typical TG/DTA curve of MgC_2O_4•$2H_2O$ obtained from reject brine under the condition of Ca^{2+}:$H_2C_2O_4$•$2H_2O$ of 1:1, Mg^{2+}:$H_2C_2O_4$•$2H_2O$ of 1.5 and pH value of 3 114
Figure 7.3 SSA of MgO produced under different calcination temperatures and durations 115
Figure 7.4 XRD diffractograms of reactive MgO produced via the calcination of MgC_2O_4•$2H_2O$ under different temperatures and durations 117
Figure 7.5 FESEM images of MgO obtained from the calcination of MgC_2O_4•$2H_2O$ under (a) 700 ℃-2h, (b) 700 ℃-6h, (c) 700 ℃-12h, (d) 800 ℃-2h, (e) 800 ℃-6h, (f) 800 ℃-12h, (g) 900 ℃-2h, (h) 900 ℃-6h and (i) 900 ℃-12h 119
Figure 8.1 Scope of comparative LCA showing the production process of reactive MgO 125
Figure 8.2 Material flow diagram for the production of reactive MgO from reject brine 126
Figure 8.3 CED of the production of 1 tonne of reactive MgO calcined from $Mg(OH)_2$ obtained from reject brine via different routes 133
Figure 8.4 GHG emission of the production of 1 tonne of reactive MgO calcined from $Mg(OH)_2$ obtained from reject brine via different routes 133
Figure 8.5 CED of the production of 1 tonne of reactive MgO calcined from $MgCO_3$•$3H_2O$ obtained from reject brine via different routes 136
Figure 8.6 GHG emission of the production of 1 tonne of MgO calcined from $MgCO_3$•$3H_2O$ obtained from reject brine via different route 137

Chapter 1 Introduction

1.1. Background

The concentration of carbon dioxide (CO_2) in the atmosphere has increseard from 325 parts per million (ppm) at the beginning of the industrial era in 1870 to 405 ppm in August 2017, ~25% higher than before (Dlugokencky and Tans 2017). CO_2 has been identified as one of the main causes of global warming and negative impacts from global warming are now becoming more significant (Zachos, Pagani et al. 2001, Root, Price et al. 2003). Due to the wide availability of its raw materials and easy manufacture, concrete made from Portland cement (PC) is the most used manmade material of the the world, with a consumption rate of nearly 4 billion tonnes per year (Oss; 2015). Cement production contributes to around 5-7% of anthropogenic CO_2 emissions worldwide (Olivier and Marilena Muntean 2014). The high carbon footprint in cement industry is mainly due to the high calcination temperature (~1450 ℃) and burning fossil fuels for high energy consumption (Olivier and Marilena Muntean 2014). As the environmental impact of construction materials is becoming a serious concern, the development of novel alternatives with lower energy requirements and associated CO_2 emissions is more crucial than ever. Even though significant improvements have been made towards reducing the impacts of the cement industry through the introduction of various kinds of industrial by-products such as pulverized fly ash (PFA) and ground granulated blast-furnace slag (GGBS) (Palomo, Grutzeck et al. 1999, Luo, Cai et al. 2003, Oner and Akyuz 2007, Ahmaruzzaman 2010), the environmental impacts associated with the energy intensive production process of cement are still a major concern.

Several sustainable improvements ranging from the use of sustainable energy sources to partial replacement of cement with low-carbon materials have been suggested by the cement industry (Hasanbeigi, Price et al. 2012). The utilization of sustainable energy sources such as wind and solar power has firstly been mentioned in the context of switching from traditional fossil fuels to renewable energy sources (Jones and Bouamane 2012). Replacement of PC with industrial by-products such as PFA and GGBS has been suggested and implemented in many projects (Palomo, Grutzeck et al. 1999, Luo, Cai et al. 2003, Oner and Akyuz 2007, Ahmaruzzaman 2010). Another approach of the sustainable initiatives in the cement industry involves the development

of alternative cement binders such as geopolymers and reactive magnesium oxide (MgO) cements (Harrison 2008, Liska, Al-Tabbaa et al. 2012a, Liska, Al-Tabbaa et al. 2012b, Al-Tabbaa 2013, Unluer and Al-Tabbaa 2013, Unluer and Al-Tabbaa 2014).

Reactive MgO cements are typically included in mixtures of PC at different proportions, depending on the actual applications, ranging from structural concrete and porous masonry units (Unluer and Al-Tabbaa 2014). Reactive MgO cements present several advantages in terms of sustainability and performance under accelerated carbonation conditions, including (i) Reactive MgO cements are manufactured at much lower temperatures than PC (700 vs. 1450 ℃); (ii) Reactive MgO cements present a high capability of combining massive industry by-products like GGBS (Yi, Liska et al. 2012) and PFA (Unluer and Al-Tabbaa 2014); (iii) Reactive MgO cements enhance durability due to the low solubility and reactivity of $Mg(OH)_2$ (Li 2012); (iv) Reactive MgO cements sequester significant amounts of CO_2 through carbonation, resulting in low or even negative CO_2 emissions (Liska, Vandeperre et al. 2008, Unluer and Al-Tabbaa 2013, Unluer and Al-Tabbaa 2014); and (v) Reactive MgO cements can be 100% recycled in applications where MgO is used as the sole binder as the carbonation of MgO produces magnesium carbonates, which are the main sources of MgO.

According to the calcination temperature during the production process, MgO can be classified into three grades. Dead-burned MgO is calcined above 1400 ℃, leading to the lowest specific surface area (SSA) and reactivity. Dead-burned MgO is mainly used in the refractory industries as an excellent fire-resistant and thermal insulation material. Hard-burned MgO is usually calcined between 1000 and 1400 ℃, with a comparatively lower reactivity and SSA. Hard-burned MgO has been successfully used in China as an expansive additive in concrete for the shrinkage compensation. Light-burned (reactive or caustic-calcined) MgO is calcined between 700 and 1000 ℃, resulting in the highest reactivity and largest SSA amongst all grades. Due to lower calcination temperatures (~700 ℃) and the ability to absorb CO_2 in the form of stable carbonates while gaining strength (Unluer and Al-Tabbaa 2013, Unluer and Al-Tabbaa 2014), reactive MgO can be considered as an alternative green cement.

Production of MgO is mainly via the calcination of natural carbonates such as dolomite ($CaMg(CO_3)_2$) or magnesite ($MgCO_3$), as shown in Equation 1-1 to 1-2.

$$MgCO_3 \rightarrow MgO + CO_2 \quad (1\text{-}1)$$

$$CaMg(CO_3)_3 \rightarrow CaO + MgO + 2CO_2 \quad (1\text{-}2)$$

In addition to the calcination of $MgCO_3$, MgO can also be synthesized from other magnesium-rich sources such as seawater or brine (a high saline water), as shown in Equations 1-3 to 1-4 (Bhatti, Dollimore et al. 1984). This contributes to ~14% of the global MgO production (Kramer).

$$CaO + H_2O + MgCl_2 \rightarrow Mg(OH)_2 + CaCl_2 \quad (1\text{-}3)$$

$$Mg(OH)_2 \rightarrow MgO + H_2O \quad \text{(via calcination)} \quad (1\text{-}4)$$

This is realized by adding an alkali source such as, lime milk (CaO solution) (Friedrich, Robinson et al. 1946), sodium hydroxide (NaOH) (Turek and Gnot 1995), or ammonia (NH_4OH) (Henrist, Mathieu et al. 2003) to seawater/brine, thereby precipitating Mg^{2+} in the form of $Mg(OH)_2$. The precipitated $Mg(OH)_2$ can be used as a flame retardant (Fellner, Híveš et al. 2011), heavy matter leaching precipitant with several industry applications (Mironyuk, Gun'ko et al. 2006, Guo, Pei et al. 2015) or can be further calcined to produce MgO (Kotsupalo, Ryabtsev et al. 2010). Friedrich et al. patented a simple process to obtain MgO calcined from $Mg(OH)_2$ precipitated from seawater at a pH of 10.5 by using a lime solution (Friedrich, Robinson et al. 1946). Petric et al. utilized dolomite composed of 57.6% CaO and 42.3% MgO to precipitate $Mg(OH)_2$ from seawater, which was then calcined at 950 ℃ to produce MgO (Petric, Martinac et al. 1997). Dave et al. used hydrated lime ($Ca(OH)_2{\cdot}2H_2O$) to precipitate $Mg(OH)_2$ from seawater at a pH ranging between 7.0 and 7.5 (Dave and Ghosh 2005). All these studies introduced Ca^{2+} into the seawater/brine solution, which resulted in the formation of gypsum ($CaSO_4{\cdot}2H_2O$) along with other precipitates due to the presence of sulphate (SO_4^{2-}) in the solution. The contamination of the final product due to the formation of gypsum necessitates the pre-treatment of seawater for desulfation via the addition of $CaCl_2$ into the seawater/brine. Turecket al. utilized sodium hydroxide (NaOH) to precipitate $Mg(OH)_2$ from brine and reported an improved precipitation at lower temperatures and higher NaOH concentrations (Turek and Gnot 1995). This improved sedimentation was attributed to the high viscosity of NaOH solution, which impeded the contact

between the precipitating agent and the brine. Henrist et al. studied several parameters such as the utilized base type, type of counter-ions and temperature on the morphological characteristics of $Mg(OH)_2$ (Henrist, Mathieu et al. 2003). Addition of NaOH to $MgCl_2$ solution led to a globular cauliflower-like morphology, while the use of aqueous NH_4OH resulted in plate-like shapes due to the structural difference of cations present in the solution. Single and circular plate-like particles were observed at lower temperatures while particles had a tendency to inter-grow at 60 ℃ (Henrist, Mathieu et al. 2003). Most of these methods that focused on precipitating $Mg(OH)_2$ from saline water suffered from low reaction kinetics and poor dewatering and filtration properties, which limited their use on an industrial scale.

Alternatively, Mg^{2+} from seawater can be precipitated in the form of carbonates, which then undergoes calcination to produce MgO. The possibility of storing CO_2 in the form of stable carbonates through the interaction of ions in aqueous solution with CO_2 has been studied by several researchers (Soong, Goodman et al. 2004, Soong, Fauth et al. 2006, Ferrini, De Vito et al. 2009, Tran, Van Luong et al. 2013). Soong et al. studied the reaction of CO_2 with natural brine and the influence of pH, temperature and CO_2 pressure on the precipitates (Soong, Goodman et al. 2004, Soong, Fauth et al. 2006). It was reported that pH values greater than 9 favoured the formation of carbonates through the addition of potassium hydroxide (KOH) and fly ash into natural brine. While changes in temperature and CO_2 pressure were less influential on the precipitates. Ferrini et al. developed a new method to synthesize nesquehonite by reacting CO_2 gas with $MgCl_2$ solution, which was further calcined to produce MgO (Ferrini, De Vito et al. 2009). The reaction kinetics was greatly improved, which led to the rapid precipitation of stable nesquehonite.

Other synthesized MgO precursors are also reported by several researchers (Simons and Vlasopoulos 2012, Tran, Van Luong et al. 2013, Baglioni, Ferraro et al. 2014). Tran et al. synthesized magnesium oxalate ($MgC_2O_4•2H_2O$) from brine and reported that while calcium oxalate ($CaC_2O_4•H_2O$) precipitated at a pH less than 1, $MgC_2O_4•2H_2O$ did not (Tran, Van Luong et al. 2013). This highlighted the pH gap that enabled a selective precipitation of Mg^{2+} and Ca^{2+}, leading to the synthesis of a high purity of $MgC_2O_4•2H_2O$ (99.5% grade), which could be further calcined to produce MgO. Another production route of MgO is from magnesium silicates, which

has received great attention due to the CO_2 capture and storage potential during the production (Simons and Vlasopoulos 2012, Baglioni, Ferraro et al. 2014). This process involves: (i) production of magnesium silicate slurry, (ii) precipitation of $MgCO_3$ by the introduction of CO_2 (iii) calcination of $MgCO_3$ to produce MgO and (iv) recycling of CO_2 to be used in step (ii). Although these methods present a great potential for the production of MgO on a larger scale, there is still some concern regarding the high energy requirements and high amounts of raw materials needed, regardless of the low calcination temperatures. A potentially more sustainable alternative production route for MgO can incorporate the use of industry waste and by-products, especially those with high magnesium contents such as reject brine from desalination plants or produced water from the oil and gas industry (Almutaz and Wagialia 1990, Ahmed, Arakel et al. 2003).

In coastal regions with limited amounts of fresh water resources such as Singapore, desalination is considered as a feasible alternative for the production of fresh water to meet residential and industrial demands. Desalination involves the removal of salts from saline water to produce fresh water. Different from natural brine which is mainly referred to as high saline water, reject brine is a concentrated by-product obtained from treating brackish water or seawater in desalination plants. At the end of this process, the most common way of disposing the reject brine is to discharge it back into the sea. However, the high concentration of salt within the brine, which is much denser than the feedstock supply, can accumulate at the bottom of the sea and create a severe impact on the environment (Ahmed, Arakel et al. 2003). Several strategies such as deep well injection and mechanical or thermal evaporation have been proposed to manage reject brine (El-Naas 2011). However, deep well injection suffers from the drawbacks of the difficulty of selecting a suitable well site and corrosion and potential leakage in the well casting; evaporation rate greatly limits the usage of thermal evaporation. The current methods to treat reject brine are rather limited and have not achieved a satisfactory result. Therefore, a feasible and practical way to treat and utilize reject brine would be very welcome. Reject brine has a much higher Mg^{2+} concentration (1700ppm) than seawater (1300ppm) (Ahmed, Arakel et al. 2003). The abundant concentration of Mg^{2+} in reject brine serves as an excellent source for the recovery of MgO. The chemical reaction between reject brine and certain additives (e.g. lime solution) for the recovery of salts provides a feasible and environmental friendly use for this waste material. Therefore

reject brine can be converted into valuable and useful solids, while the remaining brackish water can be used for irrigation (El-Naas 2011). Although there are numerous studies on the reaction of $MgCl_2$ solution or natural seawater/brine with different additives, limited research has been reported on the recovery of valuable metals from actual reject brine. This research focuses on the treatment of reject brine collected from a local desalination plant and explores the potential of recovery of MgO from reject brine.

1.2. Research objective

This research aims to investigate the potential of the production of reactive MgO with high purity and reactivity. Specifically, this study focuses on using different routes for synthesizing reactive MgO from locally sources reject brine collected from a desalination plant and identifying the key synthesis parameters. Specific objectives of this research include:

(i) To identify different routes to synthesize and characterize the precursors, i.e. $Mg(OH)_2$, hydrated magnesium carbonates (HMCs) and $MgC_2O_4•2H_2O$ from reject brine;

(ii) To study the phase change of HMCs and optimize the carbon storage efficiency via the injection of CO_2 into reject brine;

(iii) To study the separation method to synthesize $MgC_2O_4•2H_2O$ with ultra-high purity from reject brine;

(iv) To produce and characterize the reactive MgO calcined from the synthesized precursors in (i) and (iii); and

(v) To assess the energy consumption and carbon footprint of the production of reactive MgO from reject brine via different routes by means of life cycle assessment (LCA)

1.3. Methodology

The methodology of this research is shown in Figure 1-1. The synthesis of reactive MgO lies at the centre of this proposed research. Feeding into this goal are three interconnected research initiatives. Investigation on chemical synthesis of the precursors, e.g. $Mg(OH)_2$, HMC and $MgC_2O_4•2H_2O$, will be carried out. The resulting precursors will then be calcined to produce

reactive MgO and effects of calcination conditions, e.g. temperature and duration, on the properties of reactive MgO will be studied.

Secondly, comprehensive characterization techniques will be engaged to study microstructure, crystallinity, morphology and reactivity of the synthesized precursors and reactive MgO. X-ray powder diffraction (XRD) will be used to qualitatively study the compositions and crystal structures. Field emission scanning electron microscopy (FESEM) will be engaged to analyse the microstructure and morphology, whereas thermogravimetric and differential thermal analysis (TG/DTA) will be used to quantitatively analyse the compositions. Brunauer-Emmett-Teller (BET) analysis will be incorporated to quantitatively evaluate the reactivity of MgO.

Thirdly, the influence of critical synthesis parameters on the precursors will be evaluated and optimized to recover Mg from reject brine with high yield and purity. The correlation between the calcination condition (i.e. temperature and duration) and the reactivity of MgO will be established to provide the guidance on the reactivity of MgO to meet different market demands. A comprehensive assessment of economic feasibility, energy consumption and carbon footprint of the synthesized reactive MgO from locally sourced reject brine will be carried out by means of life cycle assessment (LCA).

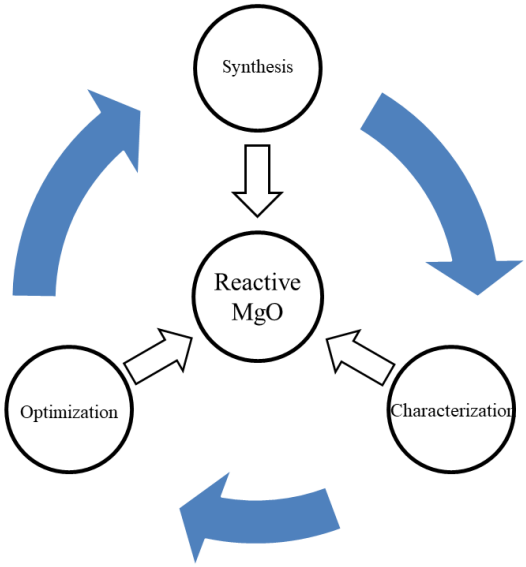

Figure 1.1 Methodology of the proposed research

1.4. Roadmap

The roadmap of research is shown in Figure 1-2 which illustrates the main research tasks of the PhD work.

Task 1: To synthesize the precursor, $Mg(OH)_2$, from reject brine. Influence of the critical synthesis parameters, such as the base type, molar ratio and reaction temperature, on the properties of $Mg(OH)_2$ precipitates will be investigated. Two types of alkalis, namely NH_4OH and NaOH, will be used to react with reject brine to precipitate $Mg(OH)_2$. Microstructure, crystallinity, and morphology of $Mg(OH)_2$ synthesized via the two different reaction routes will be characterized by means of XRD, FESEM and TGA.

Task 2: To synthesize the precursor, HMCs, from reject brine through sparging CO_2 into $Mg(OH)_2$ slurries and reject brine. Influence of critical synthesis parameters, such as the Mg : CO_2 molar ratio and pH, on the phase of HMCs will be investigated. CO_2 capture and sequestration capacity of the resulting HMCs will be evaluated. Microstructure, crystallinity, and morphology of HMCs will be characterized by means of XRD, FESEM, and TGA.

Task 3: To selectively precipitate Ca^{2+} and Mg^{2+} as $CaC_2O_4•H_2O$ and $MgC_2O_4•2H_2O$ from reject brine via the addition of oxalic acid ($H_2C_2O_4•2H_2O$) under the controlled pH. Influence of the synthesis parameters, such as the molar ratio of Ca:$H_2C_2O_4•2H_2O$ and Mg:$H_2C_2O_4•2H_2O$ and pH, on the yield and purity of $MgC_2O_4•2H_2O$ will be explored.

Task 4: To produce reactive MgO by calcining synthesized $Mg(OH)_2$ and $MgC_2O_4•2H_2O$ in Task 1 and 3, respectively. Influence of the critical factors, such as the base type, calcination temperature and duration, on the properties of MgO will be investigated. Reactivity, microstructure, crystallinity, morphology, SSA of reactive MgO will be characterized by means of XRD, FESEM, TGA, BET and acid test.

Task 5: To establish a local life cycle inventory (LCI) and to carry out the life cycle assessment (LCA) to evaluate the economic feasibility, energy consumption and carbon footprint of the production of reactive MgO from reject brine via different routes.

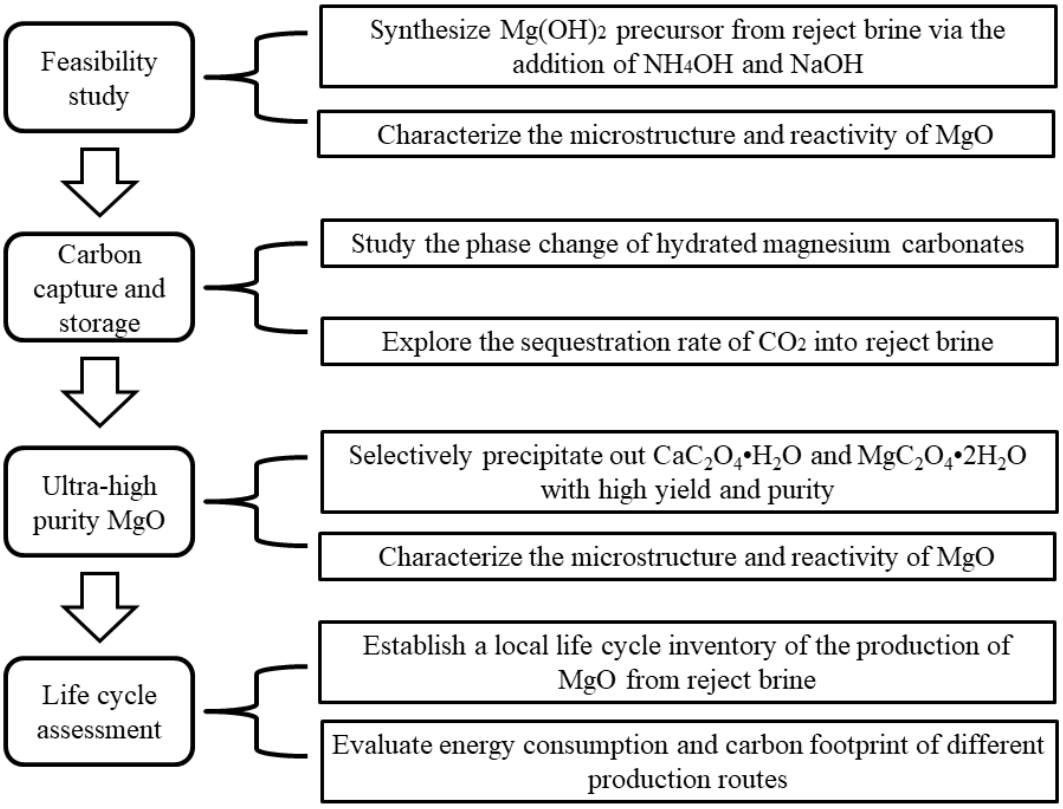

Figure 1.2 Roadmap of the proposed research

1.5. Structures of the thesis

The thesis summarizes the work that has been done over the last four years and highlights the major conclusions obtained. The thesis is divided into following chapters:

Chapter 1: Provides an introduction and overview of the issues of the research behind and addresses the aims and objectives.

Chapter 2: Presents a comprehensive study on the relevant literature focusing on the cement sustainability, reactive MgO, reject brine management, MgO production from magnesite, seawater/brine and reject brine.

Chapter 3: Reports the investigation into the feasibility of producing $Mg(OH)_2$ from reject brine by adding NH_4OH. Study the influence of the molar ratios of $Mg:NH_4OH$ on the physical and chemical properties of $Mg(OH)_2$ and characterize the $Mg(OH)_2$ in terms of crystal structures and morphologies by using XRD, FESEM and TGA. Present a case study of producing MgO calcined from $Mg(OH)_2$ synthesized from reject brine.

Chapter 4: Reports the investigation into the feasibility of producing $Mg(OH)_2$ from reject brine by adding NaOH. Study the influence of the molar ratios of Mg:NaOH on the physical and chemical properties of $Mg(OH)_2$ and characterize the calcined MgO under different conditions (i.e. temperature and duration) in terms of SSA, reactivity and morphology by using BET, acid test and FESEM.

Chapter 5: Gives a comprehensive characterization and comparison study on the influence of the synthesis environment-base type and calcination conditions (i.e. temperature and duration) on the properties of MgO calcined from the obtained $Mg(OH)_2$ via the addition of NH_4OH and NaOH into reject brine. A correlation between the calcination conditions and the reactivity, SSA of MgO is established.

Chapter 6: Studies the production of Mg-carbonates via the sequestration of CO_2 in reject brine through sparging CO_2 gas directly into reject brine. Study the synthesis parameters, such as the molar ratio of Mg:CO_2 and pH, on the change in microstructures and morphologies of HMCs. A comprehensive characterization of HMCs by means of XRD, FESEM, and TGA on the microstructure, crystallinity and morphology is discussed and CO_2 capture and sequestration capacity of reject brine is evaluated.

Chapter 7: The selective precipitation of Ca^{2+} and Mg^{2+} as $CaC_2O_4•H_2O$ and $MgC_2O_4•2H_2O$ from reject brine via the addition of $H_2C_2O_4•2H_2O$ under controlled pH is described. Study the influence of synthesis parameters, such as the molar ratio of Ca: $H_2C_2O_4•2H_2O$ and Mg: $H_2C_2O_4•2H_2O$ and pH, on the yield and purity of $MgC_2O_4•2H_2O$. A comprehensive characterization of MgO calcined from $MgC_2O_4•2H_2O$ under different conditions (i.e. temperature and duration) is presented.

Chapter 8: A local life cycle inventory (LCI) is established and a life cycle assessment (LCA) of the energy consumption and carbon footprint of the production of reactive MgO from reject brine via different routes is carried out.

Chapter 9: The conclusions and main findings of the work are summarized together with recommendations for future work.

Chapter 2 Literature review

2.1. Introduction

This chapter introduces the overview of the cement production and related environmental impacts that rise from the processing and production of cement industry. A comprehensive introduction on MgO cements in terms of grades, applications, advantages and disadvantages is discussed. Different routes on MgO production are detailed, highlighting the potential advantages and restrictions as well as the sustainability potential of each production route. A novel sustainable method to produce MgO from reject brine is introduced, followed by the current treatment of reject brine. In the end, carbon capture and storage (CCS) is introduced and combining the CCS concept with reject brine management is discussed.

2.2. Cement sustainability

2.2.1. Climate change and sustainable development

Amongst all greenhouse gases contributing to anthropogenic climate change, carbon dioxide (CO_2), whose concentration in the atmosphere recorded at Mauna Loa Observatory has risen over 25% from 315 ppm in 1960 to 395 ppm in 2013 (IPCC 2013, Pieter Tans 2014), is known as the main contributor to global warming. The main reasons behind the increase of CO_2 emissions include high rates of fossil fuel combustions (e.g. coal, oil etc.), change in land-use leading to deforestation, unlimited extraction of resources, a good example of which is the rising cement production. Various approaches have been explored with the overall goal of reducing CO_2 emissions. Some of the most notable advancements in this area include the development of renewable energy sources to partially meet the increasing energy demands, improvement of existing industrial processes to reduce the overall energy consumption and associated CO_2 emissions, and introduction of energy efficient approaches that facilitate energy conservation. Carbon capture and storage (CCS) technologies provide another suitable alternative through transporting CO_2 substantially generated from fossil fuels at large quantities to safe geological storage rather than being emitted to the atmosphere (IPCC 2007, Gibbins and Chalmers 2008).

The introduction of CCS in cement production and use offer a great potential in decreasing the overall CO_2 concentration in the atmosphere.

2.2.2. Concrete production and cement industry

Concrete is the most widely used construction material worldwide and is a composite material composed of cement and inert mineral aggregates like sand and gravel. Being the largest manufactured product in the world, concrete represents a giant energy consumer. Due to the wide availability of its raw materials and easy manufacture, concrete made from Portland cement (PC) is the most used material in the world, with a consumption rate of nearly 4 billion tonnes per year (Oss; 2015). Cement is a basic material used for building and construction and the cement industry is highly energy-intensive. Portland cement clinkers are manufactured at high calcination temperature ~1400 ℃ which are the main component of ordinary cement. This energy-intensive industry contributes to ~2% of the global primary energy consumption, direct responsible for the high CO_2 emissions. The carbon footprint of cement industry is extremely high as cement production contributes to rougly 5-7% of anthropogenic CO_2 emissions worldwide (Olivier and Marilena Muntean 2014, Unluer and Al-Tabbaa 2014). The production of one tone of cement clinker generates equal amount of CO_2 emissions, mainly due to the high calcination temperatures and energy required for the decomposition of limestone (Olivier and Marilena Muntean 2014).

$$CaCO_3 \rightarrow CaO + CO_2 \quad (2\text{-}1)$$

44% of the CO_2 comes directly from the decomposition of $CaCO_3$, while the rest comes from the combustion of fossil fuels and electricity power for crushing, grinding and transportation of raw materials. As the environmental impact of construction materials is becoming a serious concern, the development of novel alternatives with lower energy requirements and associated CO_2 emissions is more crucial than ever. Even though significant improvements have been made towards reducing the impacts of the cement industry through the introduction of various kinds of industry by-products such as pulverized fly ash (PFA) and ground granulated blast-furnace slag (GGBS), the environmental impacts associated with the energy intensive production process are still a major concern.

Several sustainable improvements ranging from sustainable energy sources usage to partial replacement of cement with low-carbon materials have been suggested in the cement industry. The utilization of sustainable energy sources such as wind and solar power has firstly been mentioned in the context of switching from traditional fossil fuels to renewable energy sources (Jones and Bouamane 2012). One approach includes the replacement of PC with industry by-products such as PFA and GGBS. Another approach of the sustainability initiatives in the cement industry involves the development of sustainable cement binders such as geopolymers and reactive magnesium oxide (MgO) cements. Recently developed reactive MgO cements require significantly lower calcination temperatures (~700 ℃) and have the ability to absorb CO_2 in the form of stable carbonates while gaining strength (Unluer and Al-Tabbaa 2013, Unluer and Al-Tabbaa 2014).

2.3. Reactive MgO cements

2.3.1. Introduction on MgO cements

Reactive MgO cements are novel hydraulic cements containing mainly reactive MgO and PC, depending on the intended application. They were firstly introduced and patented by the Australian scientist John Harrison (Harrison 2001a). Reactive MgO cements have been introduced as a potential alternative to PC with superior performances with a particular emphasis on cement sustainability and received media attention through the New Scientist (Pearce 2002) and the Guardian (Dyer 2003).

MgO cements are generally categorized into four grades depending on the calcination temperature of the parent magnesite which results in differences in particle size, reactivity and specific surface area of MgO cements:

1. Light-burned (reactive or caustic calcined) MgO is typically calcined between 700 and 1000 ℃, leading to the highest reactivity and largest specific surface area. When MgO reacts with water, a high molecular disorder is introduced to prevent the formation of precise crystalline lattice structures, resulting in the decrease of reactivity rate of MgO cements (Harrison 2004b). Reactive MgO has a similar hydration rate as PC (Liska and Al-Tabbaa 2009), serving as a better alternative to blend with PC.

2. Hard-burned MgO is calcined at slightly higher temperatures between 1000 and 1400 ℃, resulting in a comparatively low reactivity. Hard-burned MgO has been extensively used as an expansive agent to compensate shrinkage in many applications in China since 1970s (Mo, Deng et al. 2014), dam construction in particular.
3. Dead-burned MgO is calcined above 1400 ℃, resulting in a low reactive final product with a low specific surface area. When blended in PC mixes, dead-burned MgO is an unsound problematic component due to late hydration and dimensional distress (Lea and Hewlett 1998). Dead-burned MgO is usually used in the refractory industry and is one of the major components of magnesium phosphate cements.
4. Fused MgO is calcined above the fusion temperature (2800 ℃) and is the least reactive amongst all grades. It has a better performance over dead-burned MgO on strength, abrasion resistance, and chemical stability (Balkevich and Lemeshev 1968). Its main applications include its use in the refractory and electrical insulating industries (Pal and Bandyopadhyay 2008).

2.3.2. Applications, advantages and disadvantages of MgO cements

MgO in general has a broad application area due to the porous inner structure and superior properties in many aspects. Amongst a number of industrial applications, MgO is utilized in: (i) abrasives as a binder in grinding wheels, (ii) animal feed supplements and fertilizers as the source of magnesium ions for animals and plants, (iii) coatings as a pigment extender in paints, (iv) construction materials as a basic ingredient of oxychloride cements used for flooring and wallboard, (v) insulations as the light and flexible mats for insulating pipes, (vi) pharmaceuticals in antacids, cosmetics and toothpastes, and (vii) refractory, ceramic and steel industries.

Blends including reactive MgO cements through carbonation to form porous blocks have received attention particularly due to the high CO_2 sequestration potential of MgO while gaining strength in concrete mixes (Unluer and Al-Tabbaa 2013, Unluer and Al-Tabbaa 2014). Under appropriate curing conditions that enhance carbonation, reactive MgO cements can lead to significant improvements in strength and durability than those with PC (Unluer and Al-Tabbaa 2011). It has been proven that MgO can achieve 100% carbonation when blended in porous mixes, serving as a carbon sink, while PC can only achieve as high as 30% carbonation (Liska

and Al-Tabbaa 2009). The carbon footprint can be further reduced by recapturing and geo-sequestrating CO_2 generated in the production of MgO and incorporating renewable energy sources during this process. MgO cement can be fully recycled back to its original state and reused though a simple heating process. MgO cements can also make better use of much higher proportions of incorporated waste than PC since MgO has a high propensity for binding with waste and the hydration of lime in PC can cause delayed and disruptive reactions.

Although MgO cements present a great potential owing to their significant abilities in CO_2 sequestration resulting in high strength and durability, there are still certain barriers with regard to regulations, technical, and environmental aspects that need to be overcome before they can be fully commercialized in the construction sector. Concrete made from PC is the dominating construction material because of various reasons including the comprehensive regulations and documents at every level, familiarity, cost and reliability. Besides, technical problem remains due to the late hydration of MgO in clinkers causing expansion and cracking in the hardened cements. In 1884, a number of constructed bridges in France containing 16-30% periclase cracked as a result of the delayed excessive expansion of concretes due to the late hydration of periclase (Mehta 1978). Since then to avoid the unsoundness of concrete caused by delayed hydration of MgO, the content of MgO is limited around 5% for PC worldwide. However, such accidents only occur when the hydration rate of MgO is much later than other cement phases. When reactive MgO calcined at lower temperatures is introduced, reactive MgO hydrates at a similar rate with other major cement phases, avoiding the issues caused by the late hydration of MgO . Besides, research in China revealed the benefits of late hydration of MgO which can effectively compensate thermal shrinkage due to cooling of concrete with time in mass construction such as dam (Mo, Deng et al. 2014).

2.3.3. Global production of MgO cements

Currently, MgO is mainly produced via the calcination of natural carbonates such as dolomite ($CaMg(CO_3)_2$) or magnesite ($MgCO_3$) with an annual production rate of 12.5 million tonnes (commission 2010). $MgCO_3$ exists naturally with high purity of 90-95% and the estimated global reserve is around 13 billion tonnes (Shand 2006). The main production of $MgCO_3$ is located in North Korea, China, Slovakia, Turkey, Russia, Austria and India which accounts for 75% of

globe demand all together (Shand 2006). MgO can also be synthesized from seawater or natural brine (Bhatti, Dollimore et al. 1984) which contributes to ~14% of the global MgO production (Kramer). This process involves recovery of abundant magnesium ion (Mg^{2+}) from seawater to precipitate $Mg(OH)_2$ or $MgCO_3$, which then undergoes calcination and decomposes to MgO. Another production route of MgO is from magnesium silicates, which has received attention due to CO_2 sequestration potential during production (Simons and Vlasopoulos 2012, Baglioni, Ferraro et al. 2014).

2.4. Production of reactive MgO from $MgCO_3$

2.4.1. Mining and crushing

Mining of $MgCO_3$ is mainly performed via the open-pit method which includes five stages: overburden removal, drilling, blasting, loading and hauling to the processing plant (Shand 2006) as shown in Figure 2.1. Open-pit mining involves the use of one or more horizontal benches to mine a near surface deposit via surface excavation (Crawford, Hustrulid et al. 1979). Overburden removal removes the top layer of soil which is located between the surface and the ore body. Drilling is used to obtain a detailed map of the ore quality by taking samples from the drill holes, also providing holes for explosives during blasting operations. Chemical contour maps are drawn, serving for the selective purpose of mining of the core, denoting the MgO content and distinguishing the unusable ore which is later removed from the usable ore. The usable ore undergoes a series of processes like crushing, sizing and beneficiation until the required size is achieved, whereas gyratory and jaw crushers are the two main crushers used. After sizing, screening, an industrial-size separation technique is applied to reject a certain fraction size of ore, sweeping out the main impurities and removing the unsuitable materials for the following processes. Before calcination, raw materials need a third crushing step until they achieve the required size of <1 inch. The crushed and sized ore is then stockpiled over a belt tunnel feeder system, allowing loads of ore coming from different access ports onto the belt.

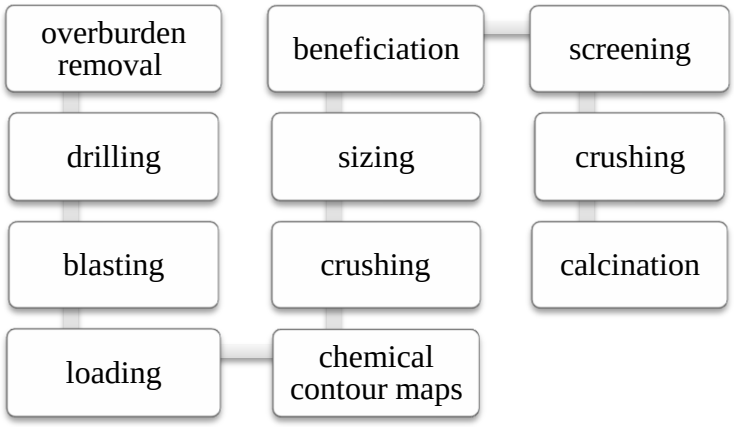

Figure 2.1 Diagram of open-pit method in mining of $MgCO_3$

2.4.2. Pyro-processing

The calcination of $MgCO_3$ takes place in a similar manner to that of $CaCO_3$, enabling the use of a similar calcination theory:

$$MgCO_3 \rightarrow MgO + CO_2 \quad (2\text{-}2)$$

A production yield of 1 kg of MgO requires decomposing 2.08 kg of pure $MgCO_3$. The decomposition kinetics of magnesite is affected by three essential factors: (i) burning the magnesite to the decomposition temperature; (ii) maintaining the minimum decomposition temperature until magnesite is fully decomposed to MgO; and (iii) removing the CO_2 gas emitted during the process to increase the decomposition rate. The decomposition temperature of $MgCO_3$ under one atmosphere CO_2 pressure has been reported to range between 402 and 750 ℃, depending on the $MgCO_3$ source, which can indicate some variations in the impurity levels, crystalline structures and microstructures (Shand 2006).

The standard heat of decomposition of $MgCO_3$ to MgO is 3,027 kJ/kg which is much higher than the decomposition of PC clinkers (1,757 kJ/kg) (Shand 2006). The energy consumption in calcinations is derived by considering three steps: (i) the energy consumed to increase the temperature from room temperature to the decomposition temperature, (ii) the enthalpy in $MgCO_3$ decomposition process, (iii) heat loss during calcinations process. Time and temperature

are the two main factors influencing the decomposition of $MgCO_3$. A significantly higher temperature above minimum decomposition temperature is employed to accelerate the rate of decomposition until CO_2 has been fully expelled in practice. Generally, temperature has a greater impact over time on the decomposition rate but a balance has to be maintained for practical profits and a high production rate. After calcination, MgO may undergo screening and grinding once more to remove certain sizes of ore with a higher level of impurities.

2.5. Production of reactive MgO from seawater/brine

Magnesium is the third most abundant element in seawater after sodium and chlorine, with an average concentration of 1300 ppm. Natural brine exists widely in brine wells and lakes, providing another abundant source for MgO production. The chemical concentration of natural brine varies according to the surrounding environment. However, natural brine generally consists of much higher salt concentrations than seawater (Shand 2006).

2.5.1. Extraction

Seawater intake structures are mostly utilized in large seawater desalination plants which mainly extract seawater from open sea under surface water arrangements (Pankratz 2004). Three main types of seawater intake structures are used during this process (Pita 2011): (i) Well intake structure extracts the water from the phreatic water-table level at the coast, having an advantage of using high quality water; (ii) direct coast intake is carried out by way of collection caissons, which are only feasible in certain enclaves since the water dynamics may bury the equipment; and (iii) open intake structures, located at a sufficient sea depth, pump seawater via the underwater pipelines to the reservoir. Seawater is then pumped into setting tanks to eliminate the suspended particles such as silts and sands before pre-treatment.

Recovery of magnesium salts from the natural brine also involves pumping the solution to the plant, similar to their extraction from the sea. However, the underground extraction is much more complicated and is usually accompanied with leaching, involving drilling and recovery techniques which are performed in a similar manner to those in the oil and gas industry (Shand 2006). A vertical borehole is firstly drilled from the surface and concentric tubes or casings are

placed along the borehole, providing the channels for liquid flow from the salt deposits. Fresh water is pumped into the boreholes via the casings so that the brine can be forced back to the surface via the inner tubes.

2.5.2. Raw materials pre-treatment

Seawater/brine pre-treatment often employs two strategies to decarbonate the solution at hand: (i) adding sulphuric acid to decrease the pH of the solution to 4, as shown in the Equation 2-3. Seawater is then passed through a desorption tower where it is aerated to remove CO_2 in case of the precipitation of $CaCO_3$ along with $Mg(OH)_2$ (Shand 2006).

$$Ca(HCO_3)_2 + H_2SO_4 \rightarrow CaSO_4 + H_2O + CO_2 \quad (2\text{-}3)$$

An alternative method involves adding milk of lime into the incoming seawater/brine. However, this method presents a difficulty in the removal of $CaCO_3$ formed in the saturated solution,

$$Ca(HCO_3)_2 + Ca(OH)_2 \rightarrow 2CaCO_3 + 2H_2O \quad (2\text{-}4)$$

2.5.3. Processing

After softening seawater/brine, it is then pumped into an agitated reactor vessel. A strong base is added into magnesium solution to raise the pH to 10.5, enabling the precipitation of magnesium (Shand 2006). Generally calcium hydroxide derived from the calcined lime or dolime is deployed in practice. Dolime is preferred due to its self-contained MgO content, so that only half of the volume of seawater or brine is required while the other half is derived from dolime to produce the same amount of MgO than lime (Al-Zahrani and Abdel-Majeed 2007). The aforementioned processes are represented in Equations 2-5 to 2-7. Besides using lime as the alkali source, researchers have proposed various additives to precipitate Mg^{2+}.

$$CaO + 2H_2O + MgCl_2 \rightarrow Mg(OH)_2 + CaCl_2 \quad (2\text{-}5)$$

$$CaO{\cdot}MgO + 2H_2O + MgCl_2 \rightarrow 2Mg(OH)_2 + CaCl_2 \quad (2\text{-}6)$$

$$CaO{\cdot}MgO + 2H_2O + MgSO_4 \rightarrow 2Mg(OH)_2 + CaSO_4 \quad (2\text{-}7)$$

Irving proposed using sodium hydroxide (NaOH) and sodium carbonate (Na_2CO_3) to precipitate Ca^{2+} and Mg^{2+} (Irving 1926). The solubility constant for the Ca^{2+} and Mg^{2+} precipitates are as follows (Johnston 1915):

$$K_{Mg(OH)2} = 1.2 \times 10^{-11} \quad (2\text{-}8)$$

$$K_{Ca(OH)2} = 4.1 \times 10^{-6} \quad (2\text{-}9)$$

$$K_{MgCO3} = 1.4 \times 10^{-4} \quad (2\text{-}10)$$

$$K_{CaCO3} = 0.98 \times 10^{-8} \quad (2\text{-}11)$$

It was found that seawater was saturated with $CaCO_3$ and addition of alkali to achieve pH 10 was enough to form precipitates in seawater.

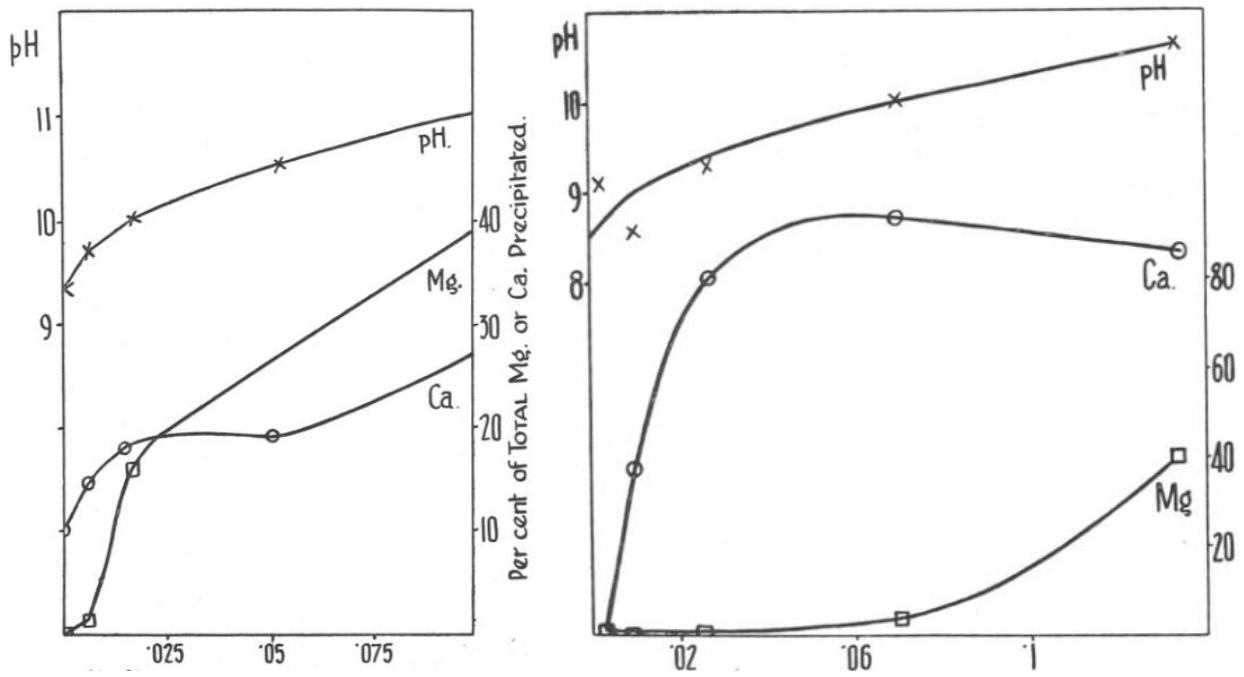

(a) (b)

Figure 2.2 (a) Titration of seawater with NaOH; (b) Titration of seawater with Na_2CO_3 (Irving 1926).

The experiment was done by adding different amount of NaOH and Na_2CO_3 into seawater as shown in (a) (b)
Figure 2.2. It was found that NaOH precipitates much more Mg^{2+} and Na_2CO_3 precipitates much more Ca^{2+} since $Mg(OH)_2$ and $CaCO_3$ have a much smaller solubility than $Ca(OH)_2$ and $MgCO_3$, respectively as shown in Equations 2-8 to 2-11.

Friedrich et al. patented a simple process to precipitate MgO calcined from $Mg(OH)_2$ precipitated from seawater at a pH of 10.5 using a lime solution in 1943 (Friedrich, Robinson et al. 1946). Petric et al. utilized dolomite composed of 57.6% CaO and 42.3% MgO to precipitate $Mg(OH)_2$ from seawater, which was then calcined at 950 ℃ to produce MgO (Petric, Martinac et al. 1997). Dave et al. used hydrated lime ($Ca(OH)_2 \cdot 2H_2O$) to precipitate $Mg(OH)_2$ from seawater at a pH ranging between 7.0 and 7.5 (Dave and Ghosh 2005). All these studies introduced Ca^{2+} into the seawater/brine solution, which resulted in the formation of gypsum ($CaSO_4 \cdot 2H_2O$) along with other precipitates due to the presence of sulphate in the solution. The contamination of the final product due to the formation of gypsum necessitates desulfation via the addition of $CaCl_2$ into the seawater/brine.

Tureck et al. utilized aqueous sodium hydroxide (NaOH) to precipitate $Mg(OH)_2$ from mine brine (Turek and Gnot 1995). The brine was firstly acidified by adding hydrochloric acid in order to remove bicarbonates which have the potential to attack Ca^{2+} to form $CaCO_3$. It was reported that an improved precipitation was achieved at lower temperatures and higher NaOH concentrations. This improved sedimentation was attributed to the high viscosity of NaOH solution and brine, which impeded the contact between the precipitating agent and the brine.

Kotsupalo et al. reported three methods to synthesize MgO from natural mineralized multicomponent brines with different $MgCl_2/CaCl_2$ ratios (Kotsupalo, Ryabtsev et al. 2010). The Mg^{2+} in the brines could be precipitated by adding lime milk (CaO of 10%) to form $Mg(OH)_2$ as shown in method I (Equations 2-12 to 2-14). After removing $Mg(OH)_2$ precipitates from the solution, CO_2 was introduced to carbonate Ca^{2+} to form $CaCO_3$.

$$Ca(OH)_2 + MgCl_2 \rightarrow Mg(OH)_2 + CaCl_2 \quad (2\text{-}12)$$

$$Mg(OH)_2 \rightarrow MgO + H_2O \quad (2\text{-}13)$$

$$Mg(OH)_2 + CaCl_2 + CO_2 \rightarrow MgCl_2 + CaCO_3 + H_2O \quad (2\text{-}14)$$

The method II (Equations 2-15 to 2-18) utilized the soda-alkali solution (Na_2CO_3 and NaOH) at room temperature to collectively precipitate $Mg(OH)_2$ and $CaCO_3$. $Mg(OH)_2$ and $CaCO_3$ were separated by introducing CO_2 into slurries. Since the introduction of CO_2 lowered the pH of the solution, $Mg(OH)_2$ were therefore dissolved into the solution while $CaCO_3$ precipitated could be separated from the solution. Then $MgCl_2$ contained in the solution could be precipitated by adding Na_2CO_3 to form hydrated magnesium carbonates which could be further calcined to produce MgO.

$$CaCl_2 + MgCl_2 + Na_2CO_3 + 2OH^- \rightarrow Mg(OH)_2 + CaCO_3 + 2NaCl + 2Cl^- \quad (2\text{-}15)$$

$$Mg(OH)_2 + CaCO_3 + CO_2 + CaCl_2 \rightarrow MgCl_2 + 2CaCO_3 + H_2O \quad (2\text{-}16)$$

$$4MgCl_2 + 3Na_2CO_3 + 5H_2O \rightarrow 3MgCO_3 \bullet Mg(OH)_2 \bullet 3H_2O + 6NaCl + 2HCl \quad (2\text{-}17)$$

$$3MgCO_3 \bullet Mg(OH)_2 \bullet 3H_2O \rightarrow 4MgO + 3CO_2 + 4H_2O \quad (2\text{-}18)$$

The method III followed a similar first stage where Ca^{2+} was precipitated by adding soda-alkali source as shown in Equations 2-15 to 2-16 but OH^- was provided by adding lime milk. In the following step after removing $CaCO_3$, soda-alkali solution was again added to precipitate Mg^{2+} as shown in Equation 2-19.

$$4MgCl_2 + 3Na_2CO_3 + Ca(OH)_2 + 3H_2O \rightarrow 3MgCO_3 \bullet Mg(OH)_2 \bullet 3H_2O + 6NaCl + CaCl \quad (2\text{-}19)$$

These three methods provided a feasible way to separate $CaCO_3$ and $Mg(OH)_2$ precipitated from the brine and natural highly mineralized multicomponent brines could be utilized as a new source of raw materials for obtaining high-quality Mg^{2+} and Ca^{2+} production. MgO binders and grouting mortars could be therefore synthesized.

Tran et al. synthesized magnesium oxalate ($Mg(C_2O_4)_2$) from Uyuni salar brine and indicated that the high purity (99.5% grade) precursor could be further calcined to produce high-purity MgO (Tran, Van Luong et al. 2013).

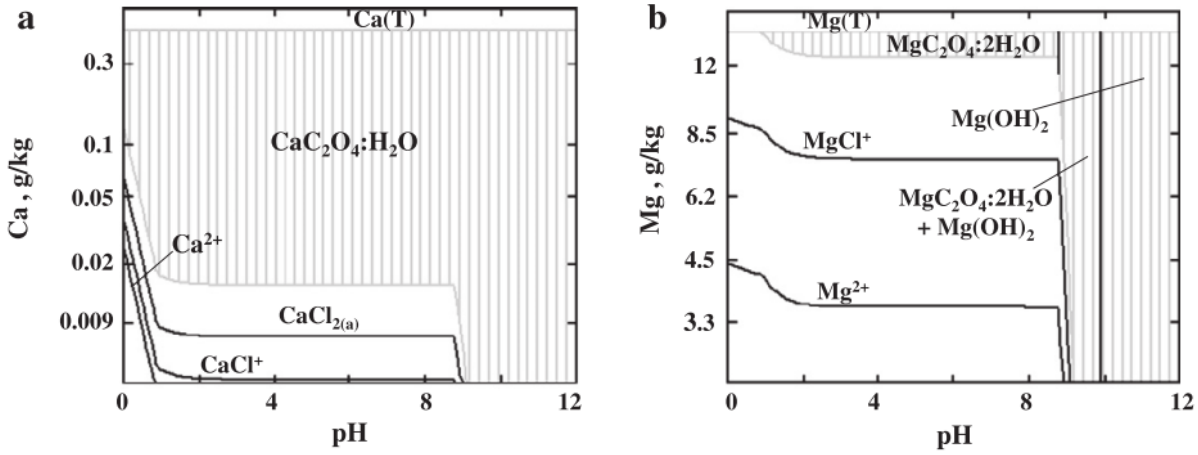

Figure 2.3 Stabcal simulation for oxalate precipitates showing the concentration of Ca^{2+} and Mg^{2+} profile versus pH (Tran, Van Luong et al. 2013).

Through stabcal simulation as shown in Figure 2.3, it was found that Ca^{2+} could be precipitated compounded with $C_2O_4^{2-}$ in acidic zone (pH 0-1) requiring only 0.02 g/kg Ca^{2+} while the precipitation of Mg oxalate would not take place when pH below 1.

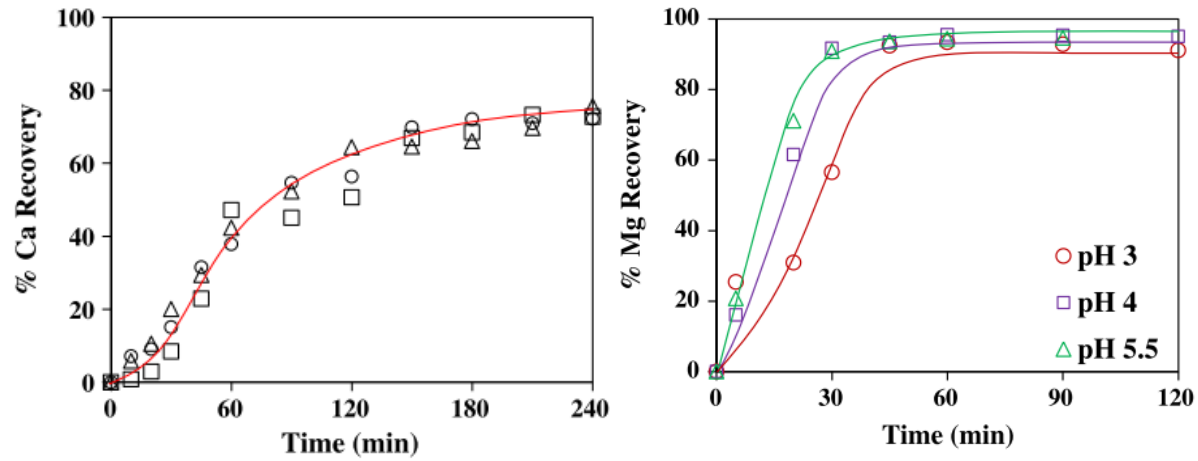

(a) (b)

Figure 2.4 (a) The percentage of precipitated Ca^{2+} at Oxalate/Ca molar ratio of 6.82:1 at pH 1. (b) Recovery of Mg at different pH (Tran, Van Luong et al. 2013).

At second stage, Ca^{2+} was precipitated by adding oxalic acid and removed from the solution. NaOH was used to adjust pH to 1. The kinetics of precipitated Ca^{2+} from the brine was shown in Figure 2.4(a) and 80% Ca^{2+} was precipitated. After removing Ca^{2+} precipitates, NaOH was added to reach different pH to precipitate Mg^{2+} as shown in Figure 2.4(b). It was found the reaction rate was higher and 90-95% Mg^{2+} was precipitated at lower pH. This highlighted the pH gap that enabled a selective precipitation of Mg^{2+} from Ca^{2+}, leading to the synthesis of a high purity of $Mg(C_2O_4)_2$ (99.5% grade), which could be further calcined to produce MgO.

2.6. Production of reactive MgO from other magnesium-containing sources

MgO can also be produced from other magnesium-containing solution like magnesium chloride and magnesium sulfate by adding alkali source. Henrist et al. studied several parameters such as the chemical nature of the utilized bases, type of counter-ions and temperature on the morphological characteristics of $Mg(OH)_2$ precipitated from magnesium salt solution (Henrist, Mathieu et al. 2003). Alkaline solution (NaOH and NH_4OH) was added to a magnesium salt solution of concentration 0.75 mol/L and reacted with Mg^{2+} at different temperature. It was found that the nature of the base source played an important role in the morphologies of precipitates formed. Addition of NaOH to $MgCl_2$ solution led to a globular cauliflower-like morphology, while the use of aqueous ammonia (NH_3H_2O) resulted in plate-like shapes due to the structural difference of cations present in the solution as shown in Figure 2.5. It was attributed to the differences in terms of pH of the solution and chemical nature of the ions. The higher pH (12) caused by NaOH created a high supersaturation level and a negative surface charge, resulting into much faster nucleation process therefore small tiny particles formed. The negative charged surface adsorbed sodium ion and therefore hindered the coming Mg^{2+} to grow particles. The small particles agglomerated to globular structure to minimize the surface the energy.

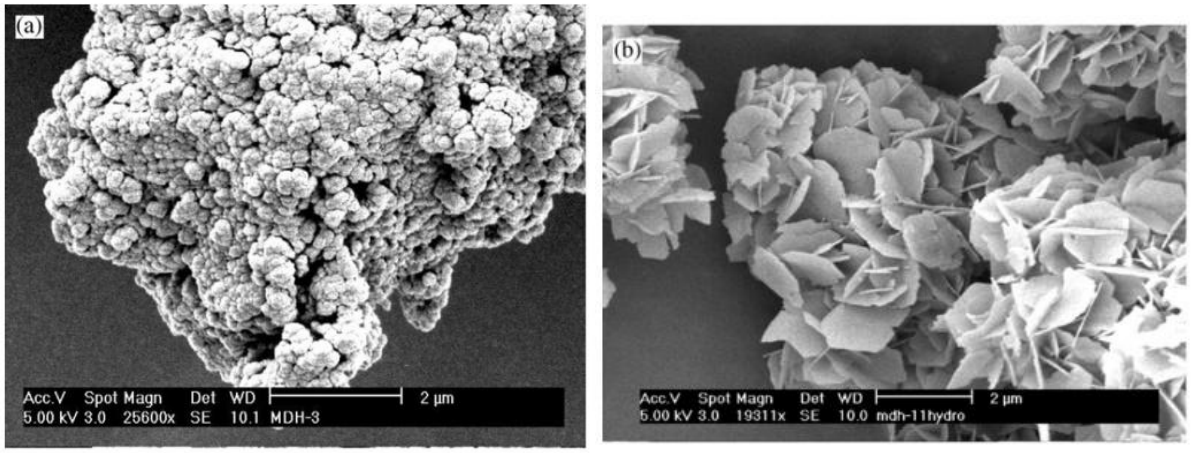

Figure 2.5 Morphology of $Mg(OH)_2$ precipitate under the condition of a) $MgCl_2$ + NaOH at 60 ℃ b) $MgCl_2$ + NH_3H_2O at 60 ℃ (Henrist, Mathieu et al. 2003).

It was also found that single and circular plate-like particles were observed at lower temperatures while particles had a tendency to inter-grow at 60 ℃. This was supported by the XRD pattern shown in Figure 2.6. The $Mg(OH)_2$ precipitate had a much higher I_{001}/I_{110} ratio at 25 ℃ than at 60 ℃, which meant a much favoured orientation of the single platelet structure. The $Mg(OH)_2$ can be further calcined to produce MgO.

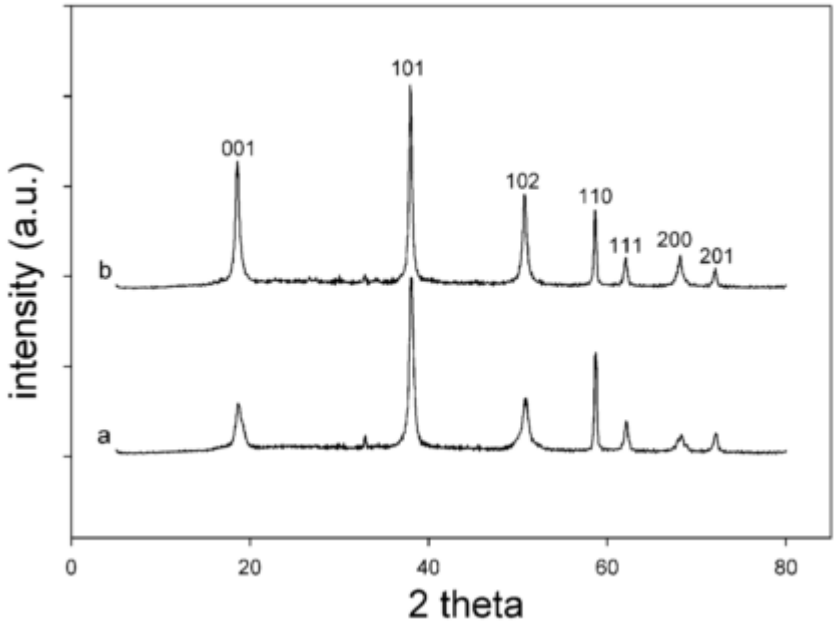

Figure 2.6 XRD pattern of $Mg(OH)_2$ precipitates reacted (a) at 60 ℃ I_{001}/I_{110}= 0.51 and (b) at 25 ℃, I_{001}/I_{110} = 1.6 (Henrist, Mathieu et al. 2003).

Yan et al. reported the synthesis of $Mg(OH)_2$ nanoflowers by a simple hydrothermal reaction of $MgCl_2$ and $CO(NH_2)_2$ without any additives (Yan, Xue et al. 2005). The pH of the magnesium chloride solution was firstly adjusted by adding HCl or NH_3H_2O to a range of 3-9.5. The solution was then sealed in the autoclave at 95-130 ℃ for 18 hours before collecting the samples. It was found that the pH value and temperature of the initial reaction solution was essential in controlling the morphology of particles as shown in Figure 2.7. The spherical particles started to be irregular and finally developed nanoflower morphology with increasing pH as shown in Figure 2.8. It was also reported that the optimum temperature for formation of $Mg(OH)_2$ nanoflowers was in the range of 80-130 ℃. The nanoflower morphology developed was because excessive Mg^{2+} and OH^- was stacked on the existing plate-like crystal seeds and therefore self-assembled into a flower like structure at high pH. This synthesized $Mg(OH)_2$ can be further calcined to produce MgO.

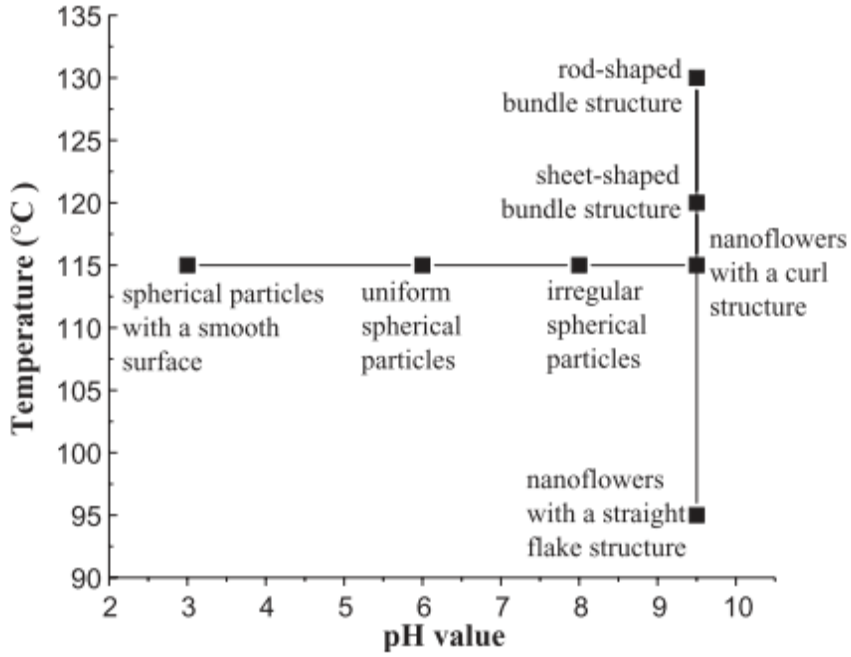

Figure 2.7 Chart of $Mg(OH)_2$ morphologies at different temperature and pH of the hydrothermal growth process (Yan, Xue et al. 2005).

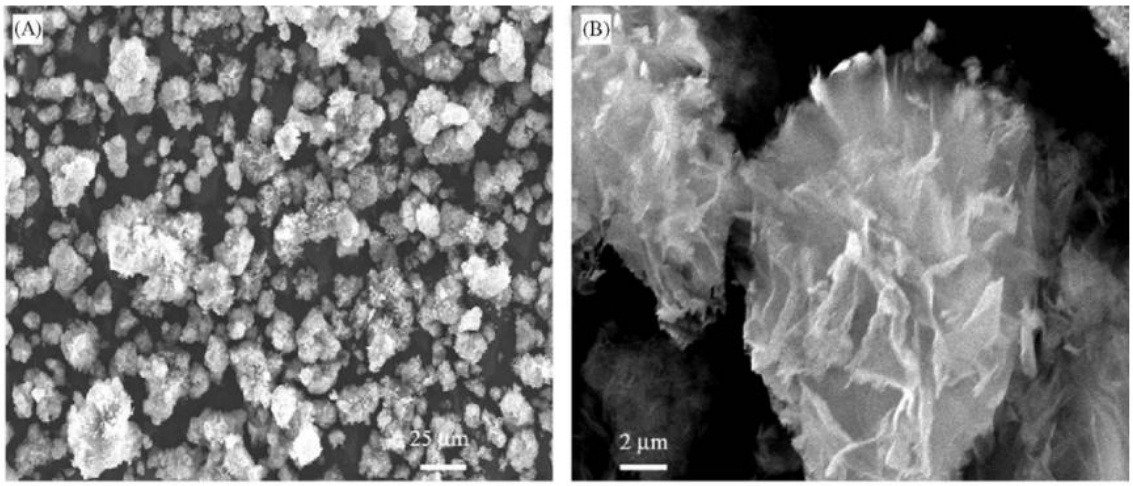

Figure 2.8 SEM images of $Mg(OH)_2$nanoflowers synthesized at pH 9.5(Yan, Xue et al. 2005).

2.7. Reject brine

Desalination is a process in which the salts are removed from saline water to produce fresh water (e.g. potable water). In coastal regions where sources of fresh water are limited such as Singapore, desalination provides a feasible alternative to produce fresh water to meet residential and industrial demands. Currently the desalinated water from two seawater reverse-osmosis plants provides 100 million gallons water a day, which meets up to 25% of Singapore's current water demand (PUB 2015).

Reject brine is the residue after desalination. The most common way to dispose reject brine is to discharge it back to the sea. With high concentration and salinity, reject brine is denser than the feedstock supply. Without sufficient mixing, reject brine discharged through an outfall tends to accumulate at the bottom of the sea. Discharge of untreated reject brine may cause negative impact to the ecosystem. Studies have shown that increased salinity has an altering effect on the flora and fauna and affects all of the organisms of that ecosystem in a negative way, either directly or indirectly (Mohamed, Maraqa et al. 2005). Several strategies such as deep well injection and mechanical or thermal evaporation have been proposed to manage reject brine (El-Naas 2011). However, deep well injection suffers from the drawbacks of the difficulty of selecting a suitable well site and corrosion and potential leakage in the well casting; evaporation rate greatly limits the usage of thermal evaporation. Alternatively, reject brine can be recycled

and mixed with concrete or asphalt to produce saltcrete (Drom; and Loveland 1998). The material can then be used for road construction. A more recent method of brine disposal is to treat brine by reverse osmosis which produces additional clean water and super concentrated brine waste. The high concentrated brine waste is then dried out to evaporate any loose water. After which the remaining salt can be harvested for resale but the process is highly costly (Arnal, Sancho et al. 2005). The current methods to treat reject brine are rather limited and have not achieved a satisfactory result. Therefore a feasible and practical way to treat and utilize reject brine is highly desirable.

2.8. A new idea to treat reject brine

Carbon capture and storage (CCS) focuses on providing a feasible and promising methond to reduce the green house emissions as it allows fossil fuels continue to be used (Rao and Rubin 2002). CCS concept covers broad fields like ocean, terrestrial, geological, biological and chemical approaches to store CO_2 gas in the long term (Botha and Strydom 2001, Kloprogge, Martens et al. 2003, Rendek, Ducom et al. 2006, Ferrini, De Vito et al. 2009). Under the concept of CCS, one novel idea is to target the reject brine as the CO_2 reservoir based on the chemical reactions of reject brine with CO_2 (El-Naas 2011).With high concentrations of magnesium and calcium ions in reject brine, the invention discloses a method to synthesize hydrated magnesium carbonates from reject brine through sequestration of CO_2 using aqueous ammonia. CO_2 therefore is reserved in the form of thermodynamically stable carbonates in the long run. The possibility of storing CO_2 in the form of stable carbonates through the interaction of ions in aqueous solution with CO_2 has been studied by several researchers.

Ferrini et al. developed a new method to synthesize nesquehonite by reacting CO_2 gas with $MgCl_2$ solution, which was further calcined to produce MgO (Ferrini, De Vito et al. 2009). NH_3H_2O was added to provide alkali source to reach desired pH. The reaction kinetics was greatly improved as shown in Figure 2.9, which led to the rapid precipitation of stable nesquehonite. The well-formed and typical needle-like morphology of nesquehonite was shown in Figure 2.10 and the elongate habit was seen under optical microscopy. The distinct needles were up to 0.5mm in length and 30 μm in diameter. A high purity of MgO can be obtained by calcining synthesized nesquehonite.

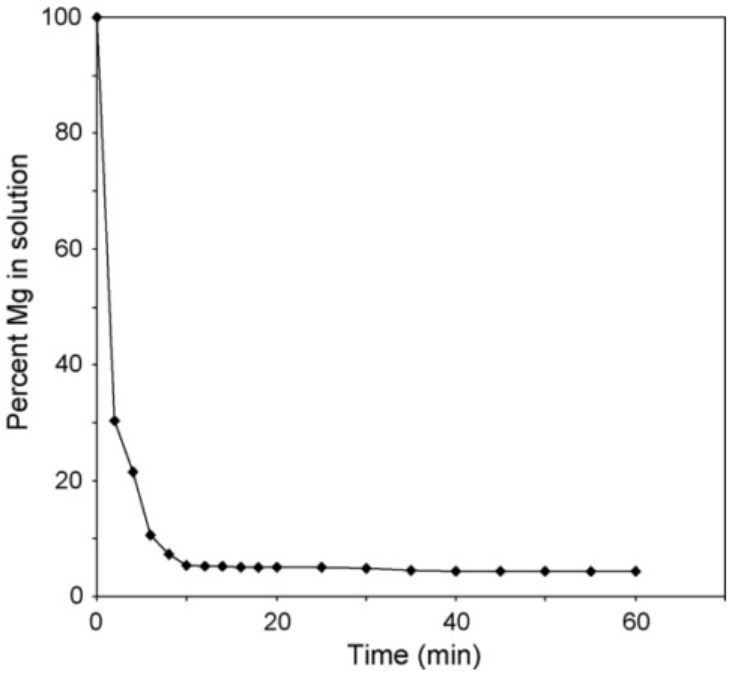

Figure 2.9 Kinetics of the carbonation reaction (Ferrini, De Vito et al. 2009).

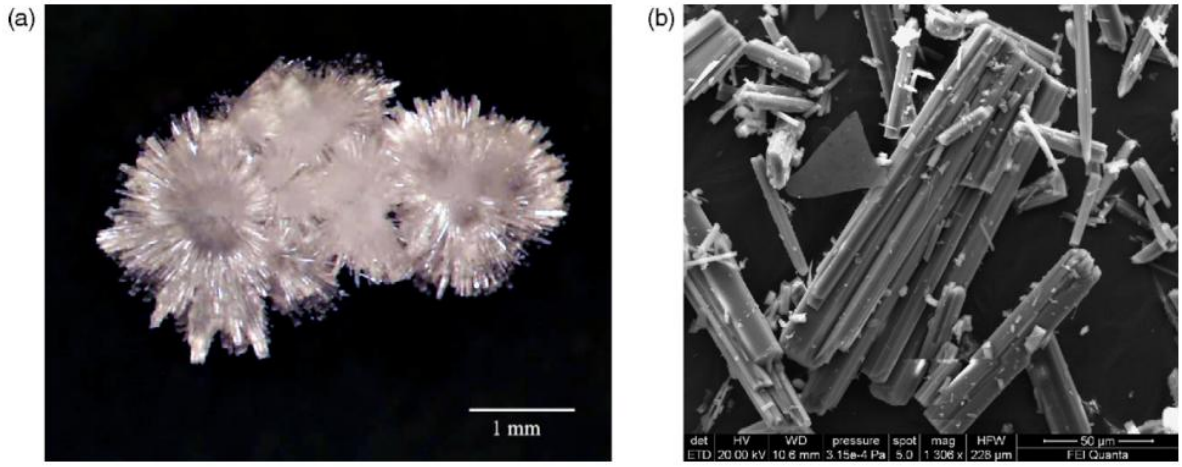

Figure 2.10 Images of synthesized nesquehonite under (a) optical microscopy; (b) under SEM at high magnification (Ferrini, De Vito et al. 2009).

Soong et al. studied the reaction of CO_2 with brine and explored the influence of pH (3.6-11), reaction time (1-6 h), CO_2 pressure (0.34-7.63 MPa) and temperature (50-170 ℃) on brine carbonation (Soong, Goodman et al. 2004). The experiment was conducted in a 1/2 1 autoclave

(Hastelloy C-276) where the brine was placed. The CO_2 was sparged into the reactor to the desired pressure while temperature was controlled. KOH was added to provide the alkali source. It was found that the reaction time had slight influence on formation of carbonates. The most noticeable difference lied in the precipitation of Ca which increased by 20% after 2 hours of reaction. pH was found to have a significant effect on brine carbonation as shown in Figure 2.11. The concentrations of Ca^{2+}, Mg^{2+} and Na^{+} in the brine were found to decrease by 25%, 17% and 17%, respectively when the pH was increased from 3.6 to 11. Both simulation and experimental results showed a similar trend of the amount of precipitates from brine with increased pH of the solution. It was found that $CaCO_3$ was the major component of the precipitates accounting for 95% by weight while the remaining part was Fe_2O_3 which was supported by XRD, FTIR and XRS. The effect of CO_2 pressure was also tested and it was found the amount of precipitates was not significantly changed when CO_2 pressure increased from 0.34 to 7.64 MPa. The reaction of temperature also did not have a significant effect on the amount of precipitates.

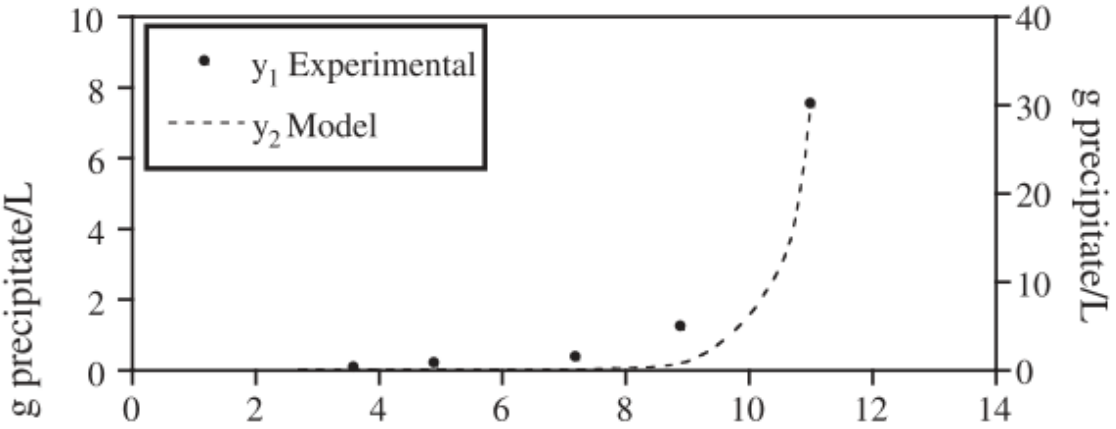

Figure 2.11 Comparison of experimental and predicted results for brine carbonation versus pH (Soong, Goodman et al. 2004).

2.9. Summary

Although there are numerous studies on the reaction of $MgCl_2$ solution, seawater or natural brine with different additives, limited research has been reported on the recovery of valuable metals from actual reject brine obtained from desalination plant. This research focuses on the treatment of reject brine collected from a local desalination plant and explores the potential of recovery of

MgO from reject brine. Precipitation of $Mg(OH)_2$ from Mg^{2+} rich water is easiest method to recover Mg^{2+}. NH_4OH was firstly proposed to study the feasibility to recover highly reactive MgO from reject brine. Unlike Ca-bearing bases, which often lead to the precipitation of a Ca-based compound (e.g. $CaCO_3$) along with Mg-phases, the use of NaOH can increase the purity of Mg-based precipitates, which serves as a pH adjuster and controls the pH of the solution. Furthermore, when compared with other bases (e.g. NH_4OH, KOH and Na_2CO_3), NaOH possesses other advantages in terms of health and safety, cost effectiveness and base strength it provides.

The key parameters affecting the properties of the synthesized $Mg(OH)_2$ and its calcination to produce reactive MgO were investigated. One of the main factors determining the efficiency of the overall synthesis was the type and amount of the base introduced into the reject brine. Accordingly, the characteristics of $Mg(OH)_2$ and resulting MgO significantly varied, especially in terms of their reactivity and microstructure, under the use of different bases. Furthermore, the synthesis temperature was accounted for the size of the platelets as the lower the synthesis temperature, the higher the diameter. However, the influence of base type, reaction condition and calcination conditions on the texture properties (SSA and pore size distribution) and reactivity of the MgO has yet been revealed. For the accurate characterization of the final product, the relationship between the reaction condition, such as the base type, and the reactivity of MgO must be clearly comprehended. Establishing clear links between its production conditions and final properties will enable the effective use of MgO and the identification of the right applications in line with its capabilities.Several techniques were utilized to characterize the synthesized $Mg(OH)_2$ and MgO including inductively coupled plasma-optical emission spectroscopy (ICP-OES), X-ray powder diffraction (XRD), field emission scanning electron microscopy (FESEM), thermogravimetric and differential thermal analysis (TG/DTA), Brunauer-Emmett-Teller (BET) analysis and acid neutralization. The obtained results shed a light on the influence of different base environments and calcination conditions on the properties of MgO and highlight potential application areas that can benefit from the end product.

The production of MgO via the calcination of $Mg(OH)_2$ suffers from the high energy consumption and low efficiency due to the bad filtration behaviour of $Mg(OH)_2$. $Mg(OH)_2$ is

spongy in the water so after filtration solids still contain high amount of water. While once $Mg(OH)_2$ going though carbonation to hydrated magnesium carbonates, the filtration behaviour of solids will be greatly improved. Although numerous researchers have conducted mineral trapping of CO_2 into saline aquafers (Soong, Goodman et al. 2004, Soong, Fauth et al. 2006, Ferrini, De Vito et al. 2009, Ballirano, De Vito et al. 2010, Mignardi, De Vito et al. 2011, Ballirano, De Vito et al. 2013), limited research has been reported to study the sequestration of CO_2 and explore the efficiency of carbon storage into $Mg(OH)_2$ slurries generated from reject brine. Furthermore, a clear relationship between the efficiency of carbon storage and the phase of HMCs must be understood. In this study, we proposed to synthesize HMCs from the highly reactive $Mg(OH)_2$ slurry generated from reject brine through the sequestration of CO_2.

The production of MgO via the calcination of $Mg(OH)_2$ usually cannot achieve ultra-high purity. Due to the presence of Ca^{2+} and HCO_3^- in the reject brine, $CaCO_3$ would co-precipitate along with $Mg(OH)_2$ with the addition of bases, which would contaminate the final MgO products and lower the economic value in the market. Therefore, this study presented a new method to recover Ca^{2+} and Mg^{2+} separately from reject brine via the use of oxalic acid ($H_2C_2O_4 \bullet 2H_2O$). The obtained $MgC_2O_4 \bullet 2H_2O$ with high purity and yield under the optimized condition was therefore calcined to produce MgO. A comprehensive characterization of MgO, i.e. microstructure and SSA, was presented and a correlation between the calcination conditions (i.e. temperature and duration) and the properties of MgO was established.

The final part focuses on the evaluation of the environmental impacts of the production of reactive MgO from reject brine via above proposed routes. There is a significant potential for the optimization of the overall process that will inevitably lead to the reduced energy requirement and CO_2 emission. Part of the success regarding the production of reactive MgO from waste streams (e.g. reject brine) is dependent on the overall environmental impacts of this process and its comparison to traditional cement production in terms of its CO_2 emission and energy requirement. This final part aims to eliminate these concerns by evaluating the energy consumption and CO_2 emission of the production of reactive MgO from reject brine via different routes and to put forward pertinent proposals concerning their sustainable development in the future, which can serve as an excellent resource for various applications ranging from food,

cosmetics, pharmaceutical and the construction industries (Lee, Jung et al. 2004, Shand 2006, Moussavi and Mahmoudi 2009, Pilarska, Klapiszewski et al. 2017).

Chapter 3 Synthesis of reactive MgO from reject brine via the addition of NH_4OH

3.1. Introduction

Magnesium oxide (MgO) is produced in different grades and used in several applications ranging from the pharmaceutical to the refractory industries due to its superior stability and chemical resistance. A majority of MgO is produced via the calcination of magnesite ($MgCO_3$) through the dry route. The properties of the resulting MgO strongly depend on the calcination conditions. Higher calcination temperatures and longer residence times lead to increases in the size of the MgO grain, which results in the decrease of its specific surface area (SSA) and reactivity (Shand 2006, Mo, Deng et al. 2010). Most of the commercially available MgO can be classified into four grades, depending on the conditions used during its production, i.e. calcination temperature and residence time. Fused MgO is produced above the fusion temperature of MgO (2800 ℃) and has the lowest SSA and reactivity, which is excellent in chemical stability and moisture resistance (Wang, Wang et al. 2012). Dead-burned MgO is obtained at calcination temperatures above 1400 ℃ and has a very low SSA and reactivity. It is widely used in the refractory industry as a fire-resistant and thermal insulation material. Hard-burned MgO is produced at 1000-1400 ℃ with a low SSA and limited reactivity. It is mostly used as an expansive additive in concrete for shrinkage compensation (Gao, Lu et al. 2008, Mo, Deng et al. 2014). Light-burned (reactive or caustic-calcined) MgO is produced at much lower temperatures ranging between 700 and 1000 ℃ and therefore retains a high SSA and reactivity. Because of its high reactivity, the light-burned MgO has been used in various applications as a fertilisers, catalyst, chemical absorbent and filtration medium (Kramer , Lee, Jung et al. 2004, Shand 2006, Caraballo, Rotting et al. 2009). Recent studies have shown that reactive MgO can also be used as a cement binder by itself or along with Portland cement (PC) and other supplementary cementitious materials, depending on the application (Liska, Al-Tabbaa et al. 2012a, Liska, Al-Tabbaa et al. 2012b, Al-Tabbaa 2013, Unluer and Al-Tabbaa 2013, Unluer and Al-Tabbaa 2014). The main advantages of reactive MgO cements over traditional PC are listed as its significantly lower calcination temperatures (700-1000 vs. 1450 ℃), ability to absorb carbon dioxide (CO_2) in the form of stable carbonates while gaining strength, and complete recyclability at the end of its lifetime.

Unlike limestone which is abundant and available worldwide, large magnesite deposits are mainly located in China and North Korea (Shand 2006). According to (RAM 2015), around 8.5 million tonnes of MgO is produced from magnesite annually, for which China is the leading provider with a 49% market share. Lack of magnesite availability on a global level highlights the need to identify alternative sources for the production of MgO, which also suffers from low purity and reactivity due to the impurities present in the parent materials. Today, a significant portion of global MgO supply is via the calcination of magnesium hydroxide $Mg(OH)_2$ generated from magnesium-rich sources such as seawater or natural brine, which contributes to about 14% of the global MgO production (Kramer). This process involves the extraction of seawater/brine, pre-treatment and final processing steps. Seawater intake structures are mostly utilized in large seawater desalination plants which mainly extract seawater from open sea (Pankratz 2004). Seawater/brine pre-treatment often employs a pH adjuster to de-carbonate the solution at hand. This involves the addition of sulphuric acid to decrease the pH of the solution to 4. Seawater is then passed through a desorption tower where it is aerated to remove CO_2 in case of the precipitation of $CaCO_3$ along with $Mg(OH)_2$ (Shand 2006). After the seawater/brine is softened, it is then pumped into an agitated reactor vessel, during which a strong base is added into the solution to raise the pH to 10.5, enabling the precipitation of magnesium (Shand 2006). Generally, calcium hydroxide ($Ca(OH)_2$) derived from calcined lime (CaO) or dolime (CaO·MgO) is deployed in practice. Friedrich et al. (1946) patented a simple process to precipitate MgO in the form of $Mg(OH)_2$ from seawater at a pH of 10.5 using a lime solution (Friedrich, Robinson et al. 1946). Dolime is preferred due to its self-contained MgO content, enabling the use of only half of the usually required volume of seawater or brine while the other half is derived from dolime to produce the same amount of MgO as would be if lime was used (Al-Zahrani and Abdel-Majeed 2007).

The precipitation of Mg^{2+} can be performed via the addition of a range of alkali sources other than lime (Turek and Gnot 1995, Dave and Ghosh 2005, El-Naas 2011, Tran, Van Luong et al. 2013, Khuyen Thi, Han et al. 2016). Hydrated lime (Ca(OH)2·2H2O) can also be used to precipitate Mg(OH)2 from seawater at a pH ranging between 7 and 7.5 (Dave and Ghosh 2005).

However the introduction of calcium-based alkalis results in the formation of gypsum ($CaSO_4 \cdot 2H_2O$) along with other precipitates due to the presence of sulphate in seawater, which necessitates the pre-treatment of seawater by adding $CaCl_2$ for desulfation. Another additive utilized for the precipitation of $Mg(OH)_2$ from natural mine brine is sodium hydroxide (NaOH). Turek and Gnot (1995) explored the effect of reaction temperature on the sedimentation of the precipitants via the addition of NaOH into mine brineand reported the improved precipitation when reaction temperature decreased from 40 to 10 ℃. The improved sedimentation was attributed to the high viscosity of NaOH solution and brine, which impeded the contact between the precipitating agent and mine brine and lowered the diffusion rate, thereby improving the crystal structure of $Mg(OH)_2$ (Turek and Gnot 1995). Ammonia solution (NH_4OH) has also been reported to precipitate $Mg(OH)_2$ from seawater/brine. The use of NH_4OH buffers the solution at a basic pH of around 10, which favours the precipitation of $Mg(OH)_2$. Unlike other alkalis such as lime or dolime, NH_4OH does not introduce additional cations which result in undesirable precipitates (e.g. $CaCO_3$), as impurities. Furthermore, NH_4OH can be recycled at the end of the reaction, which allows the design of a closed-system as suggested in the modified Solvay process and thereby eliminates the generation of waste (El-Naas 2011).

The precipitation of Mg^{2+} from synthetic solutions has also been performed by several studies (Alvarado, Torres-Martinez et al. 2000, Henrist, Mathieu et al. 2003, Yan, Xue et al. 2005). Henrist et al. (2003) studied the influence of the chemical nature of the utilized bases (NaOH and NH_4OH), type of counter-ions and temperature on the morphological characteristics of $Mg(OH)_2$ precipitated from a synthetic $MgCl_2$ solution. It was observed that the use of NaOH as the alkali source led to the formation of $Mg(OH)_2$ with a globular cauliflower-like morphology, which consisted of small particles with dispersed agglomerates; while the use of NH_4OH as the alkali source resulted in a plate-like $Mg(OH)_2$ morphology. Single and circular plate-like particles were observed at lower temperatures while particles had a tendency to inter-grow at 60 ℃ (Henrist, Mathieu et al. 2003). Yan et al. (2005) reported the synthesis of $Mg(OH)_2$ nano-flowers by a simple hydrothermal reaction of $MgCl_2$ and $CO(NH_2)_2$ without any additives. The pH of the magnesium chloride solution was first adjusted at a range of 3.0-9.5 via the addition of HCl or NH_4OH. The solution was then sealed in an autoclave at 95-130 ℃ for 18 hours before collecting the samples. It was found that the pH value and temperature during the initial reaction

was essential in controlling the morphology of particles. The initially irregular spherical particles developed a nano-flower morphology with increasing pH and temperature. This was attributed to the stacking of excessive Mg^{2+} and OH^- on the existing plate-like crystal seeds and therefore self-assembling into a flower like structure at high pH values (Yan, Xue et al. 2005).

Calcination of the resulting $Mg(OH)_2$ synthesized from seawater/brine or synthetic solutions produces MgO (Friedrich, Robinson et al. 1946, Shand 2006). A number of studies have investigated the properties of MgO calcined from $Mg(OH)_2$ (Eubank 1951, Itatani, Koizumi et al. 1988, Choudhary, Rane et al. 1994, Alvarado, Torres-Martinez et al. 2000, Bartley, Xu et al. 2012). Eubank (1951) identified that the reaction temperature and presence of impurities significantly influence the properties of MgO. The calcination of magnesium compounds was reported to take place in two distinct stages starting with the loss of water and CO_2 gases between 300 and 500 ℃, which creates a porous structure. Recrystallization or sintering takes place at higher temperatures (> 900 ℃), densifying the final material, whose porosity decreases during this process. The particle sizes of calcined MgO increase with increasing calcination temperature, resulting in the decrease of surface area and adsorptive capacity (Eubank 1951). The impurities contained in MgO can enhance the sintering process through the formation of vitreous phases. Alvarado et al. (2000) characterised MgO prepared from three precursor magnesium salts and dolomite (Alvarado, Torres-Martinez et al. 2000). The SSA of calcined MgO from different magnesium compounds precursors were found in the decreasing order: magnesium sulfate > magnesium nitrate > magnesium acetate > dolomite. On the contrary, the particle size, degree of agglomeration and porosity displayed the inverse sequence.

The main difference between MgO obtained from the calcination of magnesite and synthetically from seawater/brine or any relevant solutions is the higher purity and reactivity of the latter (Jin and Al-Tabbaa 2014). The main drawback of the production of MgO from seawater/brine is its higher energy consumption when compared to the dry route (17 vs. 5.9 GJ per tonne of MgO (Hassan 2013)). However, this can be optimized as further studies are performed on the reduction of the energy demands of MgO production from waste brine. This is particularly critical for coastal regions with a limited amount of fresh water resources such as Singapore,

where desalination is considered as a feasible approach to meet residential and industrial water demands. Desalination involves the removal of salts from saline water to produce fresh water. Currently the desalinated water from two current running seawater reverse-osmosis plants provides 100 million gallons water a day, which meets up to 25% of Singapore's current water demand (PUB 2015). According to the International Desalination Association, the global daily production of desalinated water generated by 18,426 desalination plants worldwide exceeds 86.8 million cubic meters (IDA 2015). It is estimated that an equivalent amount is generated as reject brine per m^3 of desalinated water (El-Naas 2011).

Reject brine, which is of particular interest in this study, is a concentrated by-product with a high salt concentration obtained from treating brackish water or seawater in desalination plants (Adham, Hussain et al. 2013). The most common way to dispose reject brine is through its discharge back to the sea. However, reject brine is denser than the feedstock supply due to its high salt concentration and salinity and therefore tends to accumulate at the bottom of the sea when discharged through an outfall without sufficient mixing. Discharge of untreated reject brine has an adverse effect on the ecosystem as it alters the flora and fauna through increased salinity and directly or indirectly damages all living organisms within that particular ecosystem (Mohamed, Maraqa et al. 2005). A newly proposed alternative is the re-treatment of the salt within the reject brine to obtain valuable materials such as Mg^{2+}, which can serve as an excellent source for the recovery of MgO. Therefore, reject brine can be converted into valuable and useful solids, which provides a feasible and environmental friendly use of this waste material (El-Naas 2011).

Although there are many studies on the reaction of synthetic $MgCl_2$ solution, seawater or natural brine with different alkali sources (Turek and Gnot 1995, Henrist, Mathieu et al. 2003, Dave and Ghosh 2005, Yan, Xue et al. 2005), limited research has been reported on the recovery of valuable metals from actual reject brine obtained from desalination plant (Ahmed, Arakel et al. 2003). This chapter reports the feasibility of synthesizing reactive MgO from reject brine collected from a local desalination plant in Singapore. A comprehensive study on the reaction

kinetics and the physical and chemical properties of the resulting $Mg(OH)_2$ and MgO was performed via XRD, FESEM, TG/DTA and BET analyses.

3.2. Materials and Methodology

3.2.1. Materials

In this study, NH_4OH solution with analytical grade (25.0% NH_3 content) supplied by Sigma-Aldrich (Singapore) was used as the alkali source to react with reject brine. The reject brine was collected from the Tuaspring desalination plant in Singapore, the largest desalination plant in South East Asia with a capacity of 318,500 m^3 desalinated water per day. During the desalination process, ultra-filtration membrane technology is used to remove the suspended solids and microorganisms in the seawater intake during the pre-treatment process, which is followed by a two-stage seawater reverse osmosis process. Saline feed water (seawater) is passed through semi-permeable membranes to produce a low-salinity water and a very saline concentrate (reject brine) as a by-product, which would normally be disposed back to the sea through an outfall pipe (Hyflux 2011).

Unlike seawater or natural brine, reject brine contains suspended solids through the chemicals added to precipitate the colloidal particles in the seawater before running through ultra-filtration in the desalination process. After the collection of reject brine from the plant, it was filtrated through a 45 μm membrane filter to remove suspended solids before further analysis. The chemical composition of the filtrated reject brine, determined via Inductively Coupled Plasma-Optical Emission Spectroscopy (ICP-OES), is summarized in Table 3.1. Along with a Mg^{2+} concentration of 1679 ppm, the presence of other ions (e.g. Na^+, K^+ and Ca^{2+}) was observed.

Table 3.1 Chemical composition of the reject brine used in this study

Element/ Concentration	Cl	Na	SO_4	Mg	K	Ca	Sr	B	Si	Li	P	Al
ppm	65593.1 ± 66.3	16124.3 ± 55.8	4322 ± 8.8	1679.0 ± 5.5	808.5 ± 5.4	563.6 ± 1.1	5.3 ±0 .1	4.5 ±0 .1	0. 5	0. 4	0. 2	0. 1

3.2.2. Methodology

A pre-determined amount of NH_4OH (2.12-19.08 ml) was introduced into 200 ml of reject brine as the alkaline source to investigate the influence of NH_4OH dosage on the reaction kinetics with reject brine and the chemical and physical properties of the resulting $Mg(OH)_2$ precipitates. According to stoichiometry, the reaction of 2 moles of OH^- with 1 mole of Mg^{2+} leads to the precipitation of 1 mole of $Mg(OH)_2$. However, a higher dosage of NH_4OH (up to 19.08 ml) had to be utilized due to its relatively weak nature ($K_b=1.8\times10^{-5}$) as a base.

Reject brine and NH_4OH solution were mixed with a magnetic stirrer at a constant stirring speed (300 rpm) and room temperature (25 ℃), during which a pH/thermometer probe was inserted into the beaker to monitor the temperature and pH of the reaction. The pH and temperature of the reaction were monitored by using a pH/thermometer (Mettler Toledo pH/Ion meter S220), which was calibrated before each experiment with a standard solution set at a pH of 4, 7 and 10.21, to reveal the kinetics of the chemical reactions between reject brine and NH_4OH. The experiment was terminated after 6 hours of reaction when the pH of the solution stabilized. The solids were then separated from the liquid phase through a centrifuge. Precipitates were collected and washed by ultrapure water for three times. The resulting precipitates (expected to consist mainly of magnesium hydroxide) were oven-dried at 105 ℃ until they reached a constant mass. They were then ground into powder form passing through a 125 μm sieve, after which their chemical and physical properties were determined. The remaining precipitates were calcined at a pre-determined temperature of 500 ℃ for 2 hours in the furnace to produce reactive MgO, which was then characterized for its chemical and physical properties.

Mg^{2+} and Ca^{2+} ion concentrations present in the solution after the completion of the reaction were monitored by means of an ICP-OES (PerkinElmer Optima DV2000) to determine the percentage of sequestrated ions. This provided insights on the yield of $Mg(OH)_2$ and $CaCO_3$ obtained at different levels of NH_4OH addition. The solution was diluted 10 times and filtrated through a 45 μm membrane filter to remove suspended solids. 1 ml of the reject brine/ NH_4OH solution (after the reaction) was then taken using a pipette and added to a 10 ml acidized solution

(70% nitric acid) to fully terminate the reaction. Primary Na^{+}, Mg^{2+} and Ca^{2+} solutions with concentrations of 100 ppm were used for calibration before each of the ICP-OES measurements.

Several techniques including X-ray powder diffraction (XRD), field emission scanning electron microscopy (FESEM), thermogravimetric and differential thermal analysis (TG/DTA) and Brunauer-Emmett-Teller (BET) analyses were utilized to characterize the synthesized $Mg(OH)_2$ and reactive MgO. In preparation for these analyses, all samples were vacuum dried to constant mass, followed by grinding and sieving to achieve a particle size smaller than 125 μm. XRD was performed via a Bruker D8 Advance with a Cu Kα source under the operation conditions of 40 Kv and 40 mA, emitting radiation with a wavelength of 1.5405 Å, scan rate of 0.02 °/step, and a 2θ range of 5 to 70°. The morphology and microstructure of the synthesized samples were studied by imaging powder surface using a JSM-7600F thermal FESEM. Quantitative analysis of the phases in the synthesized samples was performed via TG/DTA using a PyrisDiamond TGA 4000 operated at a heating rate of 10 ℃/min under air flow. The SSA of the synthesized samples was analysed through the BET analysis from nitrogen adsorption-desorption isotherms using a Quadrasorb Evo automated surface area and pore size analyser.

3.3. Results and Discussion

3.3.1. Reaction kinetics

Figure 3.1 shows the change in pH over time during the reaction between reject brine and NH_4OH. The rate of change of pH recorded at regular intervals revealed the kinetics of the reaction under different amounts of NH_4OH. The general trend shows a steady pH after the addition of NH_4OH, followed by a gradual decrease that stabilized at a constant level when the reaction reached equilibrium when pH of the solution was stabilized without variation. Both the initial and final pH values increased with the increase of NH_4OH dosage as more OH^- was available, which increased the reaction rate and shortened the reaction time. This enabled the time needed to achieve equilibrium to reduce significantly from 160 to 25 minutes as the amount of NH_4OH increased from 2.12 to 19.08 ml, as shown in Figure 3.2.

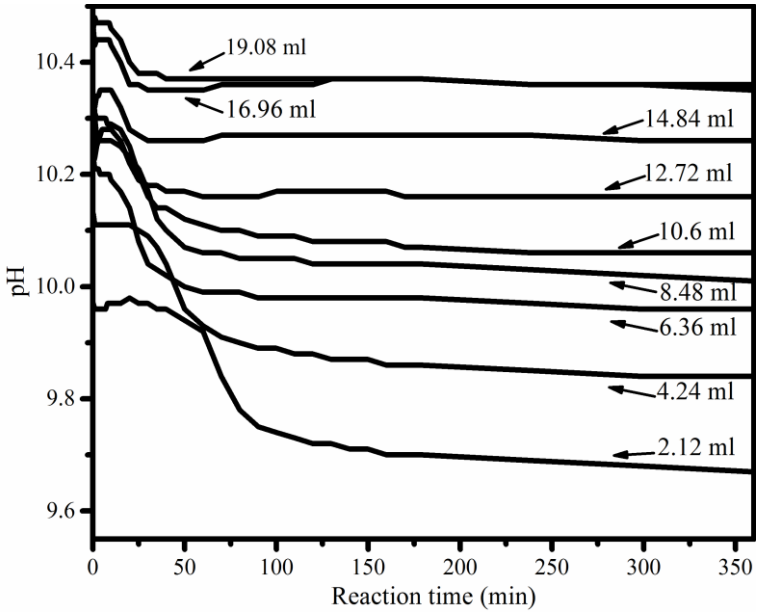

Figure 3.1 pH of the reaction of reject brine with different amounts of NH_4OH

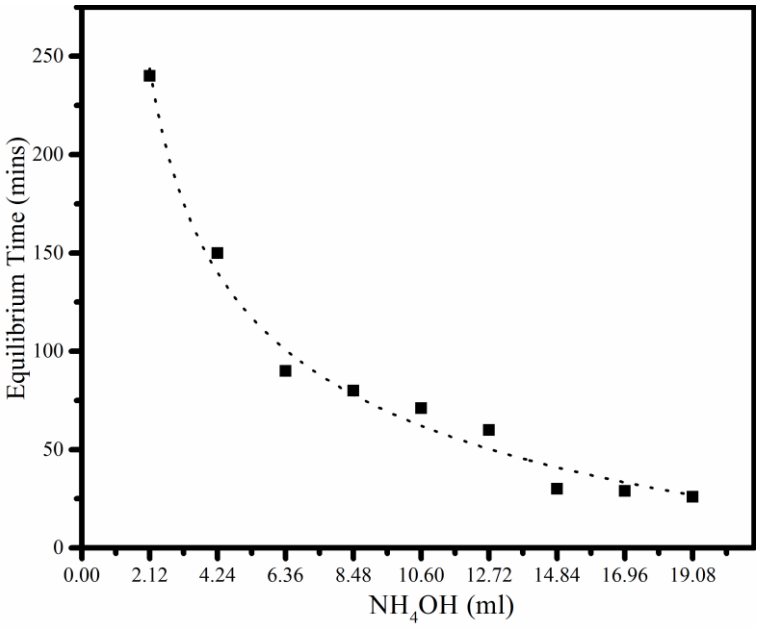

Figure 3.2 Equilibrium time as a function of NH_4OH dosage

3.3.2. Recovery of Mg^{2+} and Ca^{2+} from reject brine

The formation of $Mg(OH)_2$ was observed via the reaction between the Mg^{2+} in the reject brine and OH^- provided by NH_4OH. The addition of NH_4OH also favoured the conversion of HCO_3^-

which was present in the reject brine to CO_3^{2-}. This led to a reaction of CO_3^{2-} with Ca^{2+} and resulted in the precipitation of $CaCO_3$. The reaction paths observed during this process are shown in Equations 3-1 to 3-4 (Shand 2006).

$$NH_4OH_{(aq)} \leftrightarrow NH_4^+ + OH^- \quad (3\text{-}1)$$

$$Mg^{2+} + 2OH^- \rightarrow Mg(OH)_2 \quad (3\text{-}2)$$

$$NH_4OH_{(aq)} + HCO_3^- \leftrightarrow CO_3^{2-} + NH_4^+ + H_2O \quad (3\text{-}3)$$

$$Ca^{2+} + CO_3^{2-} \rightarrow CaCO_3 \quad (3\text{-}4)$$

Figure 3.3 shows the percentage of Mg^{2+} and Ca^{2+} recovered from reject brine through the addition of different molar amount of NH_4OH, which was calculated by measuring the ion concentration in the reject brine both before and after the reaction. The amount of Mg^{2+} and Ca^{2+} precipitated from the reject brine increased with the amount of NH_4OH addition. The ion product ($[Mg^{2+}][OH^-]^2$) was calculated to be 7×10^{-10} $mol^3\ l^{-3}$ at pH 10, which was larger than the solubility product constant of $Mg(OH)_2$ (1.8×10^{-11} $mol^3\ l^{-3}$) (Sillén, Martell et al. 1964). This formed a supersaturation for $Mg(OH)_2$ and enabled the reaction between OH^- with Mg^{2+} to form $Mg(OH)_2$. The CO_3^{2-}/HCO_3^- ratio in the solution determines the amount of carbonates formed and the equilibrium pH equals to 10.3. Since when a lower amount of NH_4OH (< 6.36 ml) was used, the pH of the solution was lower than 10.3 as shown in Figure 3.1, limiting the formation of CO_3^{2-} in the solution. Therefore, a higher content of Mg^{2+} than Ca^{2+} was precipitated when a lower amount of NH_4OH (< 6.36 ml) was used. As the amount of NH_4OH increased beyond 6.36 ml, the increased amount of OH^- in the solution achieved a sufficient level to react with both Mg^{2+}, CO_3^{2-} and Ca^{2+}, thereby increasing the amount of $CaCO_3$ in the precipitates. As the amount of NH_4OH exceeded 16.96 ml, the percentage of Mg^{2+} and Ca^{2+} recovered reached a plateau due to the equilibrium reached in the supernatant liquid.

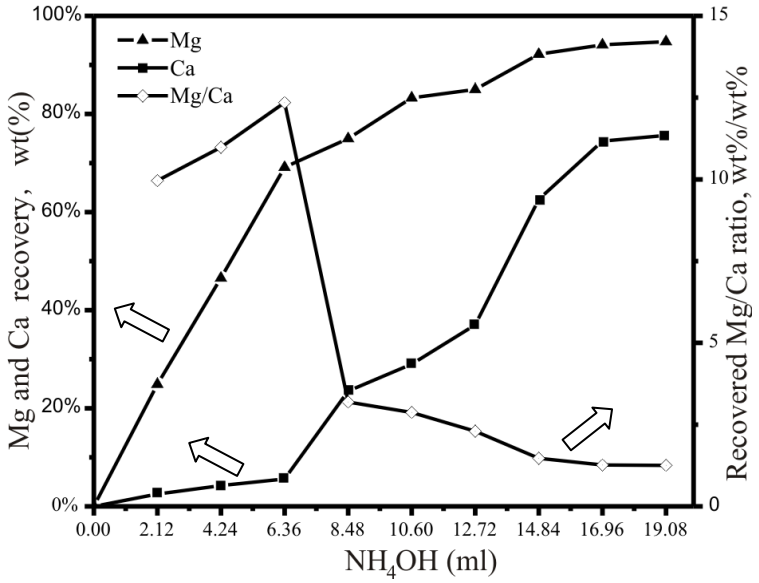

Figure 3.3 Percentage of Mg^{2+} and Ca^{2+} sequestrated from reject brine as a function of NH_4OH dosage

The Mg^{2+}/Ca^{2+} ratio was also used as an indicator of the purity level of the resulting $Mg(OH)_2$ precipitates. As seen in Figure 3.3, Mg^{2+}/Ca^{2+} peaked at about 12.5 when 6.36 ml of NH_4OH was added into the reject brine. This was because the initial pH was lower than 10.3, the formation of carbonates was prevented, therefore reducing the supersaturation for $CaCO_3$ and contributing to a lower precipitation of $CaCO_3$ in the solution. Therefore, a NH_4OH to Mg^{2+} ratio of 6 was determined as the most optimum ratio out of the different values used in this study for the precipitation of $Mg(OH)_2$, which was further calcined to produce reactive MgO with a high purity.

3.3.3. Characterization of the synthesized $Mg(OH)_2$

3.3.3.1. XRD

Figure 3.4 shows the XRD diffractograms of synthesized $Mg(OH)_2$ obtained from the reaction between reject brine and different amounts of NH_4OH. The crystalline peaks observed were mainly attributed to $Mg(OH)_2$ along with smaller amounts of $CaCO_3$, which was present in the crystal form of aragonite. The presence of Mg^{2+} in the reject brine inhibited the precipitation of calcite and favoured the formation of aragonite, which was in line with the findings of earlier

studies (Berner 1975). As shown in Figure 3.4, the relative intensity of the peaks corresponding to $Mg(OH)_2$ and $CaCO_3$ varied as the amount of NH_4OH increased, which reflected the changes in the crystallinity and chemical composition of the precipitants. The relative intensity of the peaks corresponding to $CaCO_3$ increased along with the increasing amount of NH_4OH, which indicated the increased content percentage of $CaCO_3$ in the precipitants.

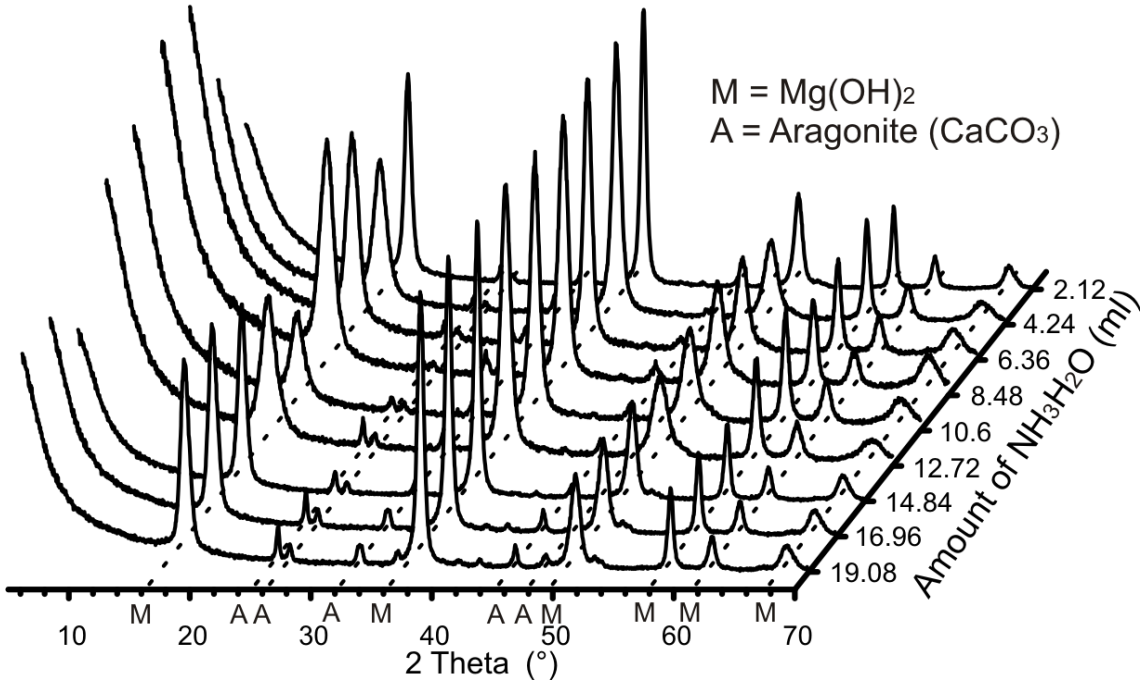

Figure 3.4 XRD diffractograms of $Mg(OH)_2$ obtained from the reaction of 200 ml reject brine with different amounts of NH_4OH

3.3.3.2. FESEM

The morphologies of the synthesized $Mg(OH)_2$ obtained with the addition of different amounts of NH_4OH are shown in Figure 3.5. A flake-like morphology with an average agglomerate size of 10-15 μm was observed in all cases, similar to the findings reported earlier in literature (Alvarado, Torres-Martinez et al. 2000, Behij, Hammi et al. 2013, Guo, Pei et al. 2015). As shown in the Figure 3.5, the amount of NH_4OH did not have a significant influence on the morphology of $Mg(OH)_2$ synthesized from reject brine.

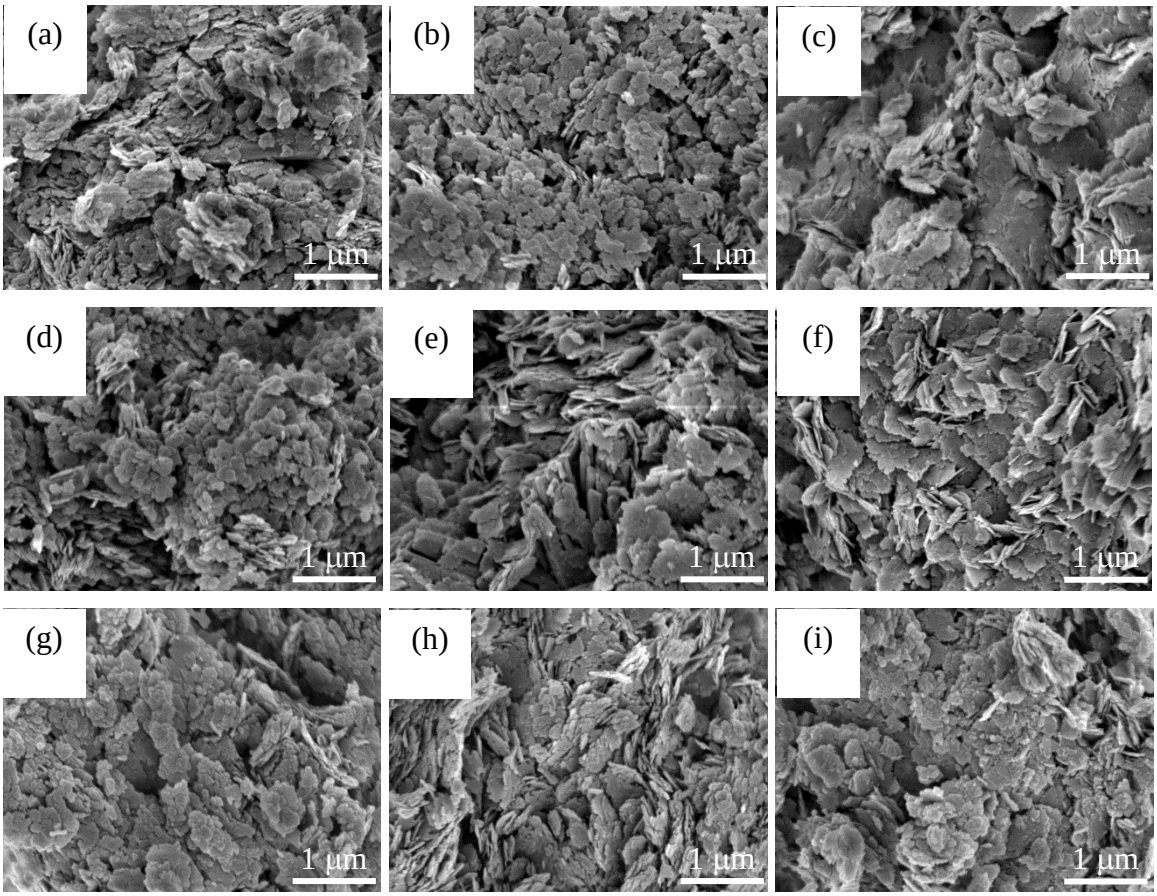

Figure 3.5 FESEM images of $Mg(OH)_2$ obtained from the reaction of 200 ml reject brine with (a) 2.12, (b) 4.24, (c) 6.36, (d) 8.48, (e) 10.6, (f) 12.72, (g) 14.84, (h) 16.96 and (i) 19.08 ml of NH_4OH as collected by filtration through a 45 μm membrane followed by vacuum drying and grinding to pass a 125 μm sieve

3.3.3.3. TG/DTA

Figure 3.6 illustrates a typical TG/DTA graph of the synthesized $Mg(OH)_2$ obtained by adding 6.36 ml of NH_4OH to react with the reject brine. The dehydration of $Mg(OH)_2$ takes place between 340 and 440 ℃ and resulted in a weight loss of around 25.5% due to the loss of H_2O from the system. The second reaction, attributed to the decarbonation of $CaCO_3$, which led to the release of CO_2, was observed between 650 and 750 ℃, resulting in a weight loss of 2.5%.

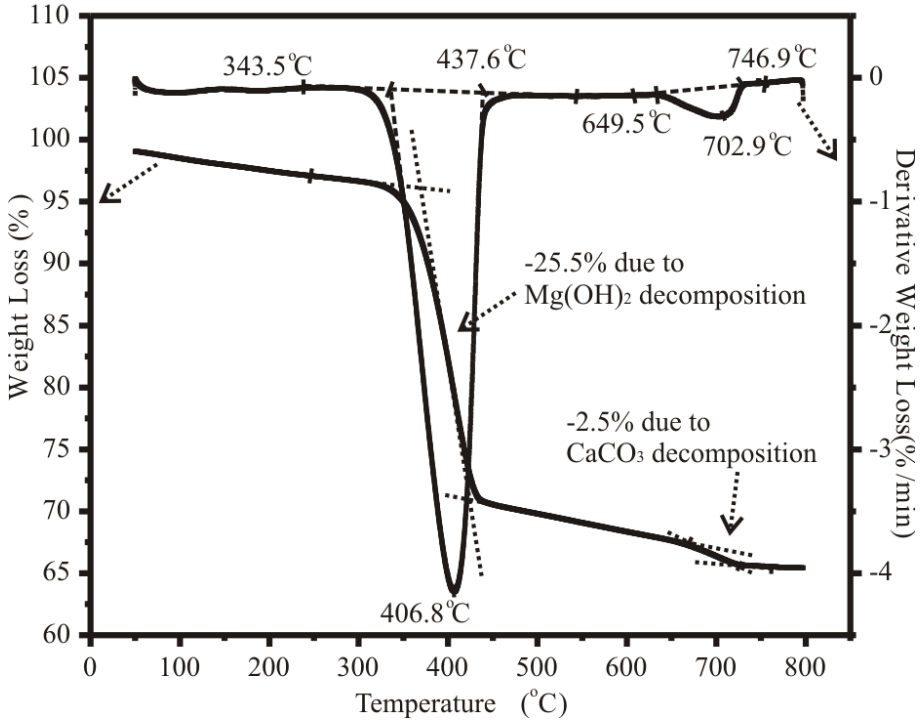

Figure 3.6 Typical TG/DTA curve of $Mg(OH)_2$ obtained from the reaction of 200 ml reject brine with 6.36 ml of NH_4OH

Table 3.2 summarizes the peak temperatures observed during the thermal decomposition of $Mg(OH)_2$ and corresponding weight losses at each reaction. The weight loss due to the dehydration of $Mg(OH)_2$ (i.e. between 340 and 440 ℃) showed a decreasing trend, while the weight loss due to the decarbonation of $CaCO_3$ (i.e. between 650 and 750 ℃) increased with the amount of NH_4OH. The peak temperature at which $CaCO_3$ decomposed into CaO and CO_2 increased significantly from 655.4 to 747.2 ℃ with the increase in the amount of NH_4OH. This could be attributed to the poorly crystalline structure of $CaCO_3$ that formed when lower amounts of NH_4OH were reacted with the reject brine (Johnson 2002). This was consistent with the XRD patterns shown earlier in Figure 3.4, where sharper and narrower $CaCO_3$ peaks were detected under higher NH_4OH dosages.

Table 3.2 TG/DTA results of $Mg(OH)_2$ obtained from the reaction of 200 ml reject brine with different amounts of NH_4OH

NH_4OH (ml)	1st peak temperature (℃)	Weight loss between 340-440 ℃ (%)	2nd peak temperature (℃)	Weight loss between 650-750 ℃ (%)
2.24	391.3	24.9	655.4	0.7
4.24	393.4	24.2	691.0	1.3
6.36	406.8	25.5	702.9	2.5
8.48	393.4	25.1	691.0	1.5
10.6	407.3	25.3	706.9	2.2
12.72	408.9	24.5	706.9	2.9
14.84	409.8	23.8	738.1	4.0
16.96	403.8	23.0	725.4	4.9
19.08	405.8	20.0	747.2	9.2

Table 3.3 lists the compositions of the synthesized $Mg(OH)_2$, which were calculated according to the TG/DTA results listed in Table 3.2 as well as the ICP-OES results shown in Figure 3.3. Both measurements revealed similar trends, which indicated a decrease in the amount of $Mg(OH)_2$ accompanied with an increase in the amount of $CaCO_3$ as the amount of NH_4OH increased. According to the result of TGA, the synthesized $Mg(OH)_2$ achieved up to 98% in purity when 2.24 ml of NH_4OH was added into the reject brine. While ICP-OES test indicated the highest purity of $Mg(OH)_2$ of 97.3% was achieved when 6.36 ml of NH_4OH was added. However, low dosages of NH_4OH cannot achieve the supersaturation for the formation of $Mg(OH)_2$, leading to a lower yield of precipitates. As such, a NH_4OH to Mg^{2+} ratio of 6 at a NH_4OH content of 6.36 ml, which led to a Mg^{2+} yield of 70% (Figure 3.3) and a $Mg(OH)_2$ with a purity of 93.5% (Table

3.3), was chosen for the large scale production of $Mg(OH)_2$, which was then calcined to produce reactive MgO.

Table 3.3 Chemical composition of the synthesized $Mg(OH)_2$ based on TG/DTA and ICP-OES results

NH_4OH (ml)	TG/DTA		ICP-OES	
	$Mg(OH)_2$ (%)	$CaCO_3$ (%)	$Mg(OH)_2$ (%)	$CaCO_3$ (%)
2.24	98.0	2.0	96.6	3.4
4.24	96.4	3.6	96.9	3.1
6.36	93.5	6.5	97.3	2.7
8.48	95.9	4.1	90.2	9.8
10.6	94.2	5.8	89.2	10.8
12.72	92.4	7.6	86.9	13.1
14.84	89.5	10.5	80.9	19.1
16.96	87.0	13.0	78.4	21.6
19.08	75.6	24.4	78.3	21.7

3.3.4. Characterization of the synthesized reactive MgO

3.3.4.1. XRD

The $Mg(OH)_2$ obtained at a NH_4OH to Mg^{2+} ratio of 6 was calcined at 500 ℃ for 2 hours in a furnace for the production of reactive MgO, whose XRD patterns are shown in Figure 3.7. The main peak positions of the synthesized reactive MgO matched well with the reference peaks of

MgO (JCPDS # 89-7746) with few minor peaks attributed to the presence of calcite, which may have formed from the transformation of aragonite at higher temperatures (Kontoyannis and Vagenas 2000). The lack of $Mg(OH)_2$ peaks was an indication that all the initially used brucite fully decomposed at the calcination conditions used (i.e. 500 ℃ for 2 hours), resulting in the formation of reactive MgO.

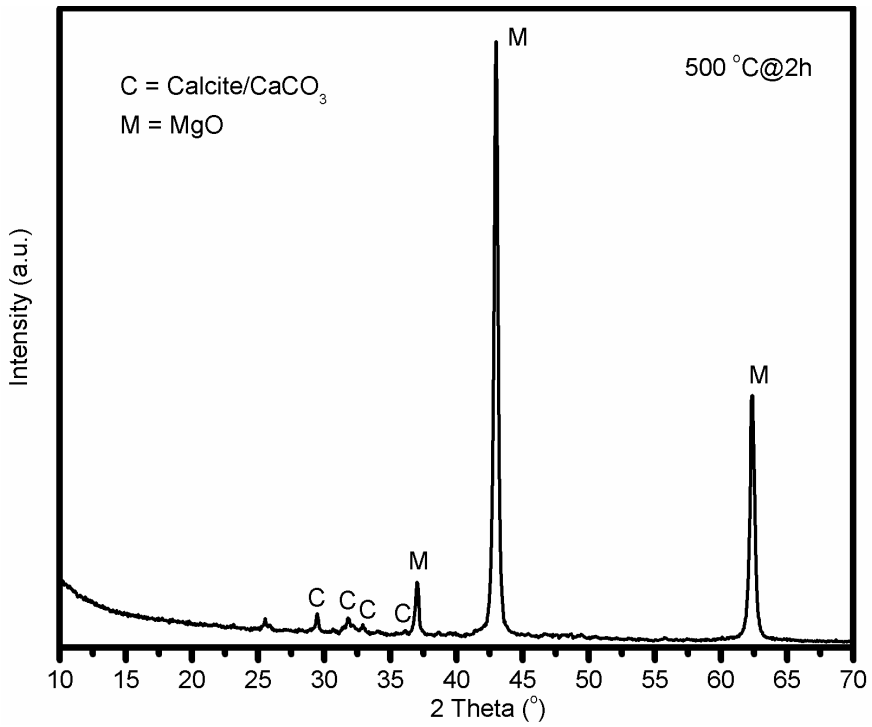

Figure 3.7 XRD diffractograms of the produced reactive MgO

3.3.4.2. FESEM

Figs. 8(a) and (b) illustrate the morphology of the reactive MgO produced from the calcination of $Mg(OH)_2$ at 500 ℃. A plate-like morphology, which was inherited from the parent material brucite as was shown in Figure 3.5, was observed throughout the microstructure of MgO. Different from the closely packed structure of brucite, MgO demonstrated a more porous structure due to the loss of water molecules during the decomposition of brucite into MgO. This finding was in agreement with previous studies (Alvarado, Torres-Martinez et al. 2000, Mo, Deng et al. 2010), in which the porous plate-like morphology of MgO calcined from magnesite

was reported. The main difference between the morphology shown in Figure 3.8 and those reported in relevant literature was the much smaller particle size of the MgO grains in the former due to the low calcination temperature (500 ℃) utilized in its production.

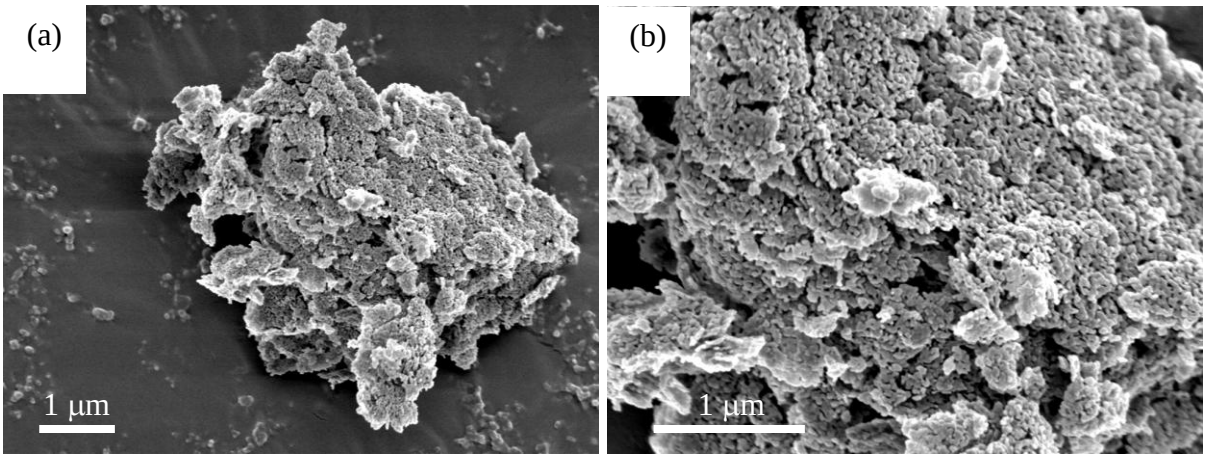

Figure 3.8 FESEM images of the reactive MgO produced at 500 ℃ at different magnifications of (a) x14,000 and (b) x30,000

3.3.4.3. BET

Figure 3.9 presents a comparison between the SSA values of the reactive MgO obtained from reject brine in this study and 12 different commercial MgO samples presented in an earlier study (Jin and Al-Tabbaa 2014). The synthesized reactive MgO, referred to as "SRM", achieved a SSA of 78.8 m^2/g, which was higher than the SSA of most of the MgO samples obtained via the dry route (i.e. through the calcination of magnesite). Alternatively, the SRM revealed a lower SSA when compared to the MgO samples obtained via synthetic routes. This could be attributed to the higher impurity level of SRM (90.8%) compared to the commercial synthetic MgO samples (e.g. DSP (99.2%) and N50 (97.7%)). The presence of the main impurity $CaCO_3$, who also possessed a low SSA, have also contributed to the generally lower reactivity of SRM amongst the synthetically produced MgO samples.

Regardless of the different SSA comparisons, the SRM obtained in this study can be classified under "category I" referring to highly reactive MgO with an SSA of over 60 m^2/g according to

the classification of reactive MgO proposed by (Jin and Al-Tabbaa 2014). Furthermore, it must be kept in mind that the SSA and therefore the reactivity of the MgO synthesized from the reject brine as presented in this study can be further increased with an optimization of production conditions.

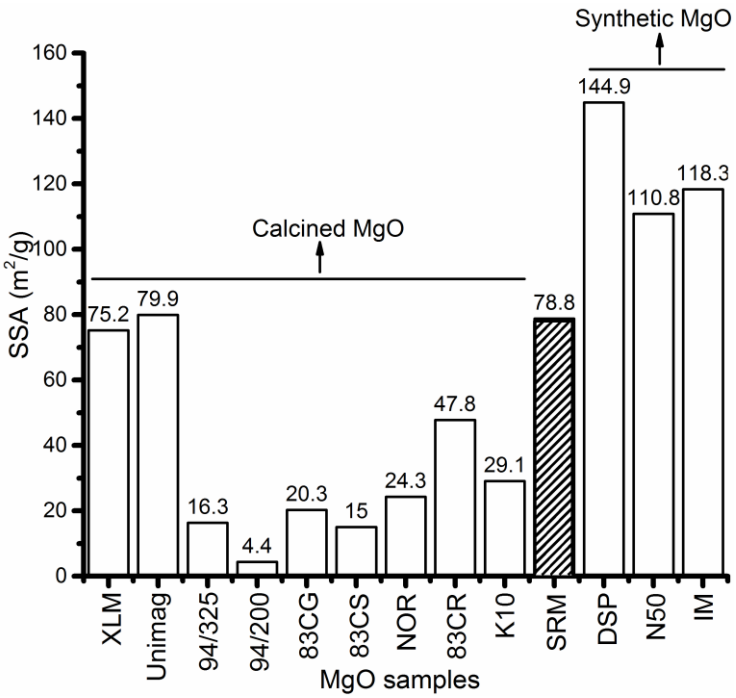

Figure 3.9 SSA of the synthesized reactive MgO (SRM) compared with 12 commercial MgO samples reported in (Jin and Al-Tabbaa 2014)

3.4. Conclusions

This study shed light on the significant potential of reject brine in the recovery of Mg^{2+} and the synthesis of reactive MgO with a wide range of potential applications. The obtained results demonstrated the feasibility of synthesizing reactive MgO from reject brine obtained from a desalination plant. NH_4OH was used as alkali source to precipitate $Mg(OH)_2$ from reject brine. The influence of the amount of NH_4OH was investigated to optimize the yield and increase the purity of the precipitates. An optimum NH_4OH to Mg^{2+} ratio of 6, which resulted in a high Mg content while minimizing Ca-based impurities, was determined. This led to the synthesis of $Mg(OH)_2$ with a high purity of 93.5%, which was further calcined at 500 ℃ for 2 hours to produce highly reactive MgO with a SSA of 78.8 m^2/g. A comparison of the produced MgO with

commercially available reactive MgO samples indicated its capability to be used in different applications necessitating the use of reactive MgO with a high SSA.

Chapter 4 Recovery of reactive MgO from reject brine via the addition of NaOH

4.1. Introduction

While previous studies (Turek and Gnot 1995, Dave and Ghosh 2005, El-Naas 2011, Tran, Van Luong et al. 2013, Khuyen Thi, Han et al. 2016, Hao 2017) have reported the synthesis of MgO or its derivatives from seawater, natural brine or synthetic solutions, this study aims to explore the feasibility of the recovery of Mg^{2+} from reject brine collected from a local desalination plant. The proposed method involves the addition of NaOH, which serves as a pH adjuster and controls the pH of the solution. Unlike Ca-bearing bases, which often lead to the precipitation of a Ca-based compound (e.g. $CaCO_3$) along with Mg-phases, the use of NaOH can increase the purity of Mg-based precipitates. Furthermore, when compared with other bases (e.g. NH_4OH, KOH and Na_2CO_3), NaOH possesses other advantages in terms of health and safety, cost effectiveness and base strength it provides (Dong, Unluer et al. 2017). This research presents a comprehensive study on the synthesis of $Mg(OH)_2$ and production of reactive MgO from reject brine via the use of NaOH. The key parameters affecting the properties of the synthesized $Mg(OH)_2$ and its calcination to produce reactive MgO were investigated. Several techniques were utilized to characterize the synthesized $Mg(OH)_2$ and MgO including inductively coupled plasma-optical emission spectroscopy (ICP-OES), X-ray powder diffraction (XRD), field emission scanning electron microscopy (FESEM), thermogravimetric and differential thermal analysis (TG/DTA), Brunauer-Emmett-Teller (BET) analysis and acid neutralization. The costs of the production of reactive MgO from reject brine via the addition of NaOH compared with NH_4OH and CaO were also calculated to evaluate the utilization of reject brine from an economic standpoint. Results obtained at the end of this study were used to demonstrate the use of reject brine as an alternative source for the recovery of MgO with a high reactivity.

4.2 Materials and Methodology

4.2.1 Materials

Reject brine was collected and sampled from a local desalination plant in Singapore, which adopts a reverse osmosis (RO) membrane system to purify saline water and produce drinkable water for human use. These membranes reject more than 99.5% of the dissolved salts and suspended materials in the feedwater, resulting in a highly concentrated reject waste stream which contains suspended constituents and a 2- to 7-fold increased concentration of dissolved salts (Fritzmann, Lowenberg et al. 2007, Greenlee, Lawler et al. 2009, Elimelech and Phillip 2011). Prior to any analysis, the reject brine was first passed through a 45 μm membrane filter to remove the large suspended solids. The pH of the as-received reject brine was measured and recorded at a value of ~8.0 throughout all experiments. The chemical composition of the reject brine, obtained via inductively coupled plasma-optical emission spectroscopy (ICP-OES) and ion chromatography (IC), is summarized in Table 4.1. Along with Mg^{2+}, which was present at a concentration of 1718 ppm, other cations such as Na^{+}, K^{+} and Ca^{2+} were also identified in the reject brine. Sodium hydroxide (NaOH, reagent grade, pellets) supplied by VWR Pte Ltd in Singapore, was used as the alkaline base in the current study.

Table 4.1 Chemical composition of the reject brine used in this study

Element	Cl	Na	SO_4	Mg	K	Ca	Sr	B	Si	Li	P	Al
Concentration (ppm)	55243 ±58.6	13580 ±41.2	4423 ±7.8	1718 ±5.4	845.7 ±4.8	471.3 ±1.2	14.6 ±0.1	3.8 ±0.1	3.7	0.3	0.2	0.1

4.2.2 Methodology

Different amounts of NaOH solution (16 M) were added into 200 ml of reject brine to study the influence of $NaOH/Mg^{2+}$ molar ratio (ranging from 2 to 4) on the recovery of Mg^{2+}. The solution was mixed at constant speed of 300 rpm by a magnetic stirrer at room temperature (25 ℃). A pH/thermometer probe was used to monitor and record the temperature and pH of the reaction in the solution. NaOH solution was added into reject brine at once and the initial pH of solution was

recorded. Experiment was terminated when the pH of the solution stabilized. The solids were separated from the residual brine through a centrifuge after precipitation. After the solids were collected, they were re-dispersed and washed thoroughly by ultra-pure water in an ultrasonic bath to remove surface-attached ions. The washed solids were separated from the solution through a centrifuge. and washed three times. The washed solids were then oven-dried at 105 ℃ for 24 hours before grinding into powder form. The ground samples were calcined at pre-determined temperatures (500-700 ℃) and durations (2-12 hours) in an electric furnace to produce reactive MgO.

Several techniques were utilized to characterize the synthesized $Mg(OH)_2$ and MgO. X-ray powder diffraction (XRD) was performed via a Bruker D8 Advance with a Cu Kα source under the operation conditions of 40 kV and 40 mA, emitting radiation with a wavelength of 1.5405 angstroms, scan rate of 0.02 °/step, and a 2θ range of 5 to 70°. A JSM-7600F thermal field emission scanning electron microscopy (FESEM) was used to analyze the microstructure of the solids by imaging powder surface. The decomposition of each sample was studied via thermogravimetric and differential thermal analysis (TG/DTA) using a PyrisDiamond TGA 4000 operated at a heating rate of 10 ℃/min under air flow. The specific surface area (SSA) of the synthesized samples was obtained by Brunauer-Emmett-Teller (BET) analysis from nitrogen adsorption-desorption isotherms using a Quadrasorb Evo automated surface area and pore size analyser. The reactivity of MgO was measured by acid neutralization, during which 0.28 grams of the synthesized MgO was added into 50 ml of 0.07 mol/L citric acid solution along with phenolphthalein (i.e. pH indicator). The neutralization time was measured and reported as an indicator of reactivity (Shand 2006, Mo, Deng et al. 2010).

Another important aspect of the production of reactive MgO from reject brine is the economic feasibility of the overall process. The whole costs are mainly from the raw material cost and the energy cost in the calcination process to obtain reactive MgO. The results were further supported to compare with the market price of MgO via a dry-route.

4.3 Results and Discussion

4.3.1 Recovery of Mg^{2+} and Ca^{2+} from reject brine

The formation of $Mg(OH)_2$ was observed via the reaction between the Mg^{2+} in the reject brine and OH^- provided by NaOH. The addition of NaOH also enabled the conversion of HCO_3^-, present in the reject brine, to CO_3^{2-}. This led to a reaction of CO_3^{2-} with Ca^{2+} and resulted in the precipitation of $CaCO_3$. The reaction paths observed during this process are shown in Equations 4-1 to 4-4 below.

$$NaOH_{(aq)} \rightarrow Na^+ + OH^- \quad (4\text{-}1)$$

$$Mg^{2+} + 2OH^- \leftrightarrow Mg(OH)_2 \quad (4\text{-}2)$$

$$NaOH_{(aq)} + HCO_3^- \leftrightarrow CO_3^{2-} + Na^+ + H_2O \quad (4\text{-}3)$$

$$Ca^{2+} + CO_3^{2-} \leftrightarrow CaCO_3 \quad (4\text{-}4)$$

The kinetics of the reaction between reject brine and NaOH reflected by the change of pH are summarized in Figure 4.1. The pH value of reject brine before the addition of NaOH was ~8.0 throughout all experiments. A rapid reaction was observed, which was completed in less than 30 minutes as the pH reached an equilibrium state. The pH increased with the molar ratio of $NaOH/Mg^{2+}$. This was due to the increased concentration of OH^- provided by the higher amounts of NaOH introduced into the solution, whereas a smaller increase was observed at $NaOH/Mg^{2+}$ ratios above 2.5.

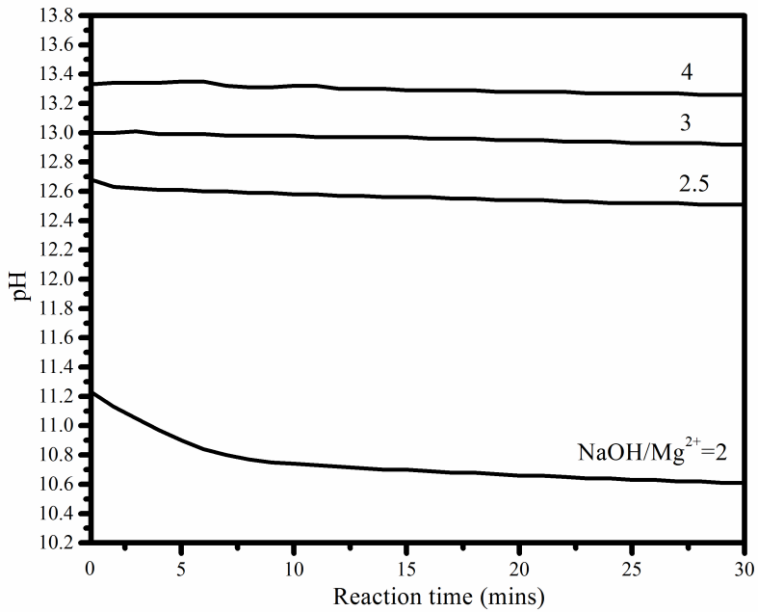

Figure 4.1 pH of the reaction between reject brine and NaOH at different $NaOH/Mg^{2+}$ ratios

Figure 4.2 shows the recovery rate of Mg^{2+} and Ca^{2+} in weight percentage after the reaction of reject brine with NaOH. As can be seen, the recovery rates for both Mg^{2+} and Ca^{2+} increased with increasing $NaOH/Mg^{2+}$ molar ratio, which achieved a similar recovery level of 94-99% of Mg as reported in (Casas, Aladjem et al. 2014). The recovered Mg^{2+}/Ca^{2+} ratio was used as an indication of the purity level of the resulting $Mg(OH)_2$ precipitates. As shown in Figure 4.2, Mg^{2+}/Ca^{2+} was highest (19.6) at a $NaOH/Mg^{2+}$ ratio of 2 and decreased with increasing $NaOH/Mg^{2+}$ ratio. This was because at a $NaOH/Mg^{2+}$ molar ratio of 2, the ion product in the solution ($[Mg^{2+}][OH^-]^2 = 7\times10^{-8.6}$ $mol^3\ l^{-3}$, pH = 11.2) was larger than the solubility product constant of $Mg(OH)_2$ (1.8×10^{-11} $mol^3\ l^{-3}$) . The supersaturation condition enabled the reaction between OH^- and Mg^{2+} and the formation of $Mg(OH)_2$. Furthermore, pH increased with increasing $NaOH/Mg^{2+}$, which provided excessive OH^- in the solution to attack HCO_3^-. This caused in a shift in Equation 4-3 towards the right hand side, resulting in the generation of additional CO_3^{2-}. The excessive CO_3^{2-} reacted with Ca^{2+} in the solution to produce more $CaCO_3$, thus lowing the overall Mg^{2+}/Ca^{2+} ratio.

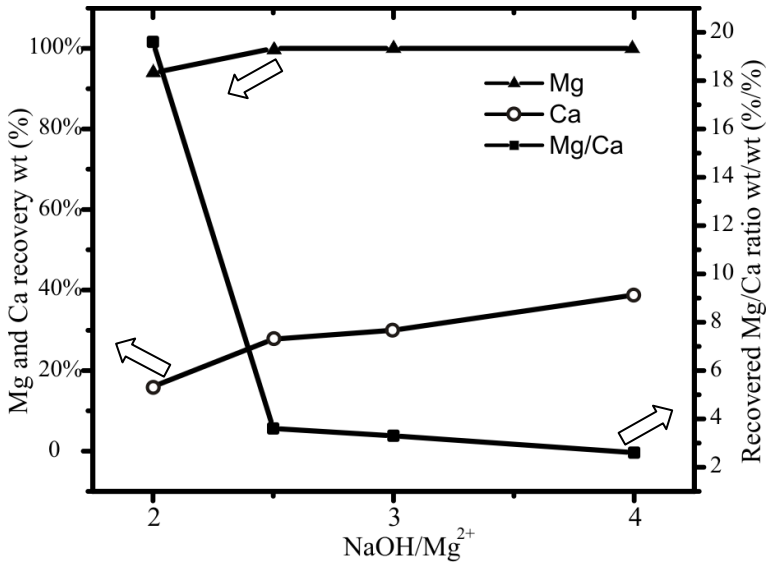

Figure 4.2 Percentage of Mg^{2+} and Ca^{2+} sequestrated from reject brine as a function of the $NaOH/Mg^{2+}$ molar ratio

4.3.2 Characterization of the synthesized $Mg(OH)_2$

4.3.2.1 XRD

Figure 4.3 shows the XRD diffractograms of $Mg(OH)_2$ obtained from the reaction of reject brine and NaOH at different $NaOH/Mg^{2+}$ molar ratios. The diffraction patterns of all samples demonstrated the presence of $Mg(OH)_2$ along with $CaCO_3$. A shift in the crystal structure of $CaCO_3$ from aragonite to calcite was observed at increased $NaOH/Mg^{2+}$ ratios. This could be attributed to the presence of Mg^{2+} in brine, which inhibited the precipitation of calcite and favored the formation of aragonite at low $NaOH/Mg^{2+}$ ratios (Berner 1975). Alternatively, the high pH of the solution at elevated $NaOH/Mg^{2+}$ ratios, at which the influence of Mg^{2+} was minimal, favored the formation of calcite.

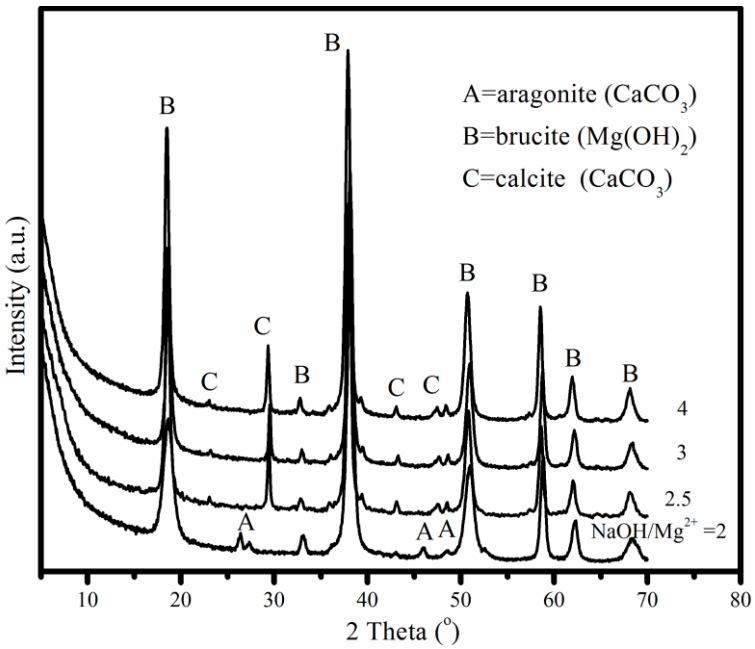

Figure 4.3 XRD diffractograms of $Mg(OH)_2$ obtained from the reaction of reject brine with NaOH at different $NaOH/Mg^{2+}$ molar ratios

4.3.2.2 FESEM

The morphologies of $Mg(OH)_2$ samples obtained at different $NaOH/Mg^{2+}$ molar ratios were investigated by FESEM, as shown in Figure 4.4. A plate-like morphology was observed at a $NaOH/Mg^{2+}$ ratio of 2. The morphology of $Mg(OH)_2$ transformed into a granular pattern consisting of a denser structure at increased $NaOH/Mg^{2+}$ ratios, which could be due to the increased pH of the solution. This was because higher pH values led to the generation of higher concentrations of OH^- in the solution. The increased availability of OH^- accelerated the nucleation of $Mg(OH)_2$ crystals and enabled the formation of larger amounts of $Mg(OH)_2$, facilitating the densification of the overall structure.

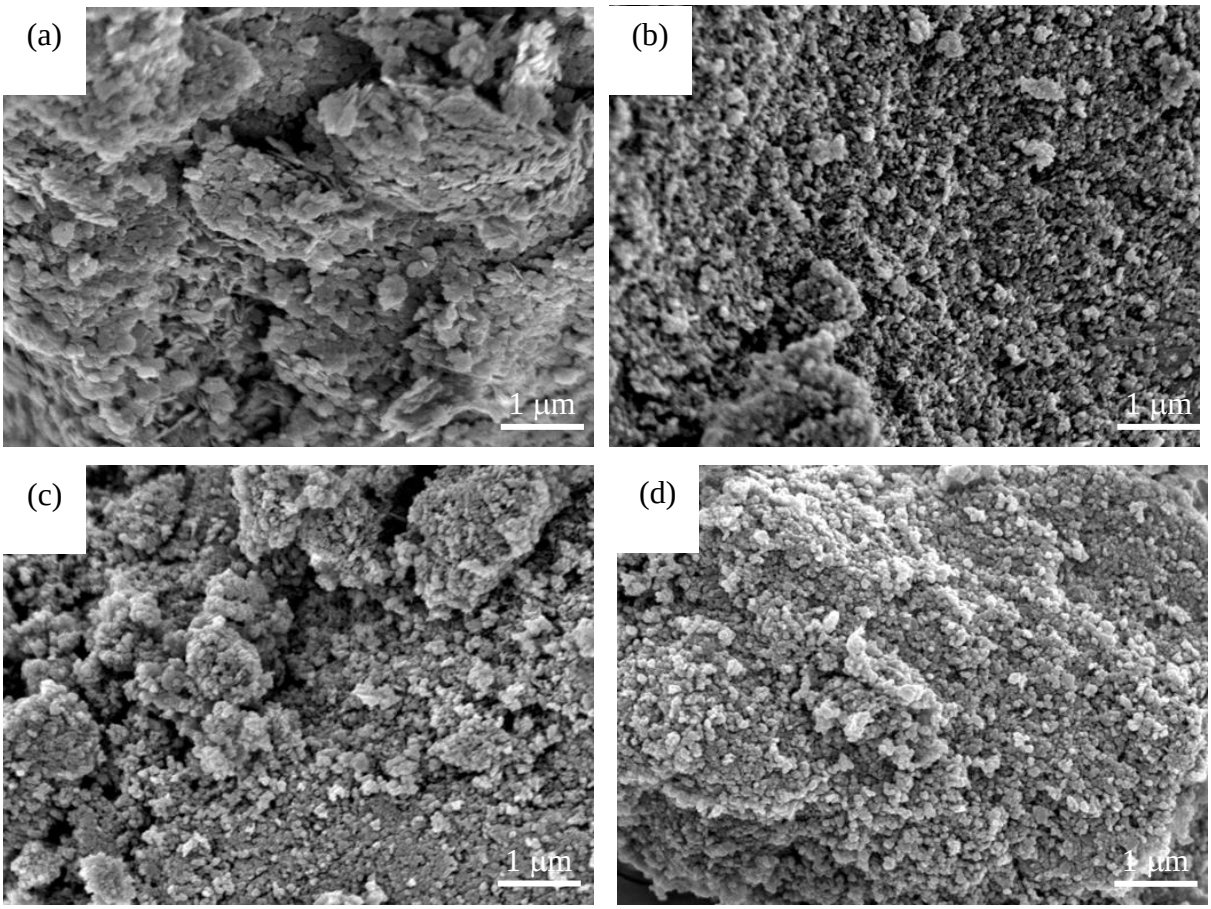

Figure 4.4 FESEM images of $Mg(OH)_2$ obtained from the reaction of reject brine with NaOH at different $NaOH/Mg^{2+}$ molar ratios of (a) 2, (b) 2.5, (c) 3 and (d) 4

4.3.2.3 TG/DTA

Figure 4.5 illustrates a typical TG/DTA graph of $Mg(OH)_2$ obtained via the reaction of brine with NaOH at a $NaOH/Mg^{2+}$ molar ratio of 2. The dehydration of $Mg(OH)_2$ took place at ~400 ℃ and resulted in a mass loss of around 24.2%, which was attributed to the loss of water. The decomposition patterns observed during TG/DTA were in line with previous studies that investigated the decomposition of $Mg(OH)_2$ into MgO (Eubank 1951, Itatani, Koizumi et al. 1988, Alvarado, Torres-Martinez et al. 2000, Mo, Deng et al. 2010). The second endothermic peak, observed at ~720 ℃, was due to the decarbonation of $CaCO_3$. The decomposition of $CaCO_3$ led to the release of CO_2, resulting in a mass loss of around 2.3%.

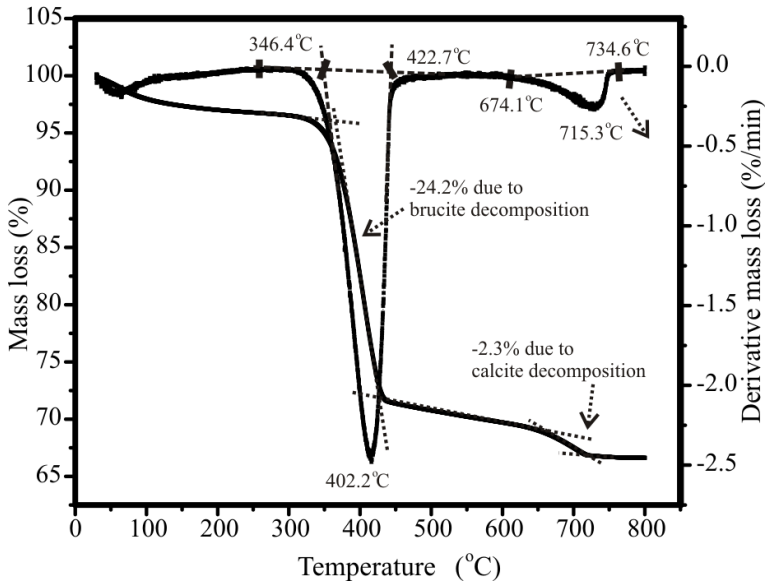

Figure 4.5 A typical TG/DTA curve of $Mg(OH)_2$ obtained from the reaction of reject brine at a $NaOH/Mg^{2+}$ molar ratio of 2

Table 4.2 summarizes the TG/DTA results of $Mg(OH)_2$ obtained from the reaction of brine with NaOH at various $NaOH/Mg^{2+}$ ratios ranging between 2 and 4. The results show that the mass loss due to dehydration of $Mg(OH)_2$ at ~400 ℃ slightly decreased (24.2 to 22.6%), while the mass loss due to decarbonation of $CaCO_3$ at ~720 ℃ slightly increased (2.3 to 3.9%) with increasing $NaOH/Mg^{2+}$ ratios. This was mainly attributed to the increased content of $CaCO_3$ in the precipitates at higher $NaOH/Mg^{2+}$ ratios, which was in line with the findings shown in Figure 4.2.

Table 4.2 TG/DTA results of the decomposition of $Mg(OH)_2$ obtained from the reaction of reject brine with NaOH at different NaOH/Mg^{2+} ratios

Mg^{2+}/ NaOH	Peak temperature (℃)	Mass loss between 340-440 ℃ (%)	Peak temperature (℃)	Mass loss between 650-750 ℃ (%)
1:2	402.2	24.2	715.3	2.3
1:2.5	401.2	23.5	721.1	3.2
1:3	400.8	23.3	719.3	3.5
1:4	404.1	22.6	724	3.9

Table 4.3 Composition of synthesized $Mg(OH)_2$ based on TG/DTA and ICP-OES results

Mg^{2+}/NaOH	TG/DTA		ICP-OES	
	$Mg(OH)_2$ (%)	$CaCO_3$ (%)	$Mg(OH)_2$ (%)	$CaCO_3$ (%)
1:2	93.7	6.3	95.4	4.6
1:2.5	91.2	8.8	91.2	8.8
1:3	90.4	9.6	90.6	9.4
1:4	89.2	10.8	88.1	11.9

Table 4.3 compares the compositions of the synthesized $Mg(OH)_2$ based on the TG/DTA (Table 4.2) and the ICP-OES (Figure 4.2) results. Both measurements revealed similar trends,

showing a decrease in the mass percentage of $Mg(OH)_2$, accompanied with an increase in the mass percentage of $CaCO_3$ (and thus a decrease in the purity of precipitates) with increasing $NaOH/Mg^{2+}$ molar ratios, which was further discussed in Section 3.1. Accordingly, the highest amount of $Mg(OH)_2$ (93.7% by TGA and 95.4% by ICP-OES) was synthesized at a $NaOH/Mg^{2+}$ molar ratio of 2. Therefore, this ratio was chosen as the optimum condition for the subsequent production and characterization of reactive MgO.

4.3.3 Characterization of the synthesized reactive MgO

4.3.3.1 SSA

Figure 4.6 presents the SSA of the reactive MgO obtained under different calcination conditions. In general, SSA reduced with increasing calcination temperature and duration, which was in line with the findings of previous studies (Eubank 1951, Itatani, Koizumi et al. 1988, Alvarado, Torres-Martinez et al. 2000, Mo, Deng et al. 2010). This was associated with the sintering and agglomeration of MgO grains at higher temperature and prolonged residence times. In the current study, the highest SSA of 51.4 m^2/g was obtained when the synthesized $Mg(OH)_2$ was calcined at 500 ^oC for 2 hours. When compared to other studies, the SSA value (51.4 m^2/g) obtained under these conditions was significantly higher than the results presented in the literature, where MgO synthesized from a magnesium chloride solution via the addition of NaOH and calcined under the same conditions (i.e. 500 ^oC for 2 hours), was reported to possess a SSA of 22.1 m^2/g (Venkatesha, Viswanatha et al. 2012). However, compared with our previous study, MgO calcined at 500 ℃ for 2 hours from reject brine via the addition of NH_4OH showed a higher SSA of 78.8 m^2/g (Dong, Unluer et al. 2017). This could be because the use of NaOH as the alkali source was found to form $Mg(OH)_2$ with a globular cauliflower-like morphology; while the use of NH_4OH resulted in a more porous plate-like morphology (Dong, Unluer et al. 2017). A relative more porous mother precursor would result in a more porous MgO, thus a higher reactivity. These values can be optimized even further with an adjustment of the calcination temperature and duration towards the lower range, while enabling the complete decomposition of $Mg(OH)_2$.

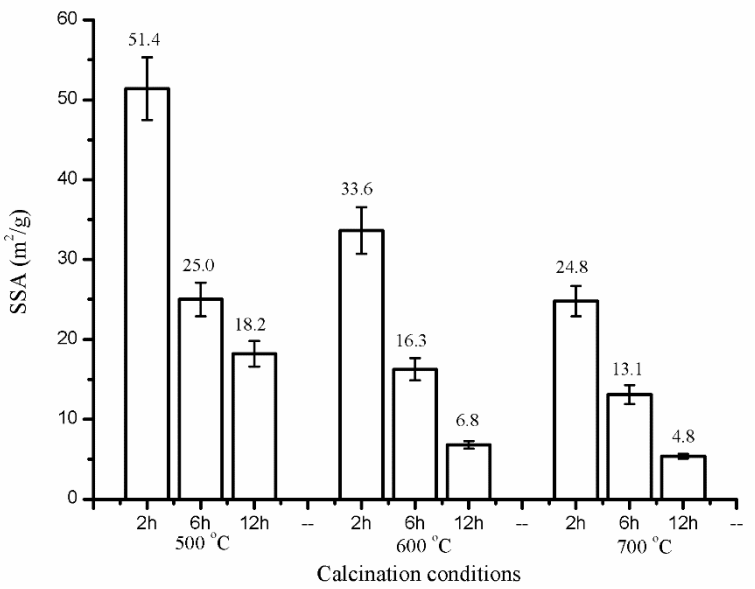

Figure 4.6 SSA of MgO produced under different calcination temperatures and durations

4.3.3.2 Reactivity

Figure 4.7 shows the acid reactivity of MgO obtained under different calcination conditions. An increase in the neutralization time was observed with increasing calcination temperature and duration, which reflected the reduction in the reactivity of MgO. This observation corresponded well with the SSA measurements reported earlier in Figure 4.6. A comparison of the reactivity and SSA of MgO is shown in Figure 4.8, where the inverse correlation between the two parameters was revealed. Accordingly, MgO samples with higher SSA resulted in shorter acid neutralization times, which was an indication of their higher reactivities. These findings were in line with those reported in earlier studies (Mo, Deng et al. 2010, Jin and Al-Tabbaa 2014), where a direct correlation between the SSA and reactivity of MgO was reported. The acid test shows a good indicator of the difference between the reactivity of various MgO samples obtained under a range of calcination conditions, as presented in this study.

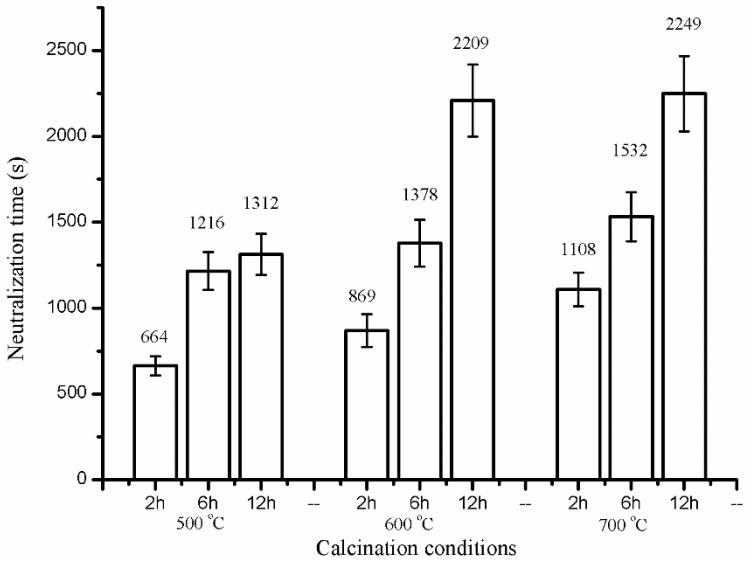

Figure 4.7 Effect of calcination temperature and duration on the reactivity of MgO

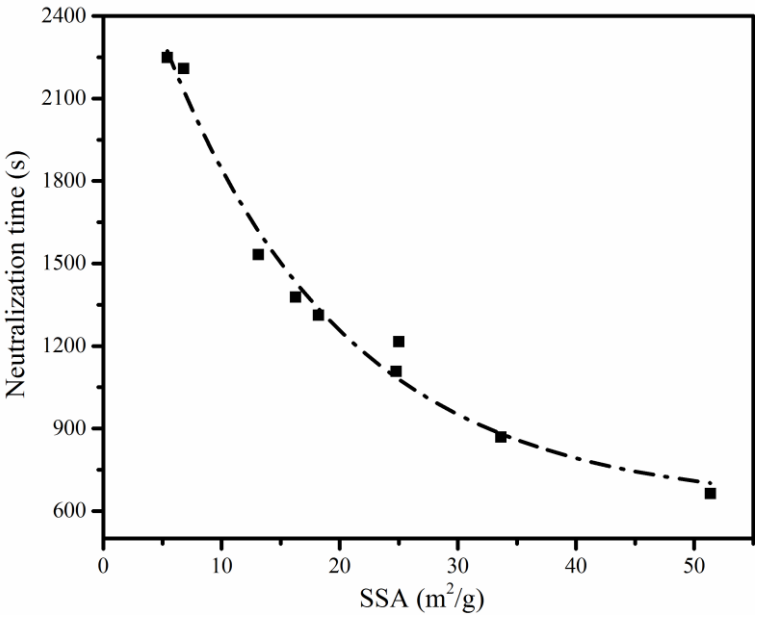

Figure 4.8 Relationship between the SSA and the reactivity of MgO

4.3.3.3 XRD

Figure 4.9 illustrates the diffractograms of MgO obtained via the calcination of $Mg(OH)_2$, which

was synthesized at a $NaOH/Mg^{2+}$ molar ratio of 2. The main peak positions of the synthesized MgO were located at ~37.0 °, 42.9 ° and 62.3 ° 2θ, which matched well with the reference peaks of MgO indicated in JCPDS card no. 89-7746. These peaks were accompanied with a few minor peaks attributed to $CaCO_3$. The absence of $Mg(OH)_2$ peaks indicated the complete decomposition of brucite under the calcination conditions adopted in this study. Aragonite, which was initially present along with $Mg(OH)_2$, transformed into calcite at higher calcination temperatures of 600 ℃ (Kontoyannis and Vagenas 2000). A further increase in the calcination temperature (700 ℃) and duration led to a reduction in the intensity of the calcite peaks due to decomposition of $CaCO_3$.

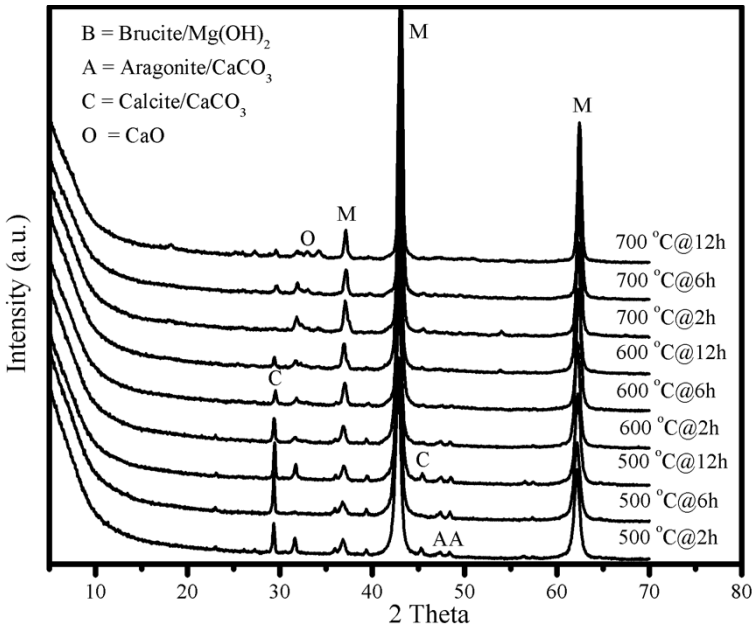

Figure 4.9 XRD diffractograms of reactive MgO produced via the calcination of $Mg(OH)_2$ under different temperatures and durations

4.3.3.4 FESEM

A further investigation on the influence of calcination temperature and duration on the SSA of MgO was revealed through FESEM. The changes in the microstructure of MgO at increased temperatures and durations are indicated in Figure 4.10, which is a good indication of the typical morphology of MgO produced at a calcination temperature of 500-700 ℃ and a residence time

of 2-12 hours. The microstructure of MgO was composed of a single particle which was a combination of several grains. A plate-like morphology, which was inherited from the parent material ($Mg(OH)_2$), was observed throughout the microstructure of MgO produced at lower temperatures. An increase in the particle size, accompanied with the creation of a more porous structure, was observed at increased temperatures and durations. The loss of water during the decomposition of $Mg(OH)_2$ led to the formation of a porous structure, which gradually reduced with the increase in the size of the MgO grains due to continued sintering, causing a reduction in the total pore volume.

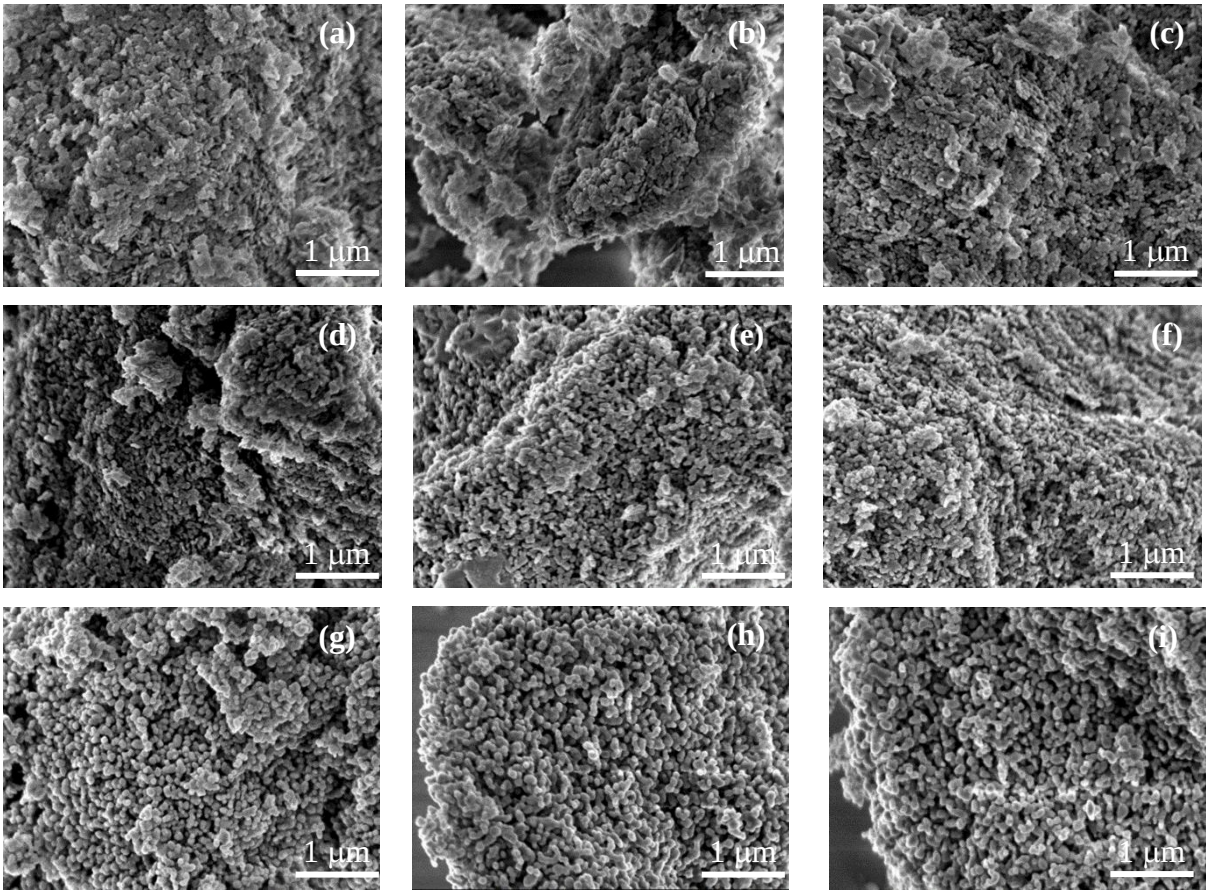

Figure 4.10 FESEM images of MgO obtained from the calcination of $Mg(OH)_2$ under different conditions: (a) 500 ℃-2h, (b) 500 ℃-6h, (c) 500 ℃-12h, (d) 600 ℃-2h, (e) 600 ℃-6h, (f) 600 ℃-12h, (g) 700 ℃-2h, (h) 700 ℃-6h and (i) 700 ℃-12h

4.3.4 Economic feasibility

The costs of the production of reactive MgO from reject brine via the addition of NaOH compared with NH_3 and CaO were also calculated to evaluate the utilization of reject brine from an economic standpoint as shown in Figure 4.11. The total costs are mainly from the raw material cost, e.g. NaOH, NH_3 and CaO, and the energy cost in the calcination process to obtain reactive MgO. Reject brine is the waste water produced at the end in the desalination plant, thus, the material cost and energy cost of reject brine are assumed to be zero. The transportation of raw materials and the grinding and packing of reactive MgO products are not considered into the calculation since they do not contribute significantly to the overall process. The prices of NaOH, NH_3 and CaO are reported to be ~$370/ton NaOH (S$571/tonne NaOH) (Fukushima 2016), ~$340 per ton NH_3 (S$525/tonne NH_3) in 2016 (Jones 2016), and ~$110/ton CaO (S$170/tonne CaO) (USGS 2012), respectively. Since a production yield of 1 tonne of reactive MgO requires 2 tonnes of NaOH, 1 tonne of NH_3 or 1.4 tonne of CaO as the base source, the material costs are calculated to be S$1142/tonne MgO, S$525/tonne MgO and S$238/tonne MgO, respectively.

After the addition of NaOH into reject brine to precipitate $Mg(OH)_2$, $Mg(OH)_2$ was in the form of filter cake which was composed of 55.2% solids. The energy consumption in the calcination of $Mg(OH)_2$ filter cake is derived by considering two steps: (i) the energy consumed to increase the temperature from room temperature (298 K, 25 ℃) to the decomposition temperature of $Mg(OH)_2$ (773K, 500 ℃), (ii) the enthalpy in the decomposition process of $Mg(OH)_2$ (Shand 2006). A production yield of 1 tonne of MgO requires decomposing 1.45 tonne of pure $Mg(OH)_2$ and the decomposition temperature of $Mg(OH)_2$ under one atmosphere CO_2 pressure is in the range between 773 K and 973 K (500 and 700 ℃). Firstly the energy required to raise the temperature from ambient air (298 K) to the decomposition temperature (773 K) is calculated using the formula: C_p × increase in temperature (K). The specific heat capacity (C_p) of $Mg(OH)_2$ at 773 K is 1.78 kJ/kg K, which results in the energy demand of 1.15 GJ in consideration of the purity of the synthesized $Mg(OH)_2$ of ~94%. The energy required for the decomposition of $Mg(OH)_2$ is calculated based on the enthalpy of decomposition (1304 kJ/kg), which brought in 1.77 GJ. As for the free water, the energy required to raise the room temperature (298 K) to boiling point (373 K) is calculated based on the specific heat capacity of water (4.18 kJ/kg K) and the percentage of water in the filter cake (44.8%), resulting in 0.37 GJ. This is followed by

the enthalpy of the vaporization of water (2283 kJ/kg), resulting in 2.69 GJ. Finally the energy required to heat up the resultant steam to 773 K is calculated via the heat capacity of water vapour (1.86 kJ/kg K), bringing in 0.88 GJ. The total energy required for the calcination process is the summation of the energy required for each individual step, resulting in a total of 6.85 GJ (1902.8 kWh) for the production of 1 tonne reactive MgO from reject brine via the addition of NaOH, which is also applicable to reactive MgO produced from reject brine via the addition NH_4OH or $Ca(OH)_2$. As of 2015, Singapore uses natural gas (95%) and others (4%) for the power generation at a price of 20.2 cents per kWh (EMA 2016), which results in an energy cost of 384 S$ to product 1 tonne reactive MgO from reject brine via the addition of NaOH, NH_3 or CaO.

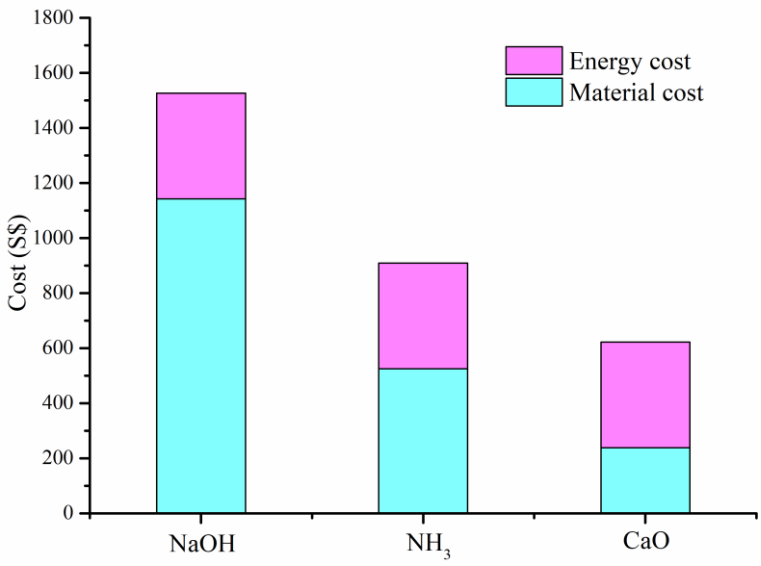

Figure 4.11 Costs of the production of reactive MgO from reject brine via the addition of NaOH compared with NH_3 and CaO

When integrating the material cost and energy cost, the overall process requests the final cost to be S$1526/tonne MgO produced from reject brine via the addition of NaOH, compared to S$909/tonne MgO via the addition of NH_4OH, which can further decrease to S$622/tonne MgO if CaO is used. The market price of MgO via a dry route in the US market was reported to be $400/ton MgO (S$617/tonne MgO) (Bogner 2015). Thus, a cheaper base alternative would make the production of reactive MgO from reject brine more economically feasible. Furthermore,

synthetic MgO from reject brine shows a much higher purity and reactivity compared to the dry route as the SSA of commercial MgO is usually ~20 m^2/g (Shand 2006), which makes it even more competitive in the global market.

4.4 Conclusions

This study presented a comprehensive investigation on the synthesis of $Mg(OH)_2$ and production of reactive MgO from reject brine via the use of NaOH. The key parameters affecting the properties of the synthesized $Mg(OH)_2$ and its calcination to produce reactive MgO were revealed. The results demonstrated the feasibility of recovering reactive MgO from reject brine obtained as a waste at the end of the desalination process. The initial set of experiments successfully demonstrated the use of NaOH as an alkali source in the precipitation of $Mg(OH)_2$ from reject brine. The effect of the $NaOH/Mg^{2+}$ ratio on the final yield was investigated with the goal of optimizing the amount and purity of the synthesized $Mg(OH)_2$. An optimum $NaOH/Mg^{2+}$ ratio of 2, which generated the highest purity of $Mg(OH)_2$, was determined and used in the subsequent production of MgO. The influence of calcination conditions (i.e. temperature and residence time) on the reactivity of MgO obtained via the calcination of the synthesized $Mg(OH)_2$ were reported. While a certain minimum temperature was required for the complete decomposition of $Mg(OH)_2$ into MgO, an increase in the calcination temperature and duration lowered the reactivity of MgO. Calcination of $Mg(OH)_2$ at 500 ℃ for 2 hours resulted in the most reactive MgO samples, with a SSA of 51.4 m^2/g. This study demonstrated that reject brine can be considered as a feasible and economic alternative source for the sustainable recovery of MgO with a high reactivity, especially suitable for those countries without magnesite reserves, which can be used in various applications within the food, cosmetics, pharmaceutical and construction industries (Kramer , Lee, Jung et al. 2004, Shand 2006).

Chapter 5 Characterization and comparison of MgO recovered from reject brine obtained from desalination plants

5.1. Introduction

The feasibility of producing MgO with a high reactivity from reject brine via the addition of NH_4OH and NaOH has been presented in previous studies (Dong, Unluer et al. 2017, Dong, Unluer et al. 2018). One of the main factors determining the efficiency of the overall synthesis was the type and amount of the base introduced into the reject brine. Accordingly, the characteristics of $Mg(OH)_2$ and resulting MgO significantly varied, especially in terms of their reactivity and microstructure, under the use of different bases. Furthermore, the synthesis temperature was accounted for the size of the platelets as the lower the synthesis temperature, the higher the diameter. However, the influence of base type, reaction condition and calcination conditions on the texture properties (SSA and pore size distribution) and reactivity of the MgO has yet been revealed.

For the accurate characterization of the final product, the relationship between the reaction condition, such as the base type, and the reactivity of MgO must be clearly comprehended. Establishing clear links between its production conditions and final properties will enable the effective use of MgO and the identification of the right applications in line with its capabilities. With this goal in mind, this paper presents a comprehensive characterization of MgO obtained via the calcination of $Mg(OH)_2$ precipitated using two different bases (NH_4OH and NaOH) and compares the properties of the final product produced under different calcination conditions. The obtained results shed a light on the influence of different base environments and calcination conditions on the properties of MgO and highlight potential application areas that can benefit from the end product.

5.2. Materials and Methodology

5.2.1. Materials

Reject brine, whose cation composition obtained via inductively coupled plasma-optical emission spectroscopy (ICP-OES) is listed in Table 5.1, was provided by a local desalination plant in Singapore. Ammonium hydroxide solution (NH_4OH, 25.0 % NH_3 content) and sodium hydroxide (NaOH), used as the alkaline sources in the synthesis of $Mg(OH)_2$, were supplied by Sigma-Aldrich and VWR Pte Ltd in Singapore, respectively.

Table 5.1 Chemical composition of reject brine used in this study

Element/ Concentration	Cl	Na	SO_4	Mg	K	Ca	Sr	B	Si	Li	P	Al
ppm	65593.1 ± 66.3	16124.3 ± 55.8	4322 ± 8.8	1679.0 ± 5.5	808.5 ± 5.4	563.6 ± 1.1	5.3 ±0 .1	4.5 ±0 .1	0. 5	0. 4	0. 2	0. 1

5.2.2. Methodology

The first step involved the synthesis of $Mg(OH)_2$ from reject brine via the addition of the bases, in line with the procedure explained in detail in previous studies (Dong, Unluer et al. 2017, Dong, Unluer et al. 2018). NH_4OH was included at a NH_4OH/Mg^{2+} molar ratio of 6, whereas NaOH was added at a $NaOH/Mg^{2+}$ molar ratio of 2, as optimized in the aforementioned previous studies. $Mg(OH)_2$ that precipitated at the end of the reaction shown in Equations 5-4 and 5-5 was calcined to produce MgO, as shown in Equation 5-6. The calcination process involved the heating of $Mg(OH)_2$ at a rate of 10 ℃/min to reach three different calcination temperatures (500, 600 and 700 ℃), which were each maintained for three different residence times (i.e. 2, 6 and 12 hours)

$$Mg^{2+} + 2NH_4^+ + 2OH^- \rightarrow Mg(OH)_2 + 2NH_4^+ \quad (5\text{-}4)$$

$$Mg^{2+} + 2\,Na^+ + 2OH^- \rightarrow Mg(OH)_2 + 2Na^+ \quad (5\text{-}5)$$

$$Mg(OH)_2 \rightarrow MgO + H_2O \quad (5\text{-}6)$$

As a detailed analysis and characterization of $Mg(OH)_2$ obtained via the reaction of reject brine with NH_4OH and NaOH was presented earlier (Dong, Unluer et al. 2017, Dong, Unluer et al. 2018), this study mainly focused on the characterization and comparison of the final product, MgO, obtained via the use of two distinct bases under different calcination conditions. A Bruker D8 Advance with a Cu Kα source was used to perform X-ray powder diffraction (XRD) under the operation conditions of 40 kV and 40 mA, emitting radiation with a wavelength of 1.5405 Å, scan rate of 0.02 °/step, and a 2θ range of 5 to 70°. The microstructure of the solids was analyzed by imaging powder surface via a JSM-7600F thermal field emission scanning electron microscopy (FESEM). The thermo-property of the solids was characterized via thermogravimetric and differential thermal analysis (TG/DTA) using a PyrisDiamond TGA 4000 operated at a heating rate of 10 ℃/min under air flow. The texture properties, namely SSA and pore volume, were determined from nitrogen adsorption-desorption isotherms using a Quadrasorb Evo automated surface area and pore size analyzer. The SSA was calculated by Brunauer-Emmett-Teller (BET) method, while the pore volume was determined by Barrett-Joynet-Halenda (BJH) method. The acid reactivity of MgO was tested via the measurement of the time duration required to neutralize the acid solution, during which 0.28 grams of the synthesized MgO was added into 50 ml of 0.07 mol/L citric acid solution while phenolphthalein was adopted as the pH indicator (Shand 2006, Mo, Deng et al. 2010).

5.3. Results and Discussions

5.3.1. Characterization of $Mg(OH)_2$

5.3.1.1. Textural properties and XRD

Figure 5.1 shows the XRD diffractograms of the synthesized $Mg(OH)_2$ obtained via the reaction between reject brine and two different base solutions involving the use of NH_4OH and NaOH. The two diffraction patterns presented similar phases, which were mainly attributed to $Mg(OH)_2$, along with minor amounts of $CaCO_3$ in the crystal form of aragonite. The purities of $Mg(OH)_2$ synthesized via the use of two different base solutions, were calculated via TG/DTA analysis. The obtained results demonstrated a similar purity level of ~94 % for both samples. Debye-Scherrer formula was used to calculate the crystallite size, as shown in the equation $G_{XRD} = K \bullet \lambda / (\beta \bullet \cos(\theta))$ (Patterson 1939). Where λ is the wavelength of Cu Kα source as 1.5405 Å, β the

full width at half-maximum intensity (FWHM) of a Bragg reflection subtracting the instrumental broadening, θ the Bragg angle and K the shape factor with a typical value as 0.9. The major characteristic peak of $Mg(OH)_2$ at 38.1 °(2 θ) was used in this calculation.

NH_4OH- and NaOH-based $Mg(OH)_2$, as calculated, possessed a crystallite size of 15.4 vs 10.5 nm, respectively. These variations could be associated with the strength of NH_4OH and NaOH as a base and the chemical nature of ions present in the solution. NaOH, which is a strong base, ionizes completely and produces a significant number of OH^- once dissolved in water. On the other hand, NH_4OH is a weaker base and electrolyte, which only ionizes to a limited extent in water, gradually releasing OH^- into the solution. The higher concentration of OH^- provided by NaOH could accelerate the reaction of Mg^{2+} and OH, which in turn enhanced the formation of $Mg(OH)_2$ crystals, therefore resulting in a shorter reaction time. The elevated pH value created a high supersaturation level, which formed many more nuclei and generated a faster nucleation process, and hence smaller crystals appeared (Markov 2016).

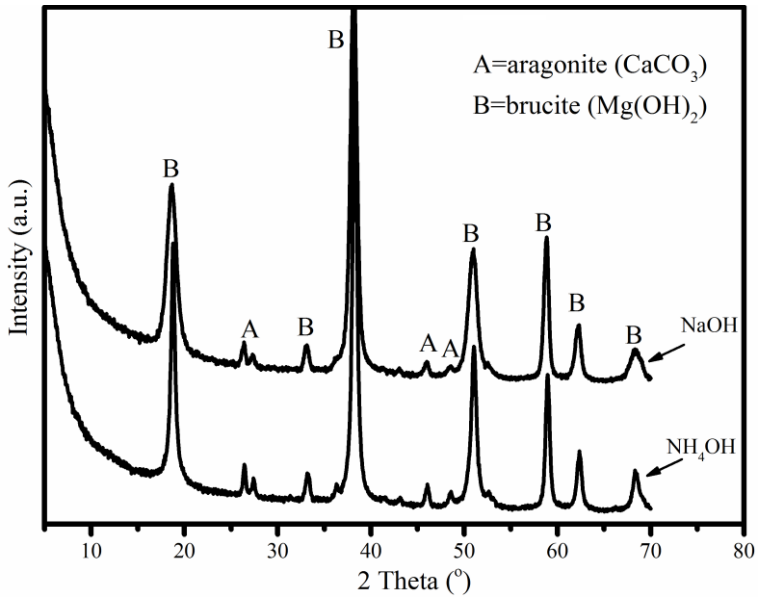

Figure 5.1 XRD diffractograms of $Mg(OH)_2$ obtained from the reaction of reject brine with NH_4OH and NaOH

Table 5.2 Chemical composition, crystallite size, SSA and pore volume of $Mg(OH)_2$ obtained from the reaction of reject brine with NH_4OH and NaOH

Base	Phase contents (%)		G_{XRD} (nm)	SSA (m^2/g)	Pore volume (cm^3/g)
	$Mg(OH)_2$	$CaCO_3$			
NH_4OH	93.5	6.5	15.4	10.6±1.1	0.055
NaOH	93.7	6.3	10.5	7.4±0.6	0.029

5.3.1.2. FESEM

The morphology of $Mg(OH)_2$ obtained via the addition of NH_4OH and NaOH to reject brine, was further investigated through FESEM, as shown in Figure 5.2. The use of NaOH generated a densely packed granular morphology with relatively clear boundaries. Alternatively, those produced via the use of NH_4OH demonstrated a flake-like morphology with a more porous structure, which was in line with the findings of previous studies (Henrist, Mathieu et al. 2003).

These microstructural observations were confirmed by BET results that revealed the SSA of $Mg(OH)_2$ produced through these two distinct routes. As shown in Table 5.2, NH4OH- and NaOH-based $Mg(OH)_2$ possessed a SSA of 10.6 vs 7.4 m^2/g, with a pore volume of 0.055 vs 0.029 cm^3/g, respectively. The morphological difference was believed to relate to pH and cations present in the solution (Henrist, Mathieu et al. 2003, Hanlon, Diaz et al. 2015). The introduction of the strong base, NaOH, set the pH of solution beyond the IEP of $Mg(OH)_2$ (~12) as explained in the aforementioned introduction section (Hanlon, Diaz et al. 2015). Furthermore, the high supersaturation generated by NaOH enhanced the nucleation of tiny crystals, which agglomerated together to grow denser, generating a much denser structure with a lower porosity, therefore leading to a lower SSA. However, the addition of weak base, NH_4OH, favored the binding of OH^- to the basal plane, encouraging anisotropic growth and hence formation of flakes.

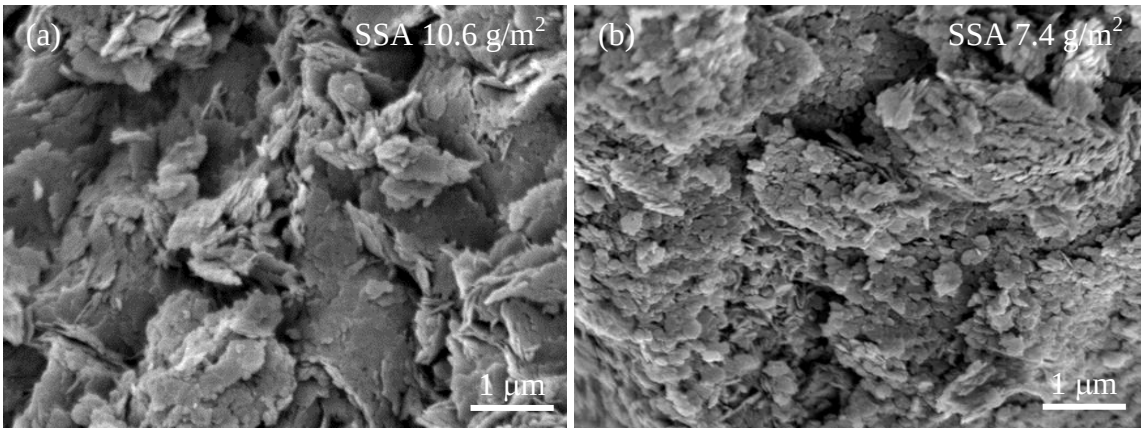

Figure 5.2 FESEM images of $Mg(OH)_2$ obtained from the reaction of reject brine with (a) NH_4OH and (b) NaOH

5.3.2. Characterization of MgO

5.3.2.1. XRD

The XRD patterns of MgO, obtained from the calcination of $Mg(OH)_2$, generated via the reaction of reject brine with NH_4OH and NaOH, under different calcination conditions are shown in Figure 5.3a and 3b, respectively. In both cases, $Mg(OH)_2$ was complete decomposed into MgO under the calcination conditions studied (i.e. 500-700 ℃ for 2-12 hours). The characteristic peaks of MgO, which were located at 37.0 °, 43.1 ° and 62.3 ° 2θ, matched well with the reference peaks of MgO indicated in JCPDS card no. 89-7746. Along with MgO, a few minor peaks attributed to $CaCO_3$ and CaO were observed in the XRD patterns of all samples. Aragonite (primary peaks at 47.5 ° and 48.6 ° 2θ) , which was initially present within the sample composition, gradually transformed into calcite (i.e. primary peaks at 29.5 ° and 43.1 ° 2θ) at higher calcination temperatures (600 ℃). This was because calcite processes a higher entropy and aragonite on heating converts to calcite at temperatures above 400 ℃ (Kontoyannis and Vagenas 2000). A clear reduction in the intensity of the calcite peak at 29.5 ° 2θ, indicated the decomposition of $CaCO_3$ into CaO as the calcination temperature further increased to 700 ℃. The overall results demonstrated the similar phase transitions of NH_4OH- and NaOH-based samples under increasing calcination temperatures and durations, which were in line with the findings reported earlier (Dong, Unluer et al. 2017, Dong, Unluer et al. 2018). These outcomes highlighted that albeit their similar compositions, the final products differed in terms of their physical properties and morphology, which were determined by the production parameters.

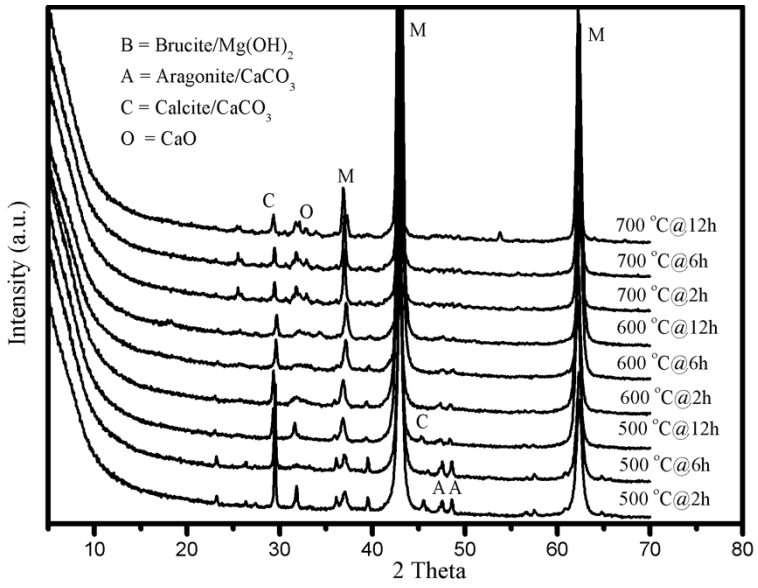

(a)

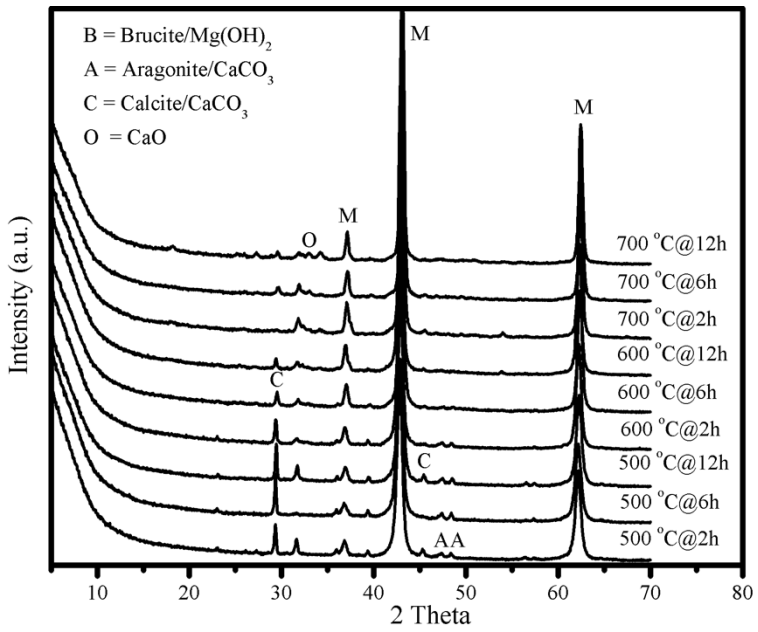

(b)

Figure 5.3 XRD diffractograms of reactive MgO obtained from the calcination of $Mg(OH)_2$ that was synthesized via the reaction of reject brine with (a) NH_4OH and (b) NaOH, under different calcination temperatures and durations

5.3.2.2. Textural properties

The SSA values of MgO, obtained from the calcination of $Mg(OH)_2$ generated via the reaction of reject brine with NH_4OH and NaOH under different calcination conditions (i.e. temperature and duration), are displayed in Figure 5.4. The SSA values ranged between 5.5 and 78.8 m^2/g, depending on the base used and calcination conditions. An increase in the calcination temperature and duration led to a consistent reduction in SSA and pore volume, indicating a decrease in the reactivity of both the NH_4OH- and NaOH-based MgO samples as shown in Table 5.3. The calcination of $Mg(OH)_2$ occurs in two steps, i.e., the release of H2O from the $Mg(OH)_2$, leaving more porous MgO (compared to $Mg(OH)_2$). Up to a certain temperature, the porous MgO starts to sinter, i.e., the breakdown of the pores in MgO and the reduction of porosity and increase of crystallite size (Eubank 1951). These findings were in line with those reported in previous studies (Eubank 1951, Itatani, Koizumi et al. 1988, Alvarado, Torres-Martinez et al. 2000, Mo, Deng et al. 2010, Jin and Al-Tabbaa 2014), where the direct influence of calcination conditions on the properties of the final product was reported.

Out of all conditions used in this study, the calcination of NH_4OH-based $Mg(OH)_2$ under 500 ^oC for 2 hours generated the highest SSA of 78.8 m^2/g, while NaOH-based samples led to corresponding SSA values of 51.4 m^2/g. Compared with NaOH-based MgO, NH_4OH-based MgO achieved higher SSA values at the lower calcination temperatures of 500 ^oC. This could be due to the difference in the textural properties of the $Mg(OH)_2$ precursor since NH_4OH-basesd $Mg(OH)_2$ possessed a higher SSA with a higher porosity. Accordingly, the calcination of NH_4OH-based $Mg(OH)_2$ generated MgO samples with more porous structures, and thereby higher SSA values, at the lower end of the calcination temperatures as shown in Table 5.3.

This trend reversed as the calcination temperature increased from 500 to 700 ^oC, indicating a sharp decline in the SSA and porosity of NH_4OH-based MgO, whereas those of NaOH-based MgO were not affected at the same rate. At the highest calcination temperature of 700 ^oC, NaOH-based samples revealed higher SSA values and porosity than NH_4OH-based ones (e.g. 24.8 vs. 10.3 m^2/g; 0.160 vs. 0.041 cm^3/g), which was especially apparent at the residence times of 2 and 6 hours. When compared to NaOH-based samples, the porous structures of NH_4OH-based samples demonstrated a larger reduction in SSA associated with the rapid growth of MgO

grains, whose originally larger areas were exposed to higher temperatures and longer durations. These differences in SSA values could be attributed to the initially highly porous structure of NH_4OH-based samples, which could be more severely influenced under elevated calcination conditions. Due to the higher porosity of NH_4OH-based $Mg(OH)_2$, the MgO possessed higher porosity at the optimum calcination condition. While under the elevated calcination temperatures, critical temperature for NH_4OH-based $Mg(OH)_2$ sintering was lower than that of NaOH-based $Mg(OH)_2$, which caused the SSA trend to reverse at high temperatures (Eubank 1951).

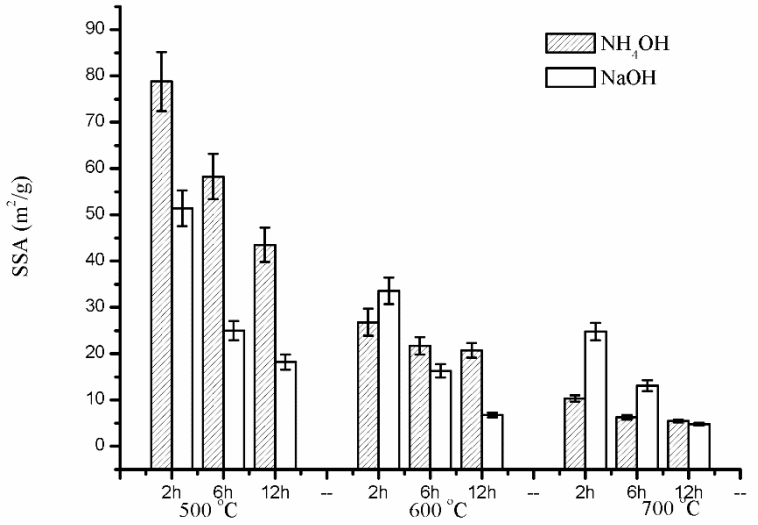

Figure 5.4 SSA of MgO produced under different calcination temperatures and durations

5.3.2.3. Crystallite size and primary particle size

The major characteristic peak of MgO at 43.1 ° (2 θ) from XRD, was used to calculate the crystallite size of MgO following the aforementioned Scherrer's equation, where the crystallite sizes of NH_4OH- and NaOH-based MgO were in the range of 10 – 25 nm. The agglomeration ratio, defined as G_{BET}/G_{XRD}, was obtained from the primary particle size, G_{BET}, which was calculated from SSA and from the crystallite size, G_{XRD}. G_{BET} was calculated following the equation: $G_{BET} = F/\rho S$. Where F is a particle-shape factor as 6, S the SSA (m^2/g), ρ theoretical density of MgO as 3.595 g/cm^3 (Itatani, Nomura et al. 1986). The G_{BET} values for NH_4OH- and NaOH-based MgO were in the range of 20–350 nm while the G_{BET}/G_{XRD} values ranged from 1.7-16.3. The lowest agglomeration ratio, 1.7, was from NH_4OH-based $Mg(OH)_2$ under 500 ^oC for 2 hours. Calcination temperature and duration had a significant influence on the crystallite sizes

and primary sizes, where the increase of temperature and duration significantly enlarged the crystallite sizes and primary sizes of MgO regardless of base type. This could be due to the spontaneous coagulation of primary particles at the growing temperatures and durations (Itatani, Itoh et al. 1993). Compared with NH_4OH -based MgO, NaOH-based MgO achieved higher agglomeration ratios at the higher calcination temperatures and durations, therefore resulting in lower SSA values as illustrated in Figure 5.4.

Table 5.3 Crystallite size, primary size and pore volume of MgO produced under different calcination temperatures and durations

		500 ℃			600 ℃			700 ℃		
		2 h	6h	12 h	2 h	6h	12 h	2 h	6h	12 h
NH_4OH-MgO	G_{XRD} (nm)	12.6	13.4	14.8	15.5	16.1	17.9	19.5	24.7	24.9
	G_{BET} (nm)	21.2	28.6	38.3	62.3	76.9	80.4	162.0	267.0	303.5
	G_{BET}/G_{XRD}	1.7	2.1	2.6	4.0	4.8	4.5	8.3	10.8	12.2
	Pore volume (cm^3/g)	0.445±0.041	0.371±0.031	0.240±0.023	0.157±0.013	0.117±0.012	0.109±0.017	0.041±0.032	0.029±0.003	0.016±0.002
NaOH-MgO	G_{XRD} (nm)	11.4	12.7	13.6	15.0	16.7	18.1	18.9	19.4	21.4
	G_{BET} (nm)	32.5	66.8	91.7	49.7	102.4	245.4	67.3	127.4	347.7
	G_{BET}/G_{XRD}	2.8	5.3	6.8	3.3	6.1	13.6	3.6	6.6	16.3
	Pore volume (cm^3/g)	0.317±0.036	0.160±0.013	0.083±0.007	0.166±0.014	0.058±0.006	0.024±0.003	0.160±0.023	0.056±0.006	0.017±0.002

5.3.2.4. Reactivity

Figure 5.5 shows the acid reactivity of MgO, obtained from the calcination of $Mg(OH)_2$, generated via the reaction of reject brine with NH_4OH and NaOH, under different calcination conditions. An increase in the neutralization time with an increase in the temperature and duration was observed in all cases, which was an indication of the reduction of reactivity. The decline in the reaction rate of MgO under elevated calcination conditions were also shown in

earlier studies (Mo, Deng et al. 2010, Jin and Al-Tabbaa 2014).

Amongst the two different bases used, NH_4OH-based MgO samples revealed shorter neutralization times in comparison to NaOH-based ones produced under lower calcination temperatures (500 ^oC). An increase in the calcination temperature from 500 to 700 ^oC caused a notable increase in the neutralization times of NH_4OH-based samples, during which those of NaOH-based samples demonstrated a gradual increase. These trends were in line with the SSA measurements reported earlier in Figure 5.4, where it was shown that the initially high SSA of NH_4OH-based samples demonstrated a sharp decrease with increasing calcination temperatures.

The influence of calcination conditions and base type on the properties of MgO can be also visualized via a comparison of the SSA and neutralization time (i.e. acid reactivity) of all the samples, as shown in Figure 5.6. The inverse correlation between SSA and reactivity could be clearly observed in all MgO samples, regardless of the utilized base type in accordance with previous studies (Aphane 2009, Mo, Deng et al. 2010, Jin and Al-Tabbaa 2014). Accordingly, higher SSA values corresponded to shorter neutralization times, which was an indication of the higher reactivity of MgO. Alternatively, lower SSA led to longer neutralization times associated with the lower reactivity and slower reaction of MgO. Although the acid reactivity test could not fully distinguish amongst MgO samples with high SSA values (> 40 m^2/g) as the neutralization time demonstrated by these samples were relatively short, the obtained results clearly indicated the relationship between the two parameters, highlighting the importance of production conditions on the properties of the final product.

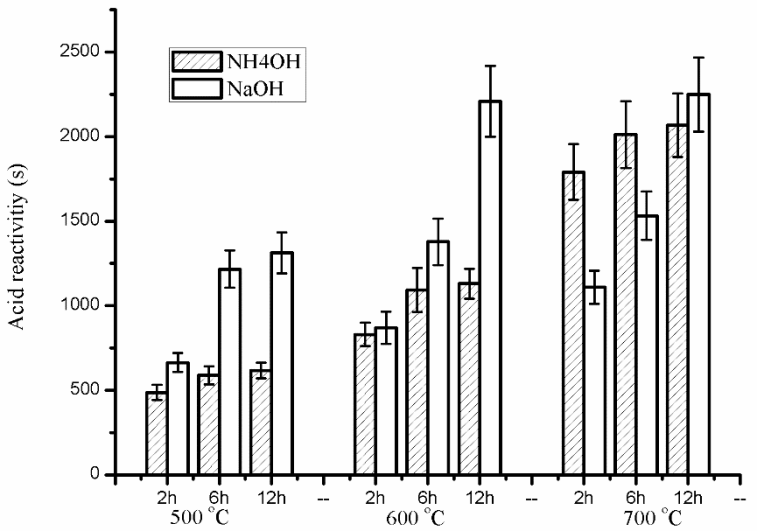

Figure 5.5 Effect of calcination temperature and duration on the neutralization time of reactive MgO

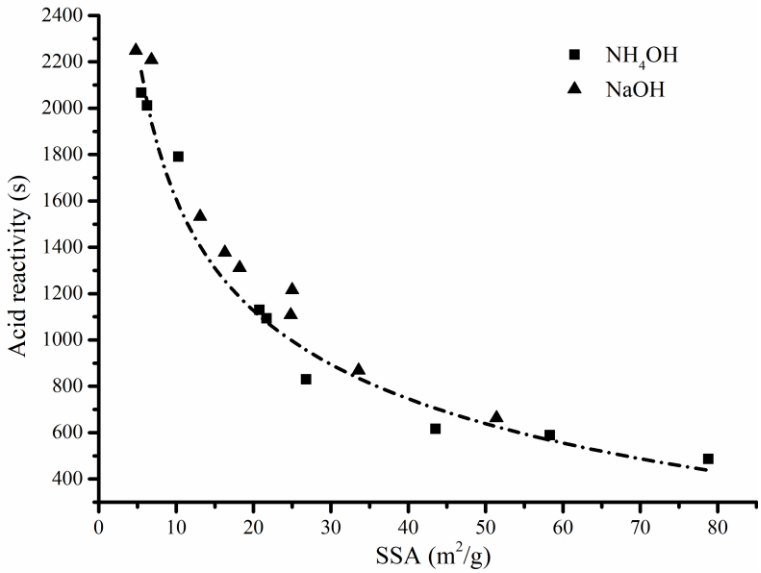

Figure 5.6 Relationship between the neutralization time and SSA of MgO

5.3.2.5. FESEM

A further investigation on the correlation of the calcination conditions (i.e. temperature and duration) and the base type (i.e. NH_4OH and NaOH) with the morphology of the final product (MgO) was revealed through FESEM images, as shown in Figure 5.7 and Figure 5.8. A single

particle of MgO consisted of layered grains, which were inherited from the parent material, $Mg(OH)_2$. Increasing the calcination temperature from 500 to 700 ℃ had a more profound effect on the size of the MgO grains, resulting in a significant growth in crystallite size, which was accompanied with the reduction of porosity, as seen in Figure 5.7a-c and Table 5.3. The effect of the calcination duration on the morphology of NH_4OH-based MgO was revealed in Figure 5.7c-e. MgO grains demonstrated a noticeable growth as the calcination duration increased from 2 to 12 hours. These changes in the morphology of MgO grains could clearly explain the reduction of SSA and the corresponding increase of neutralization time under elevated calcination temperatures and durations.

A comparison of Figure 5.7a and Figure 5.8a revealed the porous structure of NH_4OH-based MgO in comparison to NaOH-based samples produced under 500 ℃ for 2 hours. Increasing the calcination temperature and duration to 700 ℃ for 12 hours led to an increase in the growth of NH_4OH-based MgO grains, which was much more noticeable than those observed in NaOH-based samples (24.9 vs. 21.4 nm) as demonstrated in Figure 5.7e and Figure 5.8b and Table 5.3. The increase in the dimensions of the MgO grains under high calcination temperatures and durations was attributed to the loss of water during the decomposition of $Mg(OH)_2$, which facilitated the formation of a porous structure. This initial porosity was gradually reduced as the MgO grains grew further due to continuous sintering as shown in Table 5.3, which was in line with the findings reported by earlier studies (Mo, Deng et al. 2010).

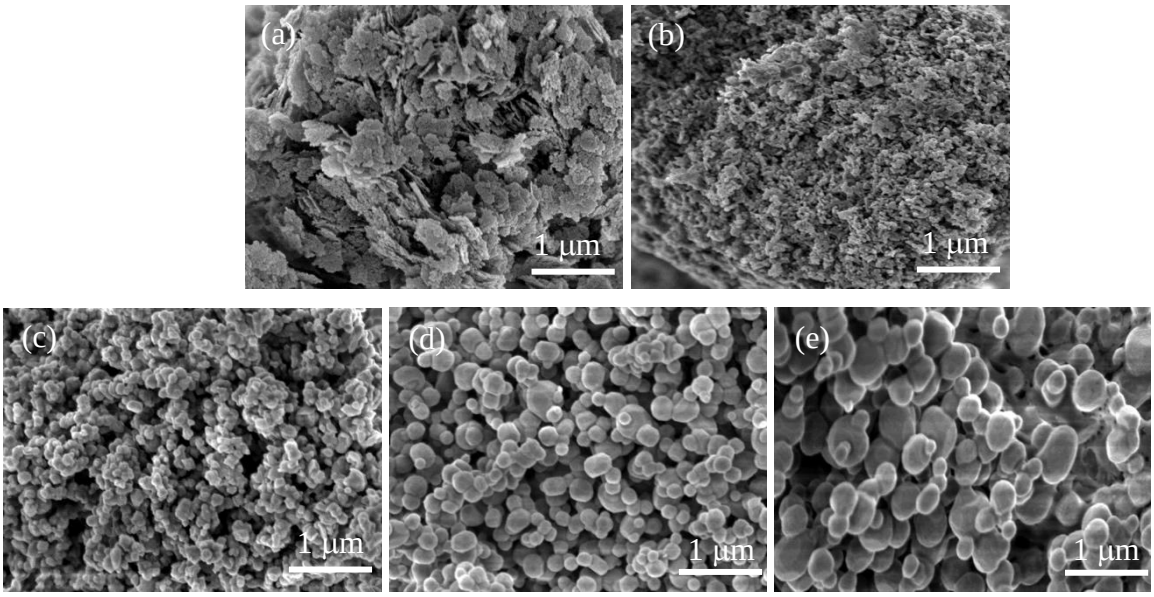

Figure 5.7 FESEM images of MgO obtained from the calcination of $Mg(OH)_2$ that was synthesized via the reaction of reject brine with NH_4OH under (a) 500 ℃-2h, (b) 600 ℃-2h, (c) 700 ℃-2h, (d) 700 ℃-6h and (e) 700 ℃-12h

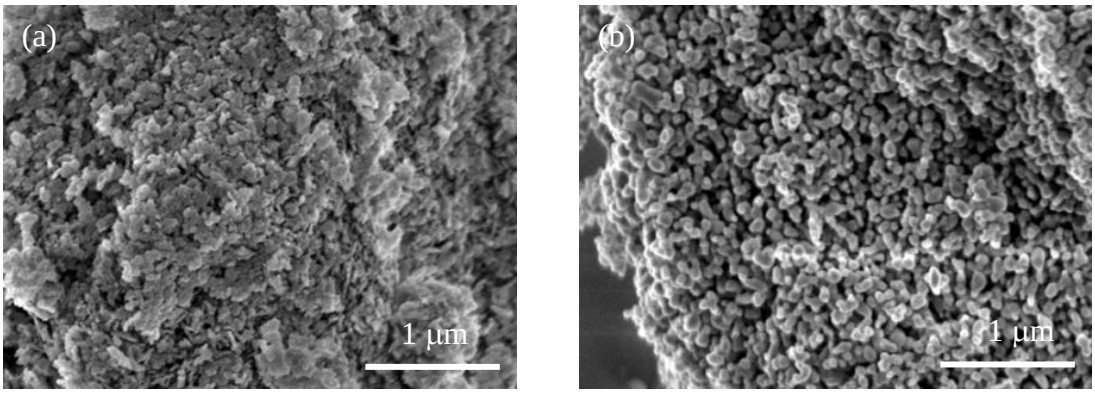

Figure 5.8 FESEM images of MgO obtained from the calcination of $Mg(OH)_2$ that was synthesized via the reaction of reject brine with NaOH under (a) 500 ℃-2h and (b) 700 ℃-12h

5.4. Conclusions

This study presented a comprehensive investigation on the properties of MgO produced through the calcination of $Mg(OH)_2$ that was synthesized from reject brine obtained from a local desalination plant. The influence of the two different alkali sources (NH_4OH and NaOH) used in

the synthesis of $Mg(OH)_2$, on the properties of $Mg(OH)_2$ and MgO was reported. The calcination conditions used during the production of MgO were varied between 500-700 ℃ (temperature) and 2-12 hours (residence time) to assess their effects on the key properties of MgO, such as the textural properties, acid reactivity, composition, and morphology.

Type of alkali source used during the synthesis of $Mg(OH)_2$ had a notable influence on not only the properties of $Mg(OH)_2$, but also the reactivity and microstructure of MgO. The use of NH_4OH generated MgO samples with porous structures, which enabled higher SSA and reactivities than those observed in NaOH-based samples calcined under lower temperatures. The SSA and reactivity of NH_4OH-based MgO were more vulnerable to the changes in the calcination conditions and therefore indicated a sharper decline at higher calcination temperatures and durations, which was associated with its relatively more porous structure in comparison to NaOH-based MgO.

Other than the alkali source, the calcination conditions were one of the key parameters controlling the properties of the final MgO. Increasing the temperature and duration of calcination led to lower SSA and reactivities in all samples, regardless of the alkali type. Analysis of the phase transitions and microstructural changes under different conditions revealed the similar compositions of all samples, albeit the clear variations that were observed in the morphologies of the final product. Out of all the samples studied, NH_4OH-based $Mg(OH)_2$ calcined at 500 ℃ for 2 hours resulted in the most reactive MgO samples, which possessed the highest SSA of 78.8 m^2/g. which can be used in various applications within the food, cosmetics, pharmaceutical and construction industries (Lee, Jung et al. 2004, Shand 2006, Moussavi and Mahmoudi 2009, Pilarska, Klapiszewski et al. 2017). Overall, the obtained results clearly indicate the feasibility of using reject brine as a reliable and possibly a sustainable source for the recovery of MgO, whose properties and therefore suitability in various applications, are based on the production conditions (i.e. calcination temperature and duration) as well as the materials (i.e. alkali source) used during this process.

Chapter 6 Production of Mg-carbonates via the sequestration of CO_2 in $Mg(OH)_2$ slurries generated from reject brine

6.1. Introduction

Desalination is a process that salts are removed from saline water to produce fresh water, e.g. potable water. In coastal regions such as Singapore where sources of fresh water are limited, desalination provides a feasible option to produce fresh water to meet residential and industrial demands. Currently, the desalinated water from two seawater reverse-osmosis plants provides 100 million gallons water per day, which delivers 25% of Singapore's current water supply. Moreover, three additional desalination plants are being built, which will bring the number of desalination plants to 5, designed to provide a total amount of 190 million gallons (852,150 m^3) of water per day by 2020 (ST 2016). Globally, production of desalinated water from 18,426 desalination plants exceeds 86.8 million cubic meters per day (IDA 2015). Production of desalinated water generates about equal amount of reject brine (El-Naas 2011), a high salt concentration waste by-product produced at the end of the desalination process (Adham, Hussain et al. 2013). The most common way to dispose of reject brine is to discharge it back to the sea. With high concentration and salinity, reject brine is denser than the feedstock supply and tends to accumulate to the bottom of the sea without sufficient mixing. Discharge of untreated reject brine may cause increased salinity of the seawater, which was shown to have an altering effect on the flora and fauna and affects all of the organisms of that ecosystem in a negative way, either directly or indirectly (Mohamed, Maraqa et al. 2005).

The disposal and management of reject brine; thus, remains a major challenge as well as an environmental threat (Mohamed, Maraqa et al. 2005, El-Naas, Al-Marzouqi et al. 2010). To solve this, several novel ideas have been proposed to make the best use of reject brine. For instance, reject brine can be recycled and mixed with concrete or asphalt to produce saltcrete (Drom; and Loveland 1998) for road construction. A more recent method of brine disposal is to treat brine by reverse osmosis which produces additional clean water and super concentrated brine waste. The high concentrated brine waste is then dried out to evaporate any loose water, after which the remaining salts can be harvested for resale (Ahmed, Arakel et al. 2003, Arnal,

Sancho et al. 2005, Kim 2011). The current treatment options of reject brine have not achieved a satisfactory solution to solve the challenge. Under the concept of carbon capture and storage (CCS), one novel idea is to target the reject brine as the CO_2 reservoir to reduce the carbon footprint of the desalination process (El-Naas 2011).

CCS provides a feasible and promising method to reduce the green house gas emissions generated from fossile fuels combustion (Herzog 1998, Rao and Rubin 2002). Fossile fuels have been the world's primiary enery source over the world, providing over 85% of the energy demands worldwide due to the low cost and reliable technology for energy production (Agency and Agency 2007). However, nearly 83% of the green house gas emissions are coming from combustion and nonfuel uses of fossil fuels (Figueroa, Fout et al. 2008). CO_2, which is the main green house gas, has caused most of the global warming since it has the highest positive radiative forcing and is far more abundent in the atmosphere than other heat-trapping gases (Morita, Robinson et al. 2001, Forster, Ramaswamy et al. 2007). The concentration of CO_2 in the atmoshere has increased ~30% from 325 parts per million (ppm) at the beginning of the industrial era in 1970 to 409.7 ppm in May 2017 measured in Mauna Loa Observatory (Dlugokencky and Tans 2017). Consequently, much attention has been drawn to the carbon management (Arakawa, Aresta et al. 2001, Lal 2004, Haszeldine 2009). CCS concept covers broad fields such as ocean, terrestrial, geological, biological and chemical approaches to store CO_2 gas in the long term (Botha and Strydom 2001, Kloprogge, Martens et al. 2003, Rendek, Ducom et al. 2006, Ferrini, De Vito et al. 2009), among which mineral carbonation via the reation of CO_2 with saline aquafers is one of the most promising geologic CO_2 storage options (Huijgen, Witkamp et al. 2005, Gerdemann, O'Connor et al. 2007, Oelkers, Gislason et al. 2008). Magnesium-based minerals have attracted great interest due to their ability to sequestrate anthropogenic CO_2 in the thermally stable and long-lasting carbonates to counterpart the global warming (O'Connor, Dahlin et al. 2002, Maroto-Valer, Fauth et al. 2005, Hanchen, Prigiobbe et al. 2008, Sanna, Uibu et al. 2014). MgO-based binders are known to gain strength via carbonation, thereby enabling the permanent sequestration of carbon dioxide (CO_2) within a range of construction products (Harrison 2008, Liska, Al-Tabbaa et al. 2012a, Liska, Al-Tabbaa et al. 2012b, Al-Tabbaa 2013, Unluer and Al-Tabbaa 2013, Unluer and Al-Tabbaa 2014).

Although the most thermodynamically stable carbonate for magnesium is the anhydrous form – magnesite (i.e., magnesium carbonate, $MgCO_3$) (Christ and Hostetler 1970, Kittrick and Peryea 1986, Wolery 1992), the formation of magnesite at the ambient condition is virtually impossible. Instead, hydrated magnesium carbonates (HMCs) will form due to the high hydration energy of Mg ions in the solution. HMCs are a class of magnesium compounds that form in MgO-CO_2-H_2O systems, where the carbonation of magnesium systems generate a variety of phases, including dypingite ($Mg_5(CO_3)_4(OH)_2 \cdot 5H_2O$) (Ballirano, De Vito et al. 2013), hydromagnesite ($Mg_5(CO_3)_4(OH)_2 \cdot 4H_2O$) (Teir, Eloneva et al. 2009), nesquehonite ($MgCO_3 \cdot 3H_2O$) (Wang, Li et al. 2008, Ferrini, De Vito et al. 2009), etc,. Ferrini et al. (2009) proposed the synthesis of needle-like nesquehonite through the reaction of CO_2 gas with magnesium chloride solution (Ferrini, De Vito et al. 2009). The process was kinetically favoured and simple and CO_2 was reserved in the thermo-stable HMCs. The efficiency of CO_2 sequestration with simulated wastewater ($MgCl_2$ solution) has been tested to achieve a high efficiency of ~80% with respect to a low-salinity solution of 7 g/L $MgCl_2$ (Mignardi, De Vito et al. 2011).

The formation of different classes of HMCs with different morphologies is influenced by several factors, e.g. temperature, pH and CO_2 partial pressure (Hanchen, Prigiobbe et al. 2008, Hopkinson, Kristova et al. 2012). The precipitation of nesquehonite with needle-like morphology from an aqueous solution occurs commonly under ambient conditions (Botha and Strydom 2001, Wang, Li et al. 2008, Ferrini, De Vito et al. 2009). With the increase of reaction temperatures (50-80 ℃) and pH values, needle-like nesquehonite transforms to hydromagnesite with sheet-like morphology (Zhang, Zheng et al. 2006). Hydromagnesite was reported to form at 120 ℃ and P_{CO2} of 3 bar, which gradually transformed to magnesite within 5–15 hours. However, a further increase of P_{CO2} to 100 bar at 120 ℃ resulted in the direct precipitation of magnesite (Hanchen, Prigiobbe et al. 2008). The thermal behaviour of the synthesized HMCs (e.g. nesquehonite) has been tested through real time X-ray diffraction (XRD), which indicated that nesquehonite and dypingite remained thermally and structurally stable up to 100 ℃ and 162 ℃, respectively (Ballirano, De Vito et al. 2010, Ballirano, De Vito et al. 2013). Under the continued thermal treatment, nesquehonite transforms into magnesite which was even thermally stable up to ~327 ℃, while dypingite transited into hydromagnesite which was thermally stable up to ~320 ℃, assuring the safety of long time storage of CO_2.

Although numerous researchers have conducted mineral trapping of CO_2 into saline aquafers (Soong, Goodman et al. 2004, Soong, Fauth et al. 2006, Ferrini, De Vito et al. 2009, Ballirano, De Vito et al. 2010, Mignardi, De Vito et al. 2011, Ballirano, De Vito et al. 2013), limited research has been reported to study the sequestration of CO_2 and explore the efficiency of carbon storage into $Mg(OH)_2$ slurries generated from reject brine. Furthermore, a clear relationship between the efficiency of carbon storage and the phase of HMCs must be understood. In this study, we proposed to synthesize HMCs from the highly reactive $Mg(OH)_2$ slurry generated from reject brine through the sequestration of CO_2. Our previous studies have revealed that highly reactive $Mg(OH)_2$ and MgO can be obtained from reject brine via the addition of alkalis and well-controlled calcination process (Dong, Unluer et al. 2017, Dong, Unluer et al. 2018, Dong, Unluer et al. 2018). In this study, $Mg(OH)_2$ was firstly precipitated from reject brine via the addition of NaOH, followed by the direct carbonation of $Mg(OH)_2$ slurry via the injection of gaseous CO_2. Commercial $Mg(OH)_2$ was also used for comparison purpose in order to understand the influences of $Mg(OH)_2/CO_2$ molar ratios and pH on the microstructure of HMCs formed. The feasibility of using the reject brine as a carbon storage source was illustrated in this paper.

6.2. Materials and Methodology

6.2.1. Materials

The composition of the reject brine collected from a local desalination plant, which was obtained via inductively coupled plasma-optical emission spectroscopy (ICP-OES), is summarized in Table 6.1. $Mg(OH)_2$ (i.e. used as a source of magnesium) and sodium hydroxide (NaOH) of analytical grade (i.e. used as an alkali source), were both supplied by VWR Pte Ltd in Singapore. Pure compressed CO_2 was provided from Leeden National Oxygen Ltd in Singapore.

Table 6.1 Chemical composition of reject brine used in this study.

Element/ Concentration	Cl	Na	SO_4	Mg	K	Ca	Sr	B	Si	Li	P	Al
ppm	65593.1 ± 67.1	13580 ±4 3.5	4322.6 ± 8.8	1718.0 ± 5.4	845.7 ± 5.3	471.3 ± 1.0	14.6 ± 0.1	3.8 ±0 .1	3. 7	0. 3	0. 2	0. 1

6.2.2. Methodology

Table 6.2 Physical properties of two type of $Mg(OH)_2$ used in this research.

	Purity %	SSA (m^2/g)
$Mg(OH)_2$ commercial	92	4.8
$Mg(OH)_2$ reject brine	94	7.4

Two types of $Mg(OH)_2$ were prepared with material properties listed in Table 6.2. One is from commercial $Mg(OH)_2$, with a purity of 92%, which was used in the section 6.3.1. The other is synthesized via the reaction of reject brine with NaOH as described in (Dong, Unluer et al. 2018), which was denoted as $Mg(OH)_2$ reject brine in short. The experiment was carried out by sparging CO_2 at a rate of ~100 ml/min through 200 ml slurry containing 0.82 g $Mg(OH)_2$ at room temperature at designed condition ($Mg(OH)_2$:CO_2 molar ratio (1:1–1:7) and reaction pH (8–14)). A pH/thermometer probe was inserted into the slurry to continuously monitor the temperature and pH during the experiment. The pH of reject brine as received was measured and recorded at a value of ~8.0 throughout all experiments while the reaction temperature was recorded around 25 ℃ throughout the reaction. 1 M NaOH was added into the slurry to maintain a constant pH environment throughout the reaction. A CO_2 flowmeter was used to monitor and record the exact volume of CO_2 diffused into the slurry. Once the volume of the diffused CO_2 reached the designed value, calculated from the $Mg(OH)_2$:CO_2 molar ratio, the reaction was terminated.

HMCs that precipitated at the end of the reaction were separated from the solution through a centrifuge and washed three times using ultra-pure water. The washed samples were then fully oven-dried at 40 ℃ (i.e. kept low to avoid any phase changes) before being ground into powder form. The prepared powder was finally passed through a 125 μm sieve for further microstructural analyses.

ICP-OES (PerkinElmer Optima DV2000) was employed to measure the chemical composition of the reject brine and the obtained residue before and after reactions. A combination of microstructural characterization techniques such as X-ray powder diffraction (XRD), field emission scanning electron microscopy (FESEM) and thermogravimetric/differential thermal analysis (TG/DTA) were utilized to characterize the precipitated solids. XRD was performed via a Bruker D8 Advance with a Cu Kα (wavelength of 1.5405 Å) source under the operation conditions of 40 kV and 40 mA, scanning rate of 0.02 °/step and 2θ range from 5 to 70°. A JSM-7600F FESEM was used to examine the morphology of the solids by imaging powder surface at an accelerating voltage of 2kv. TG/DTA was operated on a PyrisDiamond TGA 4000 at a heating rate of 10 ℃/min under air flow to provide a quantitative analysis of the phases in the synthesized samples.

6.3. Results and Discussion

6.3.1. Characterization of HMCs synthesized from $Mg(OH)_2$ slurry

6.3.1.1. Effect of $Mg(OH)_2/CO_2$ molar ratio

Figure 6.1 shows the FESEM images of all samples obtained under a constant pH of 8 while the $Mg(OH)_2$:CO_2 molar ratio was varied between 1:1 and 1:7. The morphologies of the obtained HMCs dramatically changed with the $Mg(OH)_2$:CO_2 molar ratio. For instance, the rosette-like morphology observed at a $Mg(OH)_2$:CO_2 molar ratio of 1:1 (Figure 6.1(a)) was eventually replaced by rod-like structures with smooth surfaces when this ratio gradually increased to 1:6 (Figure 6.1(b)-(f)). The boundaries of these rod-like carbonate phases became clearer with an increase in the $Mg(OH)_2$:CO_2 molar ratio. A further increase in the $Mg(OH)_2$:CO_2 molar ratio to 1:7 revealed the formation of a layer of rosette-like flakes around the original rod-like morphology, producing a “house of cards” texture (Hao and Du 2009), as shown in Figure 6.1(g).

Figure 6.2 indicates the XRD diffractograms of the same set of samples obtained under a pH of 8 at different $Mg(OH)_2$:CO_2 molar ratios. The XRD patterns confirmed that the rosette- and rod-like particles observes in Figure 6.1 could be attributed to dypingite and nesquehonite, respectively. These morphological observations were in line with the previous literature (Ferrini, De Vito et al. 2009, Hopkinson, Kristova et al. 2012, Ballirano, De Vito et al. 2013), where the distinct morphologies of dypingite and nesquehonite were reported. At a $Mg(OH)_2$:CO_2 molar ratio of 1:1, the precipitate consisted of dypingite, uncarbonated brucite and dolomite that was present as an impurity within $Mg(OH)_2$. An increase in the $Mg(OH)_2$:CO_2 molar ratio to 1:2 revealed a reduction in the amount of uncarbonated brucite, resulting in the domination of nesquehonite. These results corresponded well with the chemical composition of different carbonate phases. Accordingly, the abundance of nesquehonite could be associated with the availability of higher amounts of CO_2 introduced into the mix under higher $Mg(OH)_2$:CO_2 molar ratios. This is because nesquehonite ($MgCO_3$•$3H_2O$) requires a higher Mg:CO_2 molar ratio of 1:1 than dypingite ($Mg_5(CO_3)_4(OH)_2$•$5(H_2O)$), which can theoretically form at a corresponding ratio of 1:0.8. An increase in the $Mg(OH)_2$:CO_2 molar ratio from 1:2 to 1:7 revealed samples, in which nesquehonite continued to dominate the composition, without a significant change in the XRD patterns, which was consistent with the observations made in Figure 6.1.

As revealed in Figure 6.1, the change in the morphology of HMCs from a rod-like to a “house of cards” texture when the $Mg(OH)_2$:CO_2 molar ratio increased from 1:6 to 1:7 was also reported in previous studies (Hao and Du 2009, Hopkinson, Kristova et al. 2012), where this phenomenon was observed when nesquehonite was subjected to continuous high temperatures, gradually transferring to hydromagnesite. Nesquehonite, which is unstable at near surface ambient conditions (Hopkinson, Kristova et al. 2012), is known to transform into hydromagnesite (or dypingite as a transitional phase) at increased temperatures, CO_2 partial pressure or elevated pH, depending on the reaction conditions (Hopkinson, Kristova et al. 2012). Previous studies (Hanchen, Prigiobbe et al. 2008, Hopkinson, Kristova et al. 2012) have reported the presence of a variety of metastable phases through the dissolution-precipitation reactions involving HMCs such as nesquehonite, dypingite and hydromagnesite. This change in texture, attributed to a dissolution-recrystallization-self-assembly growth mechanism (Hao and Du 2009, Hopkinson,

Kristova et al. 2012), could indicate the dissolution of the surface of nesquehonite when exposed to high concentrations of CO_2. During this process, the presence of nesquehonite could enable the nucleation of hydromagnesite/dypingite crystals on their surfaces under the presence of elevated CO_2 levels. In this respect, the "house of cards" texture presents the transition from a previously smooth surface to a surface composed of a flaky structure, whose formation depends on the dissolving rate of nesquehonite and the nucleation rate of hydromagnesite/dypingite. When the dissolving rate of nesquehonite was lower than the precipitation rate of hydromagnesite/dypingite, the "house of cards" texture occurred (Hao and Du 2009, Hopkinson, Kristova et al. 2012).

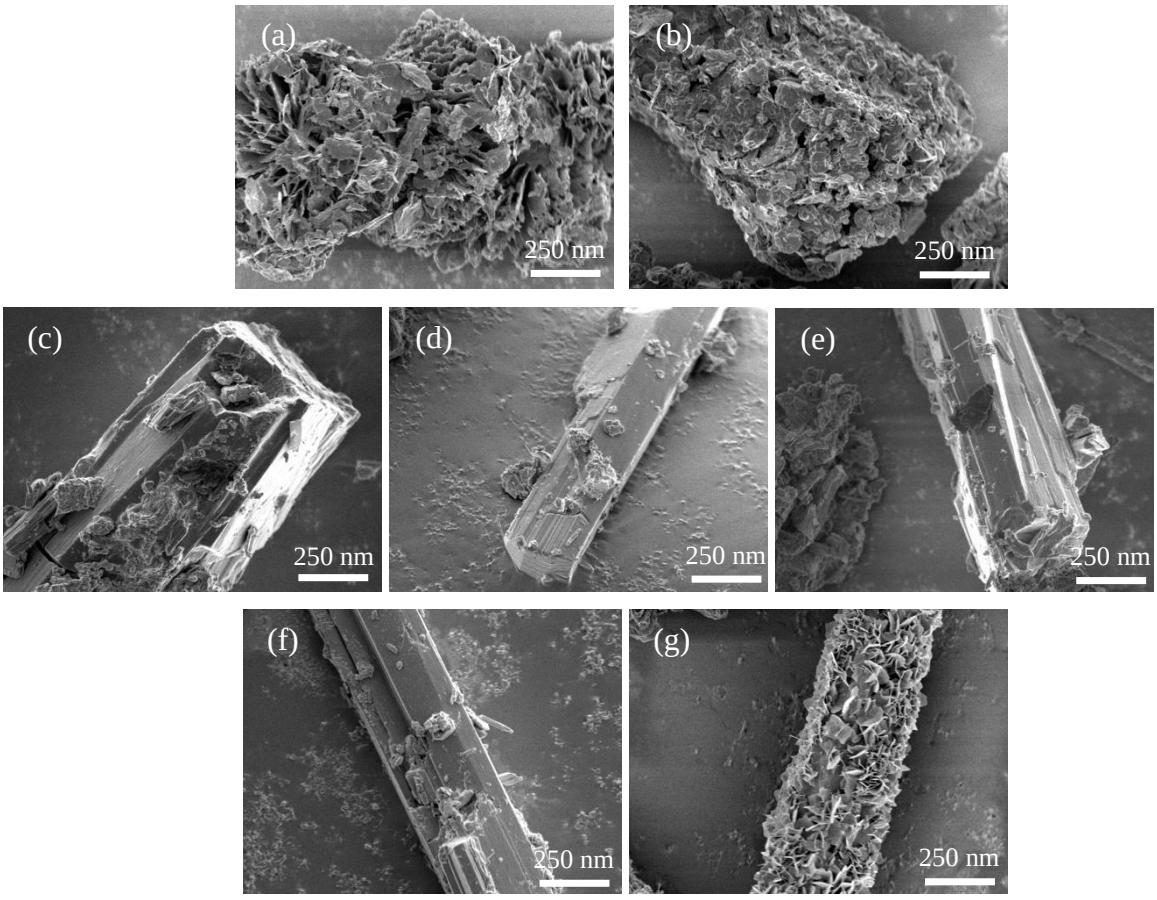

Figure 6.1 FESEM images of HMCs obtained under a pH of 8 at different $Mg(OH)_2$:CO_2 molar ratios of (a) 1:1, (b) 1:2, (c) 1:3, (d) 1:4, (e) 1:5, (f) 1:6 and (g) 1:7

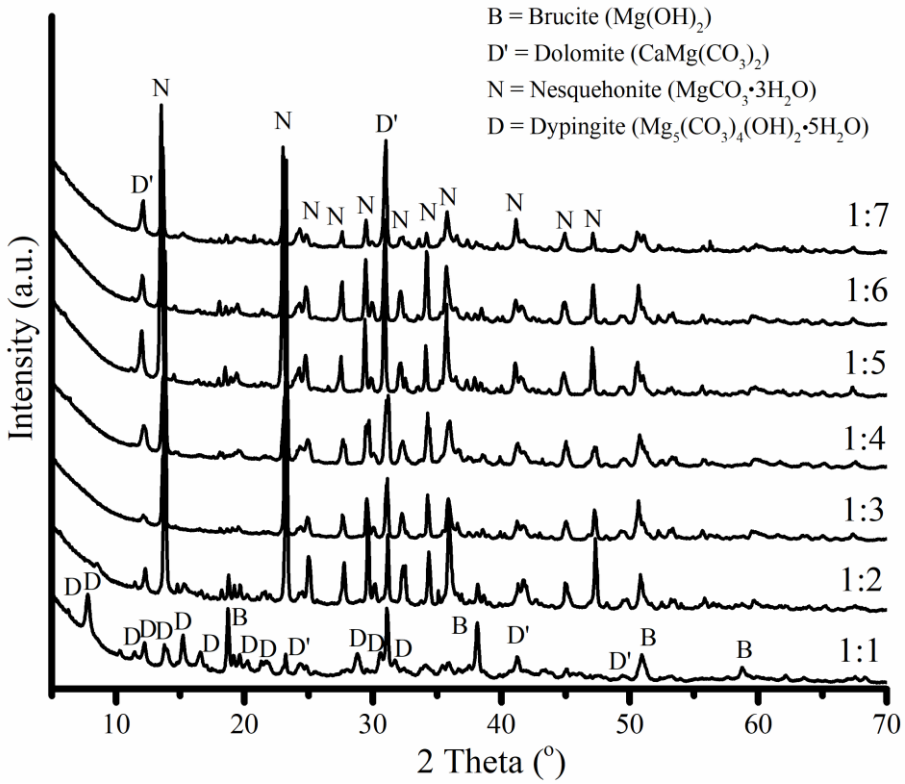

Figure 6.2 XRD diffractograms of HMCs obtained under a pH of 8 at different $Mg(OH)_2$:CO_2 molar ratios

6.3.1.2. Effect of pH at a $Mg(OH)_2$:CO_2 molar ratio of 1:1

Figure 6.3 illustrates the FESEM images of the samples obtained under different pH values ranging between 8 and 11, at a constant $Mg(OH)_2$:CO_2 molar ratio of 1:1. At the lower pH values of < 11, the obtained carbonates displayed rosette-like morphologies with an average dimension of ~2 μm, as shown in Figure 6.3(a)-(c). These rosette-like formations were confirmed to be dypingite, as shown by the XRD patterns presented in Figure 6.4. As the pH increased from 8 to 10, the intensity of the uncarbonated brucite peak revealed a decrease relative to the others, possibly indicating a reduction in the amount of brucite and an associated higher degree of carbonation at elevated pH levels. This increase in the carbonation degree could be associated with the higher CO_3^{2-}:HCO_3^- ratios in the prepared solutions at elevated pH levels. An increase in the pH led to higher concentrations of OH^-, therefore enabling the conversion of HCO_3^- to CO_3^{2-}, which then reacted with Mg^{2+}, leading to the precipitation of higher amounts of HMCs in the solution. Alternatively, brucite did not carbonate at a further increase in the pH from 11 to 14 and

remained its flake-like morphology in Figure 6.3(d), which may be because brucite is always at its supre-saturation state at high pH values. These results were in line with the findings reported in previous studies, where the optimal pH for the carbonation of brucite was shown to be around 9 (Teir, Kuusik et al. 2007, Wu, Luo et al. 2014).

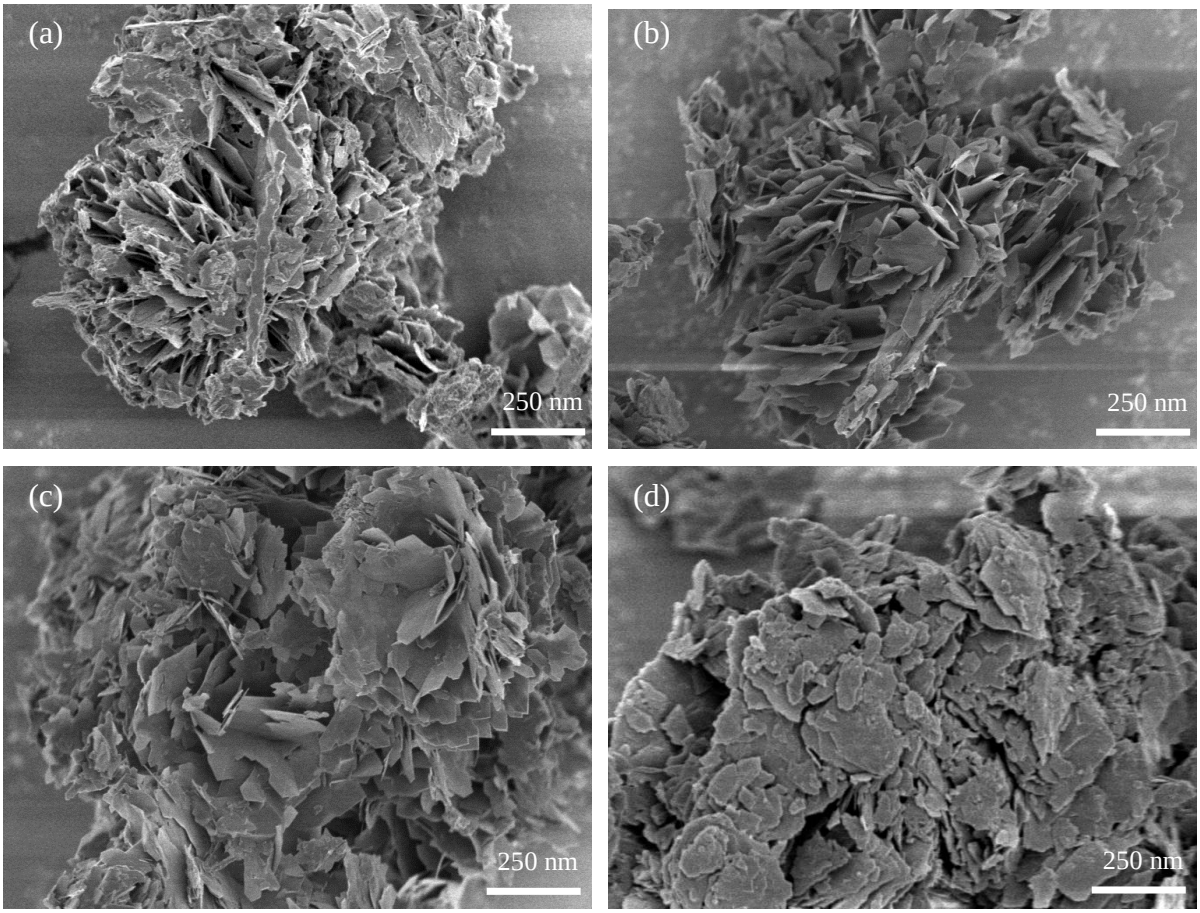

Figure 6.3 FESEM images of HMCs obtained at a $Mg(OH)_2$:CO_2 molar ratio of 1:1 under different pH values of (a) 8, (b) 9, (c) 10 and (d) 11

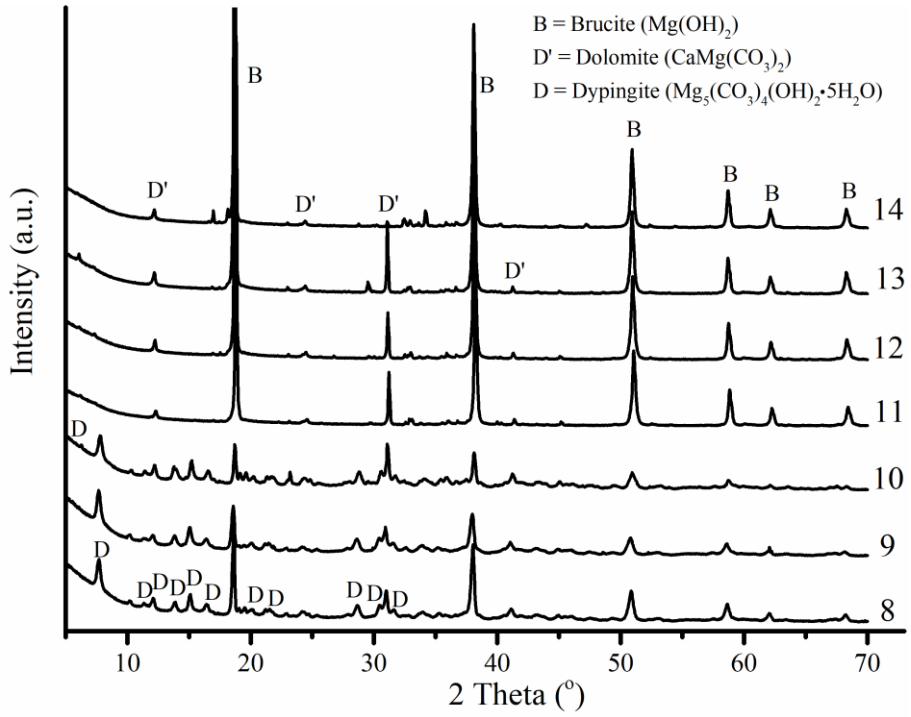

Figure 6.4 XRD diffractograms of HMCs obtained at a $Mg(OH)_2$:CO_2 molar ratio of 1:1 under different pH values

6.3.1.3. Effect of pH at a $Mg(OH)_2$:CO_2 molar ratio of 1:2

Figure 6.5 displays the morphologies of HMCs obtained under different pH values at a $Mg(OH)_2$:CO_2 molar ratio of 1:2. Different from HMCs obtained at a $Mg(OH)_2$:CO_2 molar ratio of 1:1, where the presence of dypingite with a rosette-like morphology dominated regardless of the pH value; HMCs obtained at a $Mg(OH)_2$:CO_2 molar ratio of 1:2 clearly demonstrated a different morphology. Instead of the previously observed rosette-like plates, a rod-like structure presenting the "house of cards" texture was seen in samples obtained under pH values of 8 and 9 (Figure 6.5(a) and (b)). An increase in the pH from 8 onwards resulted in the distortion of the originally clear borders of the nesquehonite crystals, whose shape transformed from the rod-like structure to a cluster of flakes forming on top. This change was mostly obvious at pH values of 10 and 11 (Figure 6.5(c) and (d)), which revealed the formation of flake-like clusters with clearly defined boundaries at a pH of 11.

The formation of nesquehonite at pH value of 8, 9 and 10 was confirmed by the XRD patterns

shown in Figure 6.6. In line with the findings obtained under a $Mg(OH)_2$:CO_2 molar ratio of 1:1 as revealed in Figure 6.4, brucite with a flake-like morphology was not observed to carbonate with the further increase in the pH to 11 till 14. This "house of cards" texture observed within the prepared samples was attributed to the dissolution-recrystallization-self-assembly growth mechanism as explained in the aforementioned text. The elevated pH used in the experiments conducted in this study increased the solubility of CO_2 in the solution, therefore accelerating the formation of this distinguished morphology at a $Mg(OH)_2$:CO_2 molar ratio of 1:2 compared to 1:7 when pH was 8. This has led to a dissolution of the surface of nesquehonite and served as the nucleation points for further hydromagnesite/dypingite plates growing with excessive CO_2 at the surface.

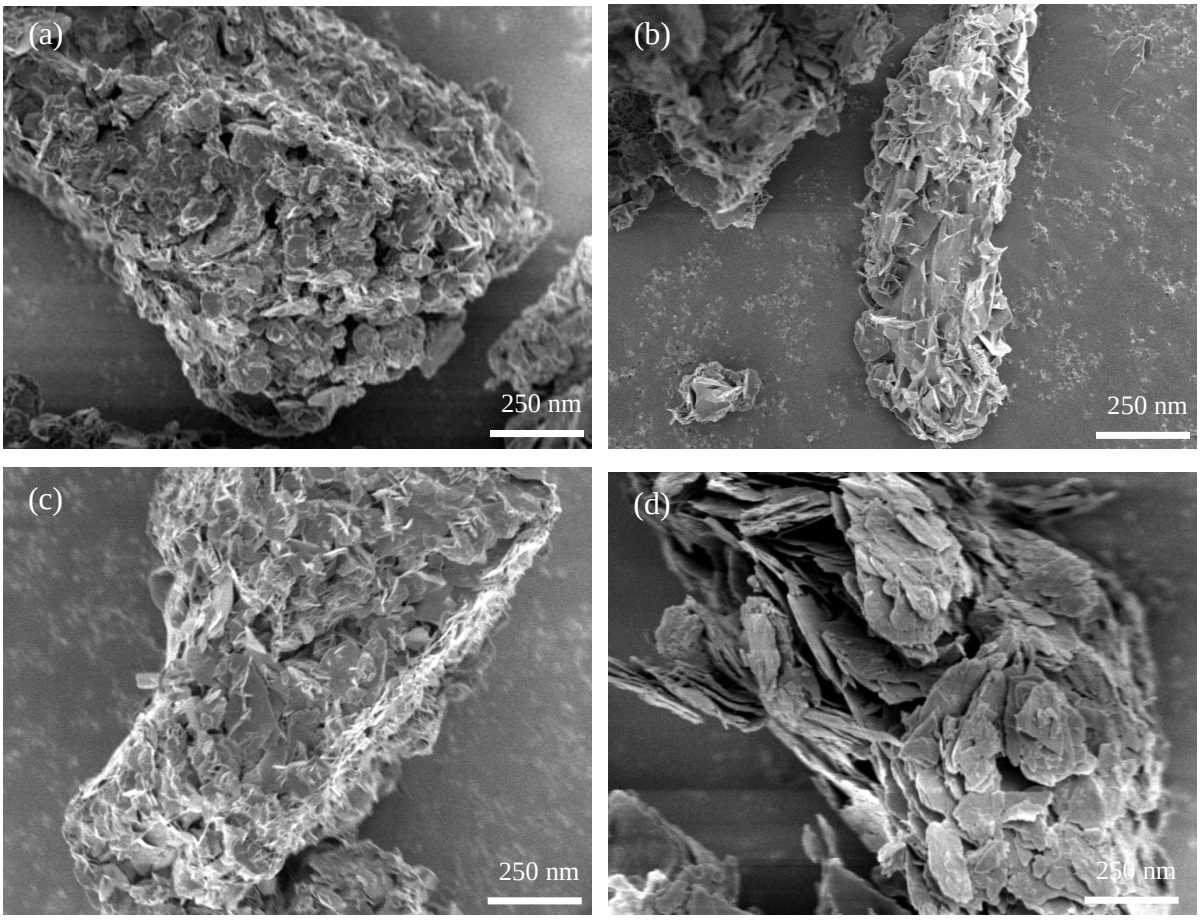

Figure 6.5 Typical FESEM images of HMCs obtained at a $Mg(OH)_2$:CO_2 molar ratio of 1:2 under different pH values of (a) 8, (b) 9, (c) 10 and (d) 11

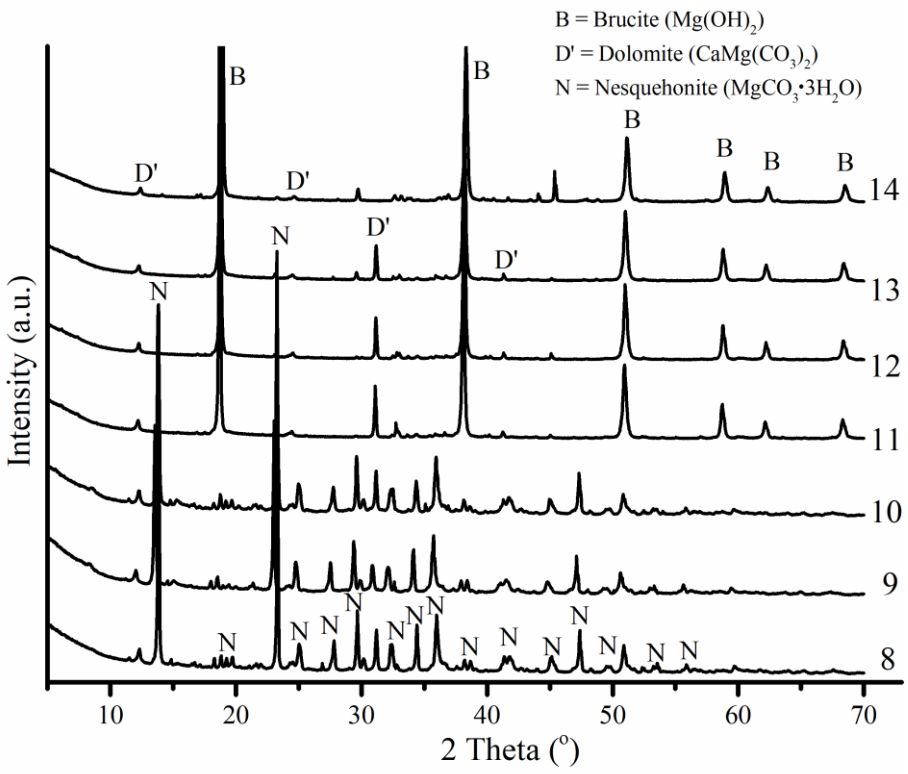

Figure 6.6 XRD diffractograms of HMCs obtained at a $Mg(OH)_2$:CO_2 molar ratio of 1:2 under different pH values

6.3.2. Comparison of reject brine vs. $Mg(OH)_2$ slurry as a source for the synthesis of HMCs

This section aims to provide a comparison of HMCs carbonated from $Mg(OH)_2$ obtained from reject brine and commercially purchased, whose detailed characterization was presented earlier in Section 3.1. The findings presented here explore the feasibility of using reject brine as a source for the long-term storage of anthropogenic CO_2.

6.3.2.1. Microstructure of the HMCs

Figure 6.7 provides a comparison of the morphologies of HMCs synthesized from $Mg(OH)_2$ slurry and reject brine under a constant pH and $Mg(OH)_2$:CO_2 molar ratio of 8 and 1:1, respectively. As shown in Figure 6.7(a), the carbonate crystals obtained via the use of $Mg(OH)_2$ slurry led to a rosette-like morphology. Alternatively, the carbonation of reject brine led to the formation of a needle-like morphology with clear boundaries, as seen in Figure 6.7(b). The

compositions of these rosette- and needle-like particles were confirmed to be nesquehonite and dypingite by XRD patterns revealed in Figure 6.8, respectively. The formation of different Mg-carbonate phases via the two sources could be associated with the relatively higher reactivity of $Mg(OH)_2$ prepared from reject brine when compared to that of $Mg(OH)_2$ slurry (i.e. with a specific surface area of 7.4 vs. 4.8 m^2/g as tested by BET analysis). The carbonation of $Mg(OH)_2$ with a higher reactivity could have captured more CO_2 and enabled the formation of nesquehonite as opposed to dypingite since nesquehonite requires a higher $Mg:CO_2$ molar ratio as explained in the aforementioned text. This difference in the reactivity of the two samples was also reflected by the absence of the residual brucite peaks in reject brine, as opposed to the clearly defined uncarbonated brucite peaks observed in the $Mg(OH)_2$ slurry, as seen in Figure 6.8.

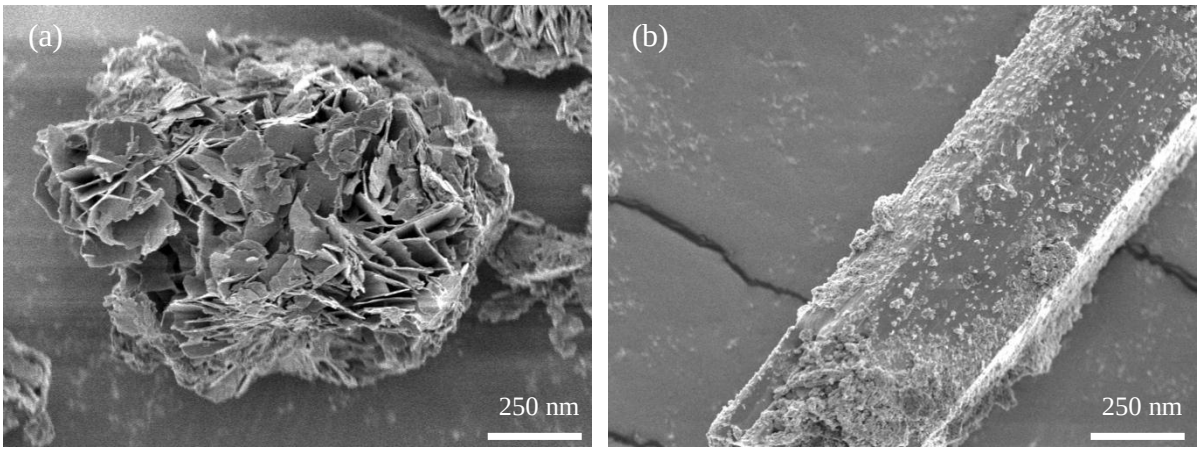

Figure 6.7 SEM images of HMCs obtained at a $Mg(OH)_2:CO_2$ molar ratio of 1:1 under a pH of 8, showing (a) $Mg(OH)_2$ slurry and (b) reject brine

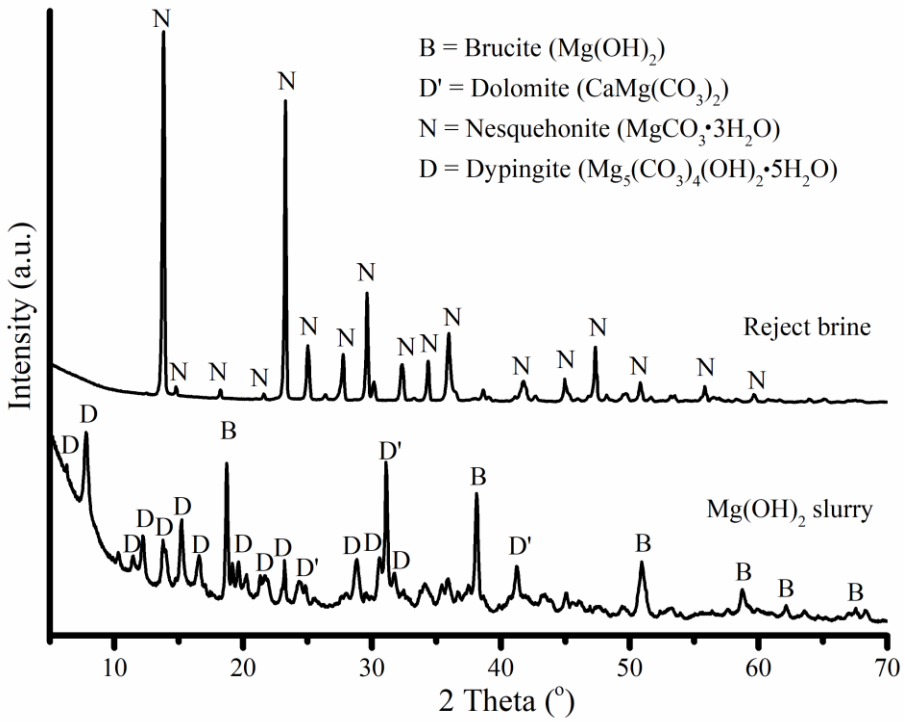

Figure 6.8 XRD diffractograms of HMCs obtained from $Mg(OH)_2$ slurry and reject brine at a $Mg(OH)_2$:CO_2 molar ratio of 1:1 under a pH of 8

6.3.2.2. Thermal properties of the HMCs

The quantitative analysis of the chemical composition of HMCs and amount of CO_2 contained in their compositions was carried out via TG/DTA and ICP-OES analyses. Figure 6.9 presents the TG/DTA graphs of HMCs obtained from $Mg(OH)_2$ slurry and reject brine at a $Mg(OH)_2$:CO_2 molar ratio of 1:1 and under a pH 8. Both systems demonstrated a similar trend with three stages of mass loss, which corresponded well with the findings of previous studies (Dell and Weller 1959, Lanas and Alvarez 2004, Ballirano, De Vito et al. 2013). Firstly, the dehydration of HMCs took place at ~100-250 ℃, resulting in the loss of H_2O. The second mass loss occurred between 250 and 550 ℃, which was attributed to the decomposition of uncarbonated $Mg(OH)_2$ into MgO as well as the decarbonation of HMCs, resulting in a loss of H_2O and CO_2. The final mass loss observed between 550 and 700 ℃ was due to the decomposition of dolomite and calcite, repectively, which was present as an impurity in the two systems (i.e. in the form of dolomite in $Mg(OH)_2$ slurry and calcite in reject brine).

The chemical composition of the final product was determined via a combination of the results generated by TG/DTA and ICP-OES, where ICP-OES was used to measure the recovery rate of Mg^{2+} and TG/DTA was used to determine the quantity of each phase derived from XRD results. Table 6.3 revealed the final composition of the precipitate obtained via the carbonation of $Mg(OH)_2$ slurry to be composed of 62.1% dypingite and 30.5% uncarbonated brucite. On the other hand, the carbonation of reject brine led to a precipitate composed of 93.1% nesquehonite and 3.7% uncarbonated brucite, as detailed in Table 6.3. These results were used in the calculation of the percentage of captured CO_2, which was derived by measuring the mass of CO_2 in the HMCs (i.e. dypingite/nesquehonite) divided by the initial input of CO_2 to the system at the $Mg(OH)_2$:CO_2 molar ratio of 1:1. The outcome of these analyses indicated that 43.7% CO_2 could be sequestered in the form of dypingite via the carbonation of the $Mg(OH)_2$ slurry, while the corresponding amount of CO_2 sequestered in reject brine was calculated to be 82.6%. The higher efficiency of CO_2 sequestration achieved via the use of reject brine was associated with the increased reactivity of $Mg(OH)_2$ obtained from reject brine.

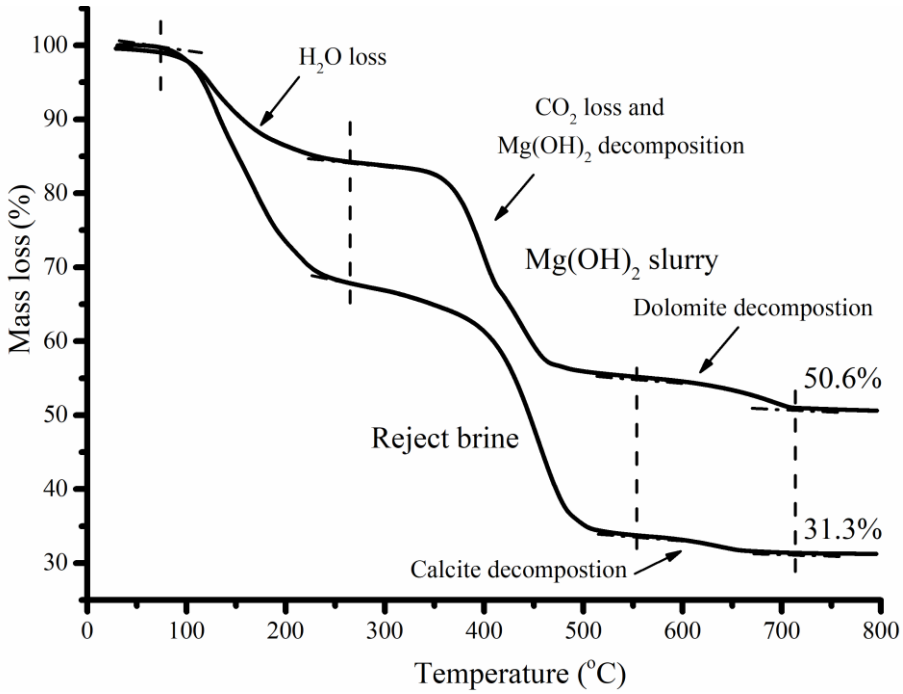

Figure 6.9 Typical TG/DTA curves of HMCs obtained from $Mg(OH)_2$ slurry and reject brine at a $Mg(OH)_2$:CO_2 molar ratio of 1:1 under a pH of 8

Table 6.3 Chemical composition of HMCs obtained from the $Mg(OH)_2$ slurry and reject brine at a $Mg(OH)_2$:CO_2 molar ratio of 1:1 under a pH of 8

Commercial $Mg(OH)_2$ slurry	Mass (g)	Mass (%)	$Mg(OH)_2$ slurry prepared from Reject brine	Mass (g)	Mass (%)
Dypingite	0.6	62.1	Nesquehonite	1.51	93.1
Brucite	0.07	30.5	Brucite	0.06	3.7
Dolomite	0.3	7.4	Calcite	0.05	3.2
CO_2 captured (%)	43.7		CO_2 captured (%)	82.6	

6.4. Conclusions

This study presented the influence of key parameters such as the $Mg(OH)_2$:CO_2 molar ratio and pH in the synthesis of HMCs through the carbonation of an $Mg(OH)_2$ slurry. The phases obtained under each experiment were characterized via a combination of various techniques including XRD, FESEM, TG/DTA and ICP-OES. The carbonation of $Mg(OH)_2$ slurry under the elevated $Mg(OH)_2$:CO_2 ratio led to the transformation of dypingite to nesquehonite. Increasing the pH from 8 to 10 was found to promote the carbonation process of $Mg(OH)_2$, resulting in a higher carbonation degree. A specific "house of cards" texture, involving the formation of rosette-like dypingite flakes on the surface of nesquehonite needles, was discovered under elevated pH and $Mg(OH)_2$:CO_2 ratios conditions. The formation of this structure was associated with to a dissolution-recrystallization-self-assembly growth mechanism as nesquehonite can function as a precursor for the further nucleation and seeding of hydromagnesite/dypingite on the surface.

To explore the feasibility of using reject brine in the long term sequestration of CO_2, the HMC phases synthesized from the carbonation of $Mg(OH)_2$ slurry were compared with those produced via the carbonation of reject brine obtained from a desalination plant. The carbonation of reject

brine led to a high yield of nesquehonite with a higher purity than the dypingite obtained from the carbonation of $Mg(OH)_2$ slurry under the same conditions. The higher degree of carbonation revealed by reject brine than that of $Mg(OH)_2$ slurry (82.6 vs. 43.7%) demonstrated its high potential to be used in the capture and long-term storage of CO_2 in the form of HMCs.

Chapter 7 Recovery of ultra-high pure MgO from reject brine obtained from desalination plants

7.1. Introduction

Magnesium and its compounds are important raw materials that have been used in a broad range of applications ranging from refractory, agricultural, pharmaceutical, chemical to construction industries (Lee, Jung et al. 2004, Shand 2006, Caraballo, Rotting et al. 2009, Moussavi and Mahmoudi 2009, Wang, Jin et al. 2016, Pilarska, Klapiszewski et al. 2017). Being physically and chemically stable at high temperatures, MgO is prized as a refractory material. Another increasingly popular use of reactive MgO is applied in the construction industry as an expansive additive (Mo, Deng et al. 2014) and as an alternative binder in the development of concrete formulations (Harrison 2008, Liska, Al-Tabbaa et al. 2012a, Liska, Al-Tabbaa et al. 2012b, Al-Tabbaa 2013, Unluer and Al-Tabbaa 2013, Unluer and Al-Tabbaa 2014). The major global production of MgO is produced from the calcination of magnesites (magnesium carbonates, $MgCO_3$) via a dry route (Equation 7-1). An alternative wet route involves its extraction from Mg-rich sources such as seawater or brine (Equations 7-2 and 7-3). Seawater contains an average Mg^{2+} concentration of 1.29-1.35 g/L, thereby constituting a significant resource of Mg (Wright and Colling 1995, Boyd 2015).

$$MgCO_3 \rightarrow MgO + CO_2 \quad (7\text{-}1)$$

$$CaO/CaO \cdot MgO + H_2O + MgCl_2 \rightarrow Mg(OH)_2 + CaCl_2 \quad (7\text{-}2)$$

$$Mg(OH)_2 \rightarrow MgO + H_2O \quad (7\text{-}3)$$

The synthetic MgO via the wet route demonstrates a higher purity and reactivity compared with MgO produced through the calcination of magnesites (Jin and Al-Tabbaa 2014), which can meet the growing competitive demands in the high-end pharmaceutical and semiconductor applications as an additive or a catalyst (Lee, Jung et al. 2004, Caraballo, Rotting et al. 2009, Pilarska, Klapiszewski et al. 2017).

The wet route production of MgO deploys a simple way of the addition of strong bases into seawater/brine to precipitate Mg^{2+}, which include a wide range of choices of bases such as lime (CaO), dolime (CaO•MgO), ammonia solution (NH_4OH) and sodium hydroxide (NaOH) etc., (Friedrich, Robinson et al. 1946, Petric, Martinac et al. 1997, Kotsupalo, Ryabtsev et al. 2010, Behij, Hammi et al. 2013). CaO or CaO•MgO is generally added to seawater/brine to raise the pH to ~10.5, enabling the precipitation of Mg^{2+} to produce $Mg(OH)_2$ (Friedrich, Robinson et al. 1946, EIPPCB 2007). CaO•MgO is preferred due to the self-contained MgO, so that only half of seawater/brine would be required to produce the same amount of MgO. However, the additional introduction of Ca^{2+} would compound with sulphate (SO_4^{2-}) which is present in the seawater/brine, to generate gypsum ($CaSO_4 \cdot 2H_2O$). $CaSO_4 \cdot 2H_2O$ will co-precipitate along with the other precipitates, which would contaminate Mg products, therefore, lowering the purity. Therefore, a necessary pre-treatment step of seawater/brine via the addition of $CaCl_2$ is needed for desulfation purpose (Shand 2006).

Apart from the addition of bases to form $Mg(OH)_2$, several studies have suggested to precipitate Mg^{2+} from seawater/brine in the form of carbonates or oxalates (Soong, Goodman et al. 2004, Soong, Fauth et al. 2006, Tran, Van Luong et al. 2013, Khuyen Thi, Han et al. 2016). Soong et al. (2004, 2006) explored the mineral trapping path way for the sequestration of CO_2 into brine via the addition of NaOH and fly ash, respectively, (Soong, Goodman et al. 2004, Soong, Fauth et al. 2006). However, due to the presence of Ca^{2+}, calcite ($CaCO_3$) would co-precipitate along with magnesium carbonates, causing the difficulty in the separation of the Mg products. When synthetic magnesium chloride ($MgCl_2$) solution used instead of seawater/brine via the direct reaction with CO_2 gas, a pure nesquehonite ($MgCO_3 \cdot 3H_2O$) could be synthesized as precursors to produce MgO (Ferrini, De Vito et al. 2009, Mignardi, De Vito et al. 2011). Tran et al. (2013) proposed to synthesize the magnesium oxalate ($MgC_2O_4 \cdot 2H_2O$) precursor from brine via the addition of the oxalic acid (Tran, Van Luong et al. 2013). pH demonstrated to be a successful separator to selectively precipitate out calcium oxalate ($CaC_2O_4 \cdot H_2O$) (pH < 1) and $MgC_2O_4 \cdot 2H_2O$ (pH > 1) from brine. $CaC_2O_4 \cdot H_2O$ was first precipitated and removed, followed by the precipitation of Mg^{2+} from the brine, leading to a production of $MgC_2O_4 \cdot 2H_2O$ of 99.5%

purity.

The properties of MgO, i.e. specific surface area (SSA) and reactivity, are known mainly depending on the calcination conditions (i.e. temperature and duration), as well as the properties of the precursors (Eubank 1951, Itatani, Koizumi et al. 1988, Choudhary, Rane et al. 1994, Alvarado, Torres-Martinez et al. 2000, Mo, Deng et al. 2010, Bartley, Xu et al. 2012). Increase in the calcination temperatures and durations has been identified to decrease the SSA values and reactivities of MgO (Mo, Deng et al. 2010). Our previous work demonstrated a correlation between the property of the precursor and the reactivity of MgO, where a more reactive of MgO with a higher SSA value could be obtained from a more porous $Mg(OH)_2$ precursor under the same calcination condition (Dong, Unluer et al. 2017, Dong, Unluer et al. 2018).

Desalinated water is expected to meet up to 30% of Singapore's future water needs by 2060 with a total of five desalination plants, two under operation and three being built, designed to provide a total of 190 million gallons (852,150 m^3) of water per day by 2020 (ST 2016). According to El-Naas (2011), an equal amount of reject brine is generated from the production of every 1 m^3 of desalinated water (El-Naas 2011). The most common and, current practice carried out for handling the reject brine is to discharge directly back to the sea. However, reject brine contains a high salinity, rising temperature and dissolved chemicals. By directly discharging back to the sea, negative environmental impacts to the marine life and quality change of sea water available for desalination are therefore expected (Mohamed, Maraqa et al. 2005, Nassar, El-Damak et al. 2007). However, studies have found out that valuable materials in the reject brine such as salts, metals, and chemicals could be recovered (Almutaz and Wagialia 1990, Ahmed, Arakel et al. 2003, Sodaye, Nisan et al. 2009, Alberti, Mosto et al. 2012, Cipollina, Misseri et al. 2012, Al Bazedi, Ettouney et al. 2014, Giwa, Dufour et al. 2017).

Reject brine, with a ~30% higher concentration of Mg^{2+} than seawater, could provide an alternative source to recover MgO. Our previous works have demonstrated feasible ways to synthesize reactive MgO from reject brine via the addition of NH_4OH and NaOH (Dong, Unluer

et al. 2017, Dong, Unluer et al. 2018, Dong, Unluer et al. 2018). However, due to the presence of Ca^{2+} and HCO_3^- in the reject brine, $CaCO_3$ would co-precipitate along with $Mg(OH)_2$ with the addition of bases, which would contaminate the final MgO products and lower the economic value in the market. Therefore, this study presented a new method to recover Ca^{2+} and Mg^{2+} separately from reject brine via the use of oxalic acid ($H_2C_2O_4 \bullet 2H_2O$). The obtained $MgC_2O_4 \bullet 2H_2O$ with high purity and yield under the optimized condition was therefore calcined to produce MgO. A comprehensive characterization of MgO, i.e. microstructure and SSA, was presented and a correlation between the calcination conditions (i.e. temperature and duration) and the properties of MgO was established.

7.2. Materials and Methodology

7.2.1. Materials

Reject brine provided by a local desalination plant in Singapore was used as the raw material for this study. To identify the composition of reject brine, the water is passed through a 45μm filter and then tested by inductively coupled plasma optical emission spectrometry (ICP-OES). It is observed that Na^+, Cl^-, SO_4^{2-}, Mg^{2+}, K^+ and Ca^{2+} are the most components in reject brine (Refer to Table 7.1 below). Oxalic acid ($H_2C_2O_4 \bullet 2H_2O$) of analytical grade and sodium hydroxide (NaOH) used as pH adjustment, were supplied by Sigma-Aldrich and VWR Pte Ltd in Singapore, respectively.

Table 7.1 Chemical composition of reject brine used in this study.

Element/ Concentration	Cl	Na	SO_4	Mg	K	Ca	Sr	B	Si	Li	P	Al
ppm	84615.1 ± 87.2	20800.3 ± 42.5	5576.2 ± 9.6	2165.9 ± 4.9	1043.0 ± 4.8	727.0 ± 4.2	6.8 ± 0.1	5.8 ± 0.1	0.6	0.5	0.3	0.1

7.2.2. Methodology

The synthesis of $MgC_2O_4•2H_2O$ was synthesized from a two-step reaction primarily from reject brine. As reject brine consists mainly of Ca^{2+} and Mg^{2+} cations, the addition of $H_2C_2O_4•2H_2O$ will precipitate out the two elements simultaneously. Previous studies showed pH could be an excellent separator to precipitate Ca^{2+} and Mg^{2+} sequentially since Ca^{2+} could be firstly precipitated from reject brine under the pH value of <1 while Mg^{2+} could be precipitated under the pH value of >1 as shown in Equations 7-4 and 7-5 (Elving and Caley 1937, Holth 1949).

$$Ca^{2+} + H_2C_2O_4•2H_2O \rightarrow CaC_2O_4•H_2O \text{ (pH < 1)} \quad (7\text{-}4)$$

$$Mg^{2+} + H_2C_2O_4•2H_2O \rightarrow MgC_2O_4•2H_2O \text{ (For pH >1)} \quad (7\text{-}5)$$

$$MgC_2O_4•2H_2O \rightarrow MgO + 2H_2O + CO + CO_2 \quad (7\text{-}6)$$

The first step involved the quick addition of $H_2C_2O_4•2H_2O$ into 600 ml reject brine to precipitate out $CaC_2O_4•H_2O$ under a control of the pH value at 1 with two different molar ratios of Ca^{2+}:$H_2C_2O_4•2H_2O$ of 1:1 and 1:2. The addition of $H_2C_2O_4•2H_2O$ into reject brine quickly brought the pH of reject brine below 1 while 1 M NaOH was added to adjust the pH to 1. Following the first step after the precipitation and removal of $CaC_2O_4•H_2O$, the addition of $H_2C_2O_4•2H_2O$ to the residue were under three different ratios of 1, 1.25 and 1.5 with pH controlled at 2 and 3, respectively. NaOH was continuously added as a pH adjuster to the solution, which allowed $H_2C_2O_4•2H_2O$ to react effectively with Ca^{2+} and Mg^{2+} in the reject brine under the controlled pH values. Different molar ratios of Ca^{2+}:$H_2C_2O_4•2H_2O$, Mg^{2+}:$H_2C_2O_4•2H_2O$ and pH conditions were tested to identify the optimum condition needed to separate Ca^{2+} and Mg^{2+} efficiently and precipitate out $MgC_2O_4•2H_2O$ with the optimum yield and purity. The constant parameters were 1 atm of air, constant speed of 200 rpm for stirring and mixing under room temperature of 25 ℃. pH and temperature were monitored continuously using a pH/thermometer (Mettler Toledo pH/Ion meter S220), which was calibrated before each experiment with three standard reference solutions set at pH 4, 7 and 10, respectively. The solids were separated from the residual brine through a centrifuge. After being collected, the solids were washed three times by ultra-pure water to remove surface-attached ions. The washed solids were then oven-dried at 105 ℃ for 24 hours before grinding into powder form. $MgC_2O_4•2H_2O$

that precipitated at the end of the reaction shown in Equations 7-4 to 7-6, was then calcined to produce MgO under different calcination temperatures (i.e. 700, 800 and 900 ℃), which were each maintained for three different residence times (i.e. 2, 6 and 12 hours).

7.2.3. Equipment

The composition of reject brine (e.g. Mg^{2+} and Ca^{2+}) before and after reaction was analysed by ICP-OES (PerkinElmer Optima DV2000). The mineralogy of solids was determined by X-ray powder diffraction (XRD), using a Bruker D8 Advance with a Cu Kα source under the operation conditions of 40 kV and 40 mA, emitting radiation with a wavelength of 1.5405 Å, scan rate of 0.02 °/step, and a 2θ range of 5 to 70°. Thermogravimetric and differential thermal analysis (TG/DTA) using a PyrisDiamond TGA 4000 were operated at a heating rate of 10 ℃/min under air flow to investigate weight changes and thermal transformations of materials. The texture properties, i.e. SSA and pore volume, were determined from nitrogen adsorption-desorption isotherms using a Quadrasorb Evo automated surface area and pore size analyzer. The SSA was calculated by Brunauer-Emmett-Teller (BET) method and the pore volume was determined by Barrett-Joynet-Halenda (BJH) method.

7.3. Results and Discussions

7.3.1. Characterization of $MgC_2O_4•2H_2O$

7.3.1.1. XRD

A controlled selective precipitation of $CaC_2O_4•H_2O$ was firstly conducted under a pH value of 1 with two different molar ratios of Ca^{2+}:$H_2C_2O_4•2H_2O$ of 1:1 and 1:2 as shown in Figure 7.1. The diffraction patterns under two conditions presented similar phases, which were mainly attributed to $CaC_2O_4•H_2O$, along with minor amounts of $MgC_2O_4•2H_2O$. Under the elevated Ca^{2+}:$H_2C_2O_4•2H_2O$ ratio of 1:2, the intensity of the $MgC_2O_4•2H_2O$ peaks revealed an increase relative to the others, possibly indicting a growing in the amount of $MgC_2O_4•2H_2O$. Once the precipitated $CaC_2O_4•H_2O$ had been removed, the further addition of $H_2C_2O_4•2H_2O$ into residual brine under different Mg^{2+}:$H_2C_2O_4•2H_2O$ ratios (i.e. 1:1, 1:1.25, 1:5) at a control pH value of 2

and 3, respectively, resulted in the precipitation of $MgC_2O_4•2H_2O$. The peaks of $CaC_2O_4•H_2O$ were not observed in the diffractorgrams of the second stage, indicating a complete removal of Ca^{2+} in the first step.

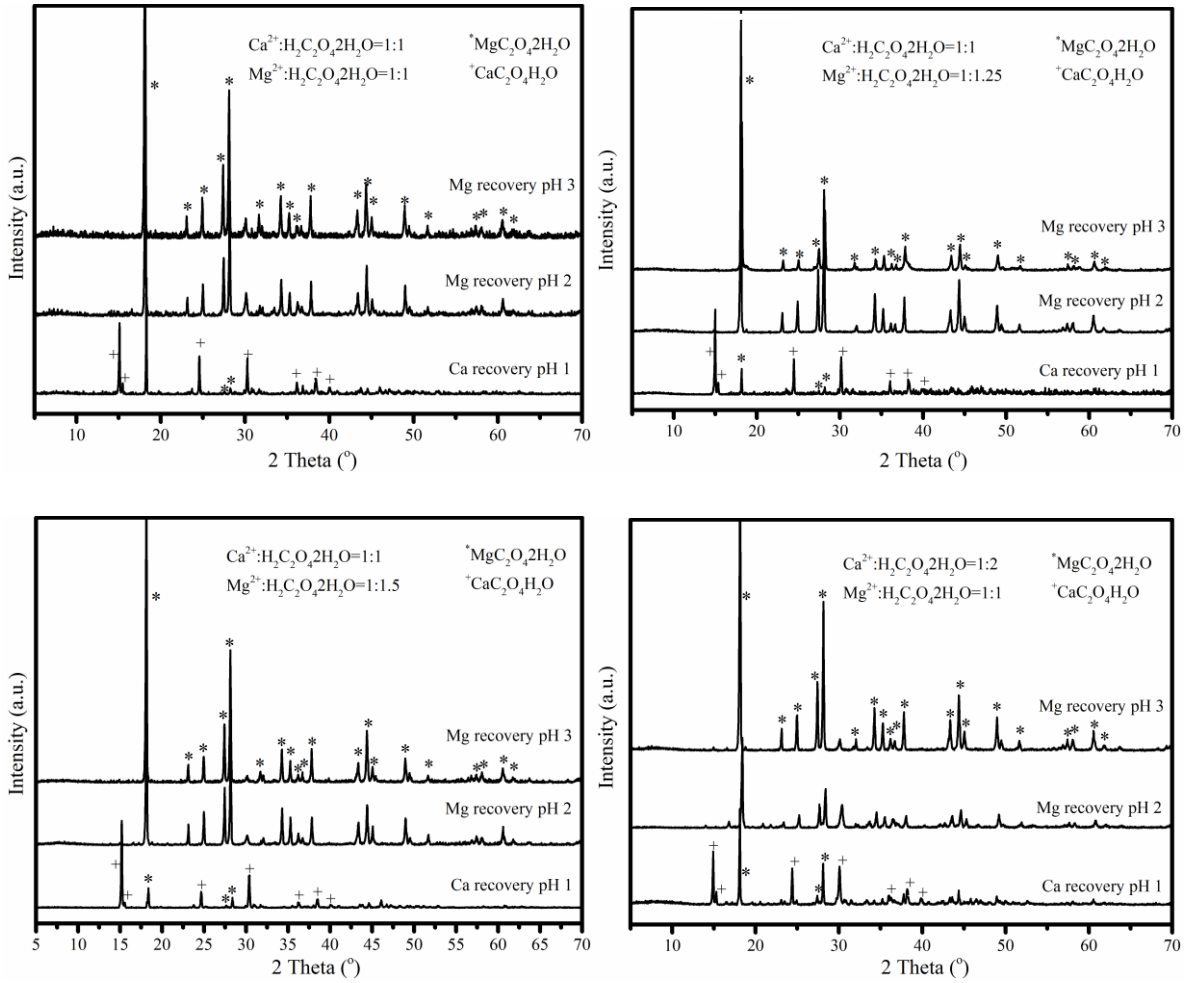

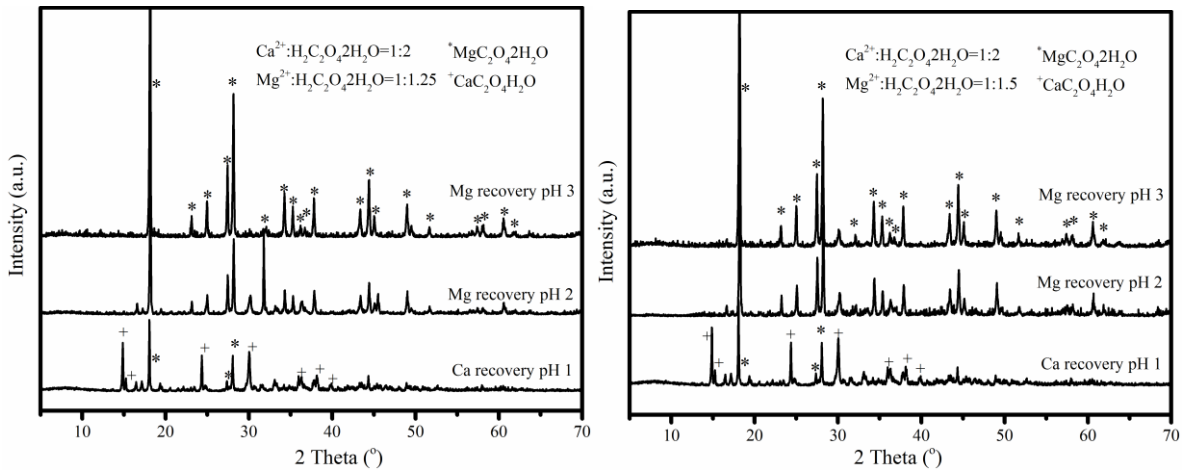

Figure 7.1 XRD diffractograms of precipitates obtained from the reaction of reject brine with $H_2C_2O_4$•$2H_2O$ from a two-step reaction

7.3.1.2. ICP-OES

The concentrations of Ca^{2+} and Mg^{2+} in the residual brine after the sequential precipitation of CaC_2O_4•H_2O and MgC_2O_4•$2H_2O$ are shown in Table 7.2. At the molar ratio of Ca^{2+}:$H_2C_2O_4$•$2H_2O$ of 1:1 under the pH value of 1, the recovery rate of Ca^{2+} is ~96%. Meanwhile, ~12% of Mg^{2+} was also precipitated out as MgC_2O_4•$2H_2O$, which explained the appearance of the minor peaks of MgC_2O_4•$2H_2O$ in the first stage of XRD diffractograms. The further increase of Ca^{2+}:$H_2C_2O_4$•$2H_2O$ to 1:2 under pH value of 1, the recovery rate of Ca^{2+} increased to nearly 100%, which explained the absence of CaC_2O_4•H_2O in the second stage of XRD diffractograms. After the removal of CaC_2O_4•H_2O, pH played a main role in controlling the recovery rate of Mg^{2+}, while the increase of the molar ratios of Mg^{2+}:$H_2C_2O_4$•$2H_2O$ from 1:1 to 1:1.5 slightly increased the recovery rate of Mg^{2+}. Under a pH value of 2, ~70% of Mg^{2+} could be precipitated out while the increase of pH to 3 can achieve a recovery rate as high as 94.9%.

Table 7.2 Concentrations of Ca^{2+} and Mg^{2+} in the residual brine.

Ca^{2+}:$H_2C_2O_4$•$2H_2O$	Mg^{2+}:$H_2C_2O_4$•$2H_2O$								
1:1	1:1			1:1.25			1:1.5		
pH	1	2	3	1	2	3	1	2	3
Ca^{2+} (ppm)	30.0	13.1	0	27.4	10.1	0	34.4	13.1	0
Recovery (%)	95.9	98.2	100.0	96.2	98.6	100.0	95.3	98.2	100.0
Mg^{2+} (ppm)	1930	829.9	187.4	1878	655.0	334.5	1894	605.2	152
Recovery (%)	10.9	61.7	91.3	13.3	69.8	84.6	12.6	72.1	93.0
Ca^{2+}:$H_2C_2O_4$•$2H_2O$	Mg^{2+}:$H_2C_2O_4$•$2H_2O$								
1:2	1:1			1:1.25			1:1.5		
pH	1	2	3	1	2	3	1	2	3
Ca^{2+} (ppm)	2.1	9.8	0	1.8	0.02	0	0	0	0
Recovery (%)	99.7	98.7	100.0	99.8	100.0	100.0	100.0	100.0	100.0
Mg^{2+} (ppm)	1902	704.1	149.5	1894	666.2	217.1	1884	624	110.9
Recovery (%)	12.2	67.5	93.1	12.6	69.2	90.0	13.0	71.2	94.9

7.3.1.1. TG/DTA

The quantitative analysis of the composition of the obtained MgC_2O_4•$2H_2O$ under the condition of Ca^{2+}:$H_2C_2O_4$•$2H_2O$ of 1:1, Mg^{2+}:$H_2C_2O_4$•$2H_2O$ of 1.5 and pH value of 3, was carried out via TG/DTA analysis. The decomposition of MgC_2O_4•$2H_2O$ follows the steps as shown in Equations 7-7 to 7-10:

$$MgC_2O_4•2H_2O \rightarrow MgC_2O_4 + 2H_2O \quad (7\text{-}7)$$

$$MgC_2O_4 \rightarrow MgCO_3 + CO \quad (7\text{-}8)$$

$$CO + 1/2O_2 \rightarrow CO_2 \quad (7\text{-}9)$$

$MgCO_3 \rightarrow MgO + CO_2$ (7-10)

As shown in Figure 7.2, the dehydration of $MgC_2O_4 \cdot 2H_2O$ firstly took place at ~200 ℃ to become MgC_2O_4 as H_2O molecules escaped, resulting in a weight loss of 23.9%. The second weight loss occurred between 400 ℃ and 600 ℃ due to the decomposition of MgC_2O_4 to MgO, causing a weight loss of 46.8% because of the liberation of CO and CO_2, where the theoretical weight losses due to the dehydration and decarbonation of $MgC_2O_4 \cdot 2H_2O$ are calculated as 24.3% and 48.6%, respectively. The final product was analysed to take up a mass of 27.5% of the initial sample, where the purity of the synthesized $MgC_2O_4 \cdot 2H_2O$ therefore was calculated to be 99.5 % which was compatible with the previous study (Tran, Van Luong et al. 2013). Finally, $MgC_2O_4 \cdot 2H_2O$ produced under the condition of Ca^{2+}:$H_2C_2O_4 \cdot 2H_2O$ of 1:1, Mg^{2+}:$H_2C_2O_4 \cdot 2H_2O$ of 1.5 and pH value of 3, due to the high purity and yield, was chosen for further calcination to produce reactive MgO under different conditions.

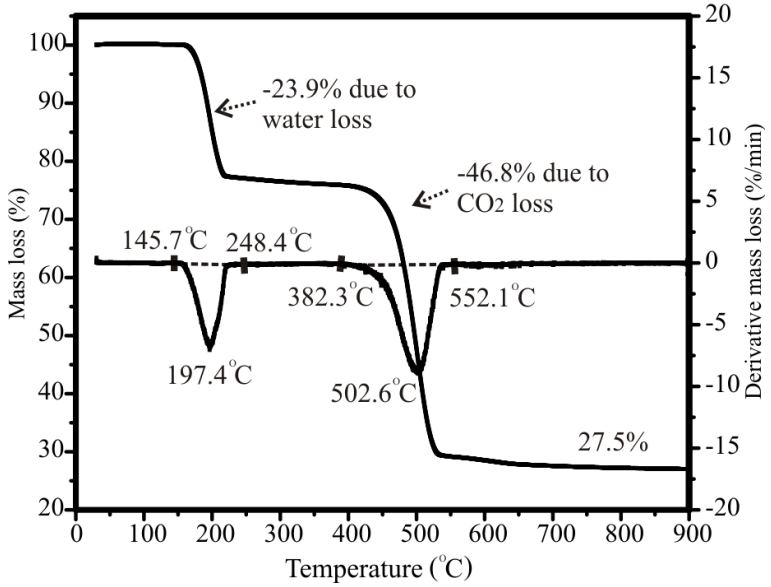

Figure 7.2 A typical TG/DTA curve of $MgC_2O_4 \cdot 2H_2O$ obtained from reject brine under the condition of Ca^{2+}:$H_2C_2O_4 \cdot 2H_2O$ of 1:1, Mg^{2+}:$H_2C_2O_4 \cdot 2H_2O$ of 1.5 and pH value of 3

7.3.2. Characterization of MgO

7.3.2.1. Textural properties

The SSA values of MgO, obtained from the calcination of $MgC_2O_4•2H_2O$ under different calcination conditions (i.e. temperature and duration), are displayed in Figure 7.3. The SSA values ranged between 4.4 and 30.2 m^2/g, depending on the calcination temperatures and durations. Out of all conditions used in this study, the calcination of $MgC_2O_4•2H_2O$ under 700 ^oC for 2 hours generated the highest SSA of 30.2 m^2/g. An increase in the calcination temperature and duration led to a consistent reduction in the SSA values and pore volumes, indicating a decrease in the reactivities of MgO as shown in Table 7.3. The calcination of $MgC_2O_4•2H_2O$ occurs in two steps, i.e., the dehydration and decarbonation causing the release of H_2O, CO and CO_2 from $MgC_2O_4•2H_2O$, leaving more porous MgO. Up to a certain temperature, the porous MgO starts to sinter, i.e., the breakdown of the pores in MgO and the reduction of porosity and the increase of crystallite size (Eubank 1951). These findings were in line with those reported in previous studies (Eubank 1951, Itatani, Koizumi et al. 1988, Alvarado, Torres-Martinez et al. 2000, Mo, Deng et al. 2010, Jin and Al-Tabbaa 2014), where the direct influence of calcination conditions on the properties of MgO was reported.

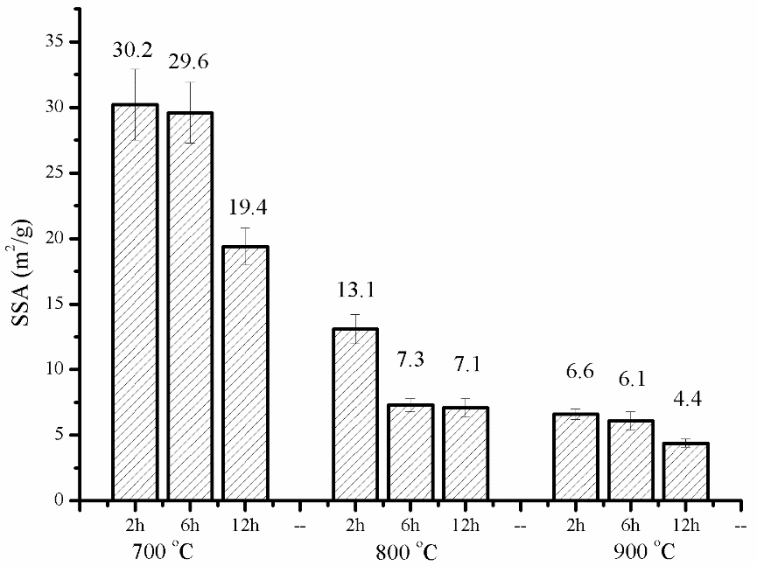

Figure 7.3 SSA of MgO produced under different calcination temperatures and durations

7.3.2.2. Crystallite size and primary particle size

The XRD diffractograms of all MgO calcined under different conditions (i.e. temperature and duration) are shown in Figure 7.4, where the characteristic peaks for MgO were situated at 37.0 °, 43.0 ° and 62.5 ° 2θ, matched well with the reference peaks of MgO indicated in JCPDS card no. 89-7746. Owing to the high purity of the MgC_2O_4•$2H_2O$ precursor, no other phases were detected. Debye-Scherrer formula was used to calculate the crystallite size, as shown in the equation $G_{XRD} = K•\lambda/(\beta•\cos(\theta))$ (Patterson 1939). Where λ is the wavelength of Cu Kα source as 1.5405 Å, β the full width at half-maximum intensity (FWHM) of a Bragg reflection subtracting the instrumental broadening, θ the Bragg angle and K the shape factor with a typical value as 0.9. The major characteristic peak of MgO at 43.0 ° (2 θ) from XRD, was used to calculate the crystallite size of MgO, where the increase of the calcination temperatures and durations prolonged the crystallite sizes of MgO ranging from 14 to 28 nm. The agglomeration ratio, defined as G_{BET}/G_{XRD}, was obtained from the ratio of the primary particle size, G_{BET}, to the crystallite size, G_{XRD}. G_{BET} was calculated following the equation: $G_{BET} = F/\rho S$. Where F is a particle-shape factor as 6, S the SSA (m^2/g), ρ theoretical density of MgO as 3.595 g/cm^3 (Itatani, Nomura et al. 1986). The G_{BET} values for MgO were in the range of 52–170 nm while the G_{BET}/G_{XRD} values ranged from 3.6-13.5, increasing along under the elevated calcination temperatures and durations. The lowest agglomeration ratio, ~3.6, was obtained under 700 ^oC. The calcination temperatures and durations had a significant influence on the crystallite sizes, primary sizes and pore volumes of MgO, where the increase of the temperatures and durations significantly enlarged the crystallite sizes and primary sizes of MgO, resulting in the decrease of pore volumes. This could be due to the expansion of MgO grains and the spontaneous coagulation of primary particles at the growing temperatures and durations (Itatani, Itoh et al. 1993), resulting in the higher agglomeration ratios and the low pore volumes, therefore resulting in the lower SSA values of MgO as illustrated in Figure 7.3.

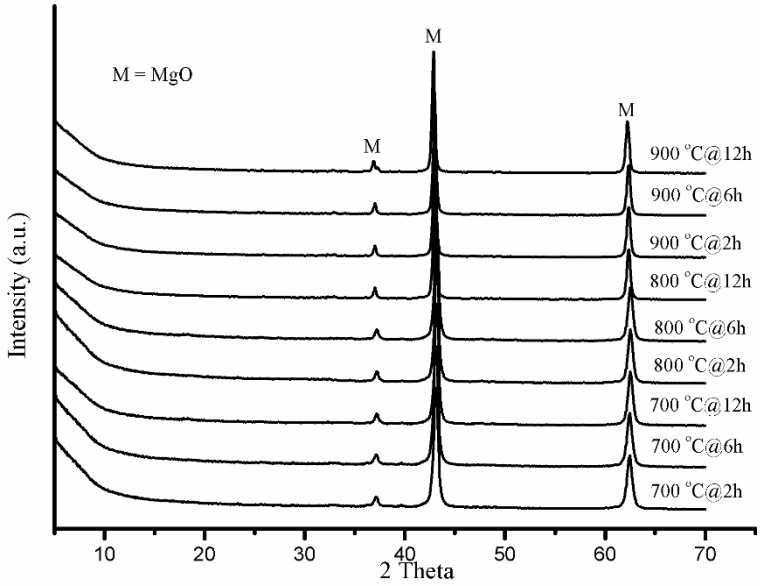

Figure 7.4 XRD diffractograms of reactive MgO produced via the calcination of $MgC_2O_4 \cdot 2H_2O$ under different temperatures and durations

Table 7.3 Crystallite size, primary particle sizes and pore volumes of MgO produced under different calcination temperatures and durations

	700 ℃			800 ℃			900 ℃		
	2 h	6h	12 h	2 h	6h	12 h	2 h	6h	12 h
G_{XRD} (nm)	14.3	15.6	17.8	18.1	18.1	20.2	21.7	26.3	28.1
SSA (m^2/g)	30.2	29.6	19.4	13.1	7.3	7.1	6.6	6.1	4.4
G_{BET} (nm)	52.3	62.3	115.1	115.1	146.4	173.9	123.6	137.9	157.5
G_{BET}/G_{XRD} (nm)	3.9	3.6	4.8	7.0	12.6	11.6	11.6	10.4	13.5
Pore volume (cm^3/g)	0.175	0.205	0.109	0.086	0.029	0.028	0.024	0.016	0.023

7.3.2.4. FESEM

A further investigation on the correlation of the calcination conditions (i.e. temperature and duration) with the microstructures of MgO was revealed through FESEM images, as shown in Figure 7.5. Increasing the calcination temperatures from 700 to 900 ℃ had a more profound effect on the sizes of the MgO grains, resulting in a significant growth in the crystallite sizes, which was accompanied with the reduction of porosity, as seen Table 7.3. MgO grains demonstrated a noticeable growth and expansion as the calcination duration increased from 2 to 12 hours. These changes in the morphology of MgO grains could clearly explain the reduction of SSA under the elevated calcination temperatures and durations. The increase in the dimensions of the MgO grains under the high calcination temperatures and durations was attributed to the liberation of H_2O, CO and CO_2 during the decomposition of $MgC_2O_4 \cdot 2H_2O$, which facilitated the formation of a porous structure. This initial porosity was gradually reduced as the MgO grains grew further due to continuous sintering as shown in Table 7.3, which was in line with the findings reported by earlier studies (Mo, Deng et al. 2010).

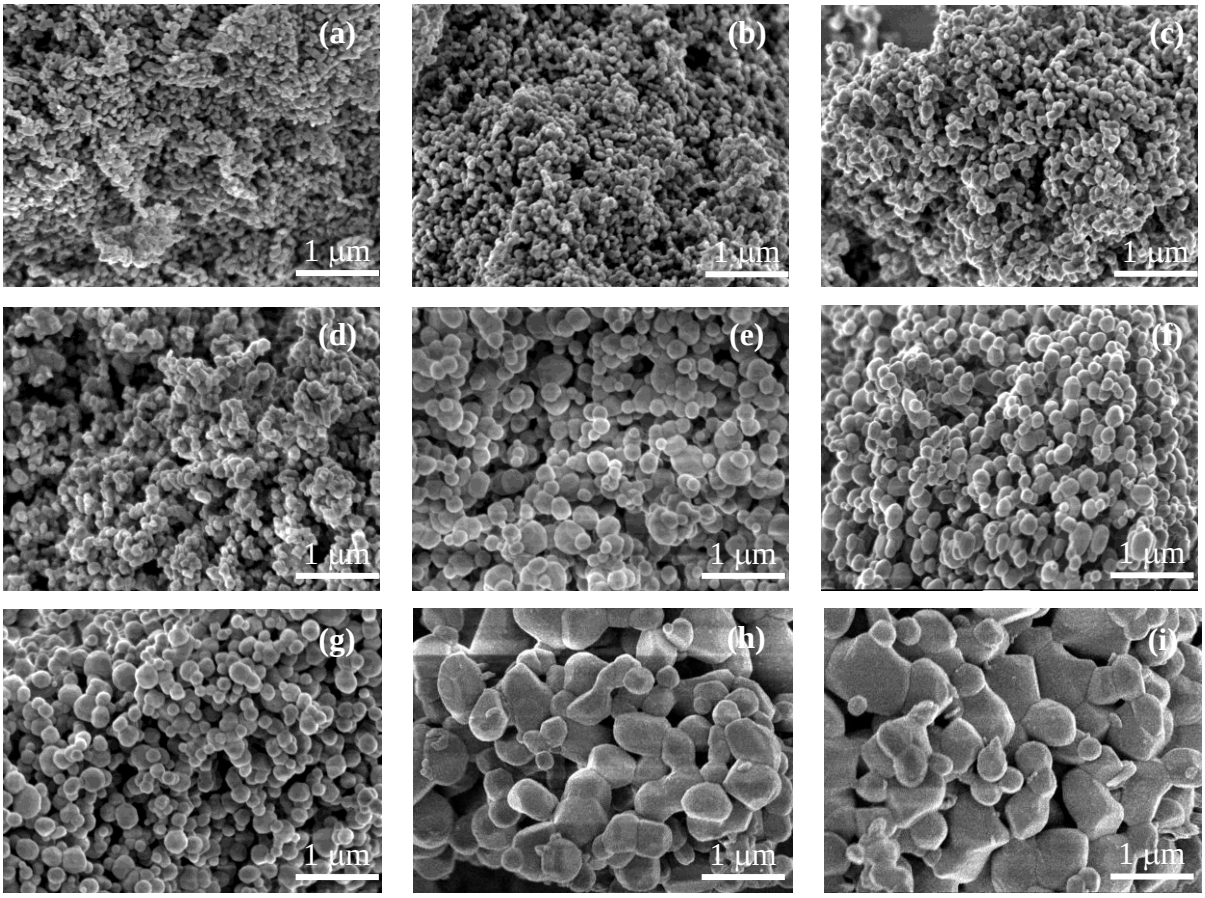

Figure 7.5 FESEM images of MgO obtained from the calcination of $MgC_2O_4•2H_2O$ under (a) 700 ℃-2h, (b) 700 ℃-6h, (c) 700 ℃-12h, (d) 800 ℃-2h, (e) 800 ℃-6h, (f) 800 ℃-12h, (g) 900 ℃-2h, (h) 900 ℃-6h and (i) 900 ℃-12h

7.4. Conclusions

This study presented a comprehensive investigation on a two-step synthesis of $MgC_2O_4•2H_2O$ from reject brine via the use of $H_2C_2O_4•2H_2O$ and the production of reactive MgO with ultra-high purity. The key parameters affecting the purity and yield of the synthesized $MgC_2O_4•2H_2O$ and its calcination to produce reactive MgO were revealed. The results demonstrated the feasibility of recovering reactive MgO with high purity from reject brine obtained as a waste at the end of the desalination process. The addition of $H_2C_2O_4•2H_2O$ into reject brine proved to be a successful method to selectively precipitate out $CaC_2O_4•H_2O$ and $MgC_2O_4•2H_2O$ under a controlled pH. The effects of Ca^{2+}:$H_2C_2O_4•2H_2O$, Mg^{2+}:$H_2C_2O_4•2H_2O$ and pH on the final yield and purity was investigated with the goal of optimizing the yield and purity of the synthesized $MgC_2O_4•2H_2O$. $MgC_2O_4•2H_2O$ with a ultra-high purity of 99.5% was obtained, achieving a high recovery rate of Mg^{2+} of 94.9%.

An optimum condition of Ca^{2+}:$H_2C_2O_4•2H_2O$ of 1:1, Mg^{2+}:$H_2C_2O_4•2H_2O$ of 1.5 and pH value of 3, which generated $MgC_2O_4•2H_2O$ with high purity and yield, was determined and used in the subsequent production of MgO. The influence of the calcination conditions (i.e. temperature and duration) on the reactivities of MgO obtained was reported. An increase in the calcination temperatures and durations lowered the SSA values of MgO. Calcination of $MgC_2O_4•2H_2O$ at 700 ℃ for 2 hours resulted in the most reactive MgO samples, with a SSA of 30.2 m^2/g, which could be can be used in the high-end applications in the food, cosmetics pharmaceutical and semiconductor applications (Lee, Jung et al. 2004, Caraballo, Rotting et al. 2009, Pilarska, Klapiszewski et al. 2017). Overall, reject brine proved to be as an alternative and reliable source for the sustainable recovery of MgO with a high purity and reactivity.

Chapter 8 Comparative life cycle assessment of reactive MgO produced from local reject brine

8.1. Introduction

Concrete is the most widely used material on earth, other than water. Portland cement (PC) is the most common binder used in concrete and construction materials and its production is estimated to be 3 billion tonnes yearly at a global scale (Schneider, Romer et al. 2011, USGS 2012). The production of PC contributes to 5-7% of anthropogenic CO_2 emissions worldwide, mainly due to the high calcination temperatures (~1450 ℃) used during the calcination of limestone and intensive energy required for power generation (Huntzinger and Eatmon 2009, Schneider, Romer et al. 2011, Olivier and Marilena Muntean 2014). CO_2, the primary greenhouse gas (GHG), has been identified as one of the main causes of global warming while negative impacts from global warming are becoming more significant, thus, turning the world towards a more environmental consciousness. As the environmental impacts of PC-based construction materials are becoming a serious concern, the development of novel alternatives with lower energy requirements and associated CO_2 emissions is more crucial than ever. Reactive magnesia (MgO) cement has received attention as an alternative binder due to the lower calcination temperatures (~700 ℃) used during its production, its ability to store CO_2 permanently while gaining strength, and complete recyclability at the end of use (Dung and Unluer 2017).

Currently a majority of MgO worldwide is produced from the calcination of magnesium carbonate (magnesite, $MgCO_3$) via a dry route (Equation 8-1).

$$MgCO_3 \rightarrow MgO + CO_2 \quad (8\text{-}1)$$

The theoretical energy demand via the dry route is around 5.89 GJ / tonne of rective MgO compared with 4.87 GJ/tonne of PC, which includes the mining and crushing, pre-treatment, calcination and grinding process as presented in Table 8.1 (Hassan 2013).

Table 8.1 Energy consumption of PC and MgO production via the dry-route (Hassan 2013).

Process	Production of PC from limestone (GJ /tonne of PC)	Production of MgO from magnesite (GJ /tonne of MgO)
Mining and crushing	0.04	0.06
Pre-treatment	0.06	0.11
Calcination	4.69	5.62
Finish grinding	0.08	0.10
Total	4.87	5.89

The CO_2 emissions associated with reactive production are due to (i) the combustion of fuels required to provide the energy needed for each production step and the chemical reaction involving the decomposition of $MgCO_3$ to MgO. The sum of these two steps is equivalent to the emission of ~1.7 tonne CO_2 /tonne of MgO compared with ~1 tonne CO_2 /tonne of PC (Hassan 2013). While as reported in (Ruan and Unluer 2016), the GHG emission of the production of reactive MgO, via using an IPCC climate change factor with a timeframe of 100 years, was calculated to be 1.36 tonne CO_2 /tonne of MgO compared with 0.97 tonne CO_2 /tonne of PC. Although both reported the CO_2 emission of the production of MgO is higher than the production of PC, the capability of MgO to sequester CO_2 and gain strength from this process can enable the reduction of its net CO_2 emissions. Several studies on the use of MgO cement in concrete products have shown that formulations involving reactive MgO cement can fully carbonate and achieve a carbonation degree of 100% (Liska, Al-Tabbaa et al. 2012a, Liska, Al-Tabbaa et al. 2012b, Al-Tabbaa 2013, Unluer and Al-Tabbaa 2013, Unluer and Al-Tabbaa 2014). When this carbonation capability of MgO is integrated in the calculation of its overall emissions, the CO_2-eq of reactive MgO cement is calculated to be up to 73% (i.e. 0.71 tonne/tonne) lower than PC by revealing a net amount of around 0.26 tonne CO_2-eq/tonne of MgO after carbonation. This makes use of the ability of reactive MgO cement-based formulations to enable a stable and permanent storage of CO_2 within construction products, while gaining strength.

An alternative wet route involves its extraction from magnesium-rich sources such as seawater or brine. Synthetic MgO contributes to around 14% of the world MgO production from seawater or brine (Kramer). Magnesium is the third most abundant element in seawater after sodium and chorine, with an average concentration of ~1300 ppm (Wright and Colling 1995, Boyd 2015). Natural brine exists widely in brine wells and lakes, providing another abundant source for MgO production. The chemical concentration of brine varies depending on the surrounding environment, consisting of much higher salt concentrations than seawater. After softening seawater/brine, it is then pumped into an agitated reactor vessel. A strong base is added into magnesium solution to raise the pH to 10.5, enabling the precipitation of magnesium (Turek and Gnot 1995, Dave and Ghosh 2005, El-Naas 2011, Tran, Van Luong et al. 2013, Khuyen Thi, Han et al. 2016). Generally lime (CaO) or dolime (CaO•MgO) are deployed in practice as shown in Equations 8-2 to 8-4.

$$MgCl_2 + Ca(OH)_2 \rightarrow CaCl_2 + Mg(OH)_2 \quad (8\text{-}2)$$

$$MgCl_2 + CaMg(OH)_4 \rightarrow CaCl_2 + 2Mg(OH)_2 \quad (8\text{-}3)$$

$$Mg(OH)_2 \rightarrow MgO + H_2O \quad (8\text{-}4)$$

The production process of reactive MgO from seawater/brine involves four main stages (i) extraction and pre-treatment of seawater/brine (1.30 GJ/tonne MgO); (ii) the preparation of CaO (6.61 GJ/tonne MgO); (iii) the precipitation of $Mg(OH)_2$ (exothermic), and (iv) pyro-processing/calcination (8.18 GJ/tonne MgO) (Hassan 2013). As a result, the energy consumptions associated with the production of reactive MgO from seawater/brine are mainly coming from the preparation of CaO and the calcination of $Mg(OH)_2$ during the production of MgO in the final step. The overall process results in a total energy demand of 16.09 GJ/tonne MgO, which is significantly higher (~2.7 times) than the dry route.

In addition to its ability to carbonate within concrete applications to reduce the CO_2 emission, another environmental friendly advantage of MgO can be achieved via its production from waste streams such as reject brine compared with the use of seawater/brine. Reject brine is a concentrated by-product obtained from treating brackish water or seawater in desalination plants. Desalination (i.e. removal of salts from saline water to produce fresh water) is considered as a feasible approach to meet residential and industrial water demands in Singapore. Currently the desalinated water from two currently running seawater reverse-osmosis plants provides 100 million gallons water a day, which meets up to 25% of Singapore's current water demand (PUB 2015). According to the International Desalination Association, the global daily production of desalinated water generated by 18,426 desalination plants worldwide exceeds 86.8 million cubic meters (IDA 2015). It is estimated that an equivalent amount is generated as reject brine per m^3 of desalinated water (El-Naas 2011). The most common way of disposing reject brine is currently through its discharge back to the sea. However, as brine is denser than the feedstock supply due to its high salt concentration and salinity, it accumulates at the bottom of the sea when discharged through an outfall without. Discharge of untreated reject brine has an adverse effect on the ecosystem by permanently altering the flora and fauna through increased salinity and damaging all living organisms within that particular ecosystem (Mohamed, Maraqa et al. 2005). A new idea has been proposed to target reject brine as an excellent source for the recovery of reactive MgO due to its high Mg^{2+} content and abundance on both local and global levels. Therefore, reject brine can be converted into valuable and useful solids, which provides a feasible and environmental friendly use of this waste material.

Although there are a number of studies on the environmental impacts of the production of MgO from magnesite and seawater, it must be noted that very limited studies have been performed on the production of reactive MgO from reject brine and environmental impacts of the production of reactive MgO from reject brine have to date not been explored. Our previous studies have revealed that $Mg(OH)_2$ can be synthesized from reject brine, which can be calcined to produce reactive MgO under different conditions (Dong, Unluer et al. 2017, Dong, Unluer et al. 2018, Dong, Unluer et al. 2018), or can be further carbonated to synthesize HMCs (Dong, Unluer et al. 2018), which could serve as a reservoir to store CO_2 in the form of carbonates. There is a

significant potential for the optimization of the overall process that will inevitably lead to the reduced energy requirement and CO_2 emission. Part of the success regarding the production of reactive MgO from waste streams (e.g. reject brine) is dependent on the overall environmental impacts of this process and its comparison to traditional cement production in terms of its CO_2 emission and energy requirement. This project aims to eliminate these concerns by evaluating the energy consumption and CO_2 emission of the production of reactive MgO from reject brine via different routes and to put forward pertinent proposals concerning their sustainable development in the future, which can serve as an excellent resource for various applications ranging from food, cosmetics, pharmaceutical and the construction industries (Lee, Jung et al. 2004, Shand 2006, Moussavi and Mahmoudi 2009, Pilarska, Klapiszewski et al. 2017).

8.2. Materials and methods

The LCA methodology follows the ISO 14040 standards which have been widely adopted by previous researchers. SimaPro 7.3 was used to evaluate the environment impacts and provide a comprehensive comparison between reactive MgO produced from reject brine via different routes through four steps:

1. Define the goal, scope and system boundary of the study;
2. Build up a model of reactive MgO life cycle inventory with all products and process inputs and outs;
3. Evaluate the environmental impact data (i.e. inputs and outputs) in the inventory;
4. Interpret the results and provide recommendations for progress.

8.2.1. Goal, functional unit and scope

The main goal of this study is to compare and identify key issues (i.e. energy consumption and GHG emission) associated with the life cycle of reactive MgO produced from reject brine. One tonne of MgO recovered from reject brine via different routes is chosen as the functional unit. A cradle-to-gate LCA has been performed and the system boundary are given in Figure 8.1, ranging from the acquisition of raw materials to the final shipping of products, while the major raw materials and the process flow diagram are shown in Figure 8.2. This process involves the

precipitation of precursors (i.e. $Mg(OH)_2$) via the addition of different bases into reject brine, which could either be directly calcined to produce reactive MgO or be carbonated to sequestrate CO_2 into HMCs. The obtained HMCs could be sold as the end product or further be calcined to produce reactive MgO. The energy consumption and GHG emission of the production of reactive MgO are mainly from the steps of the production of chemicals and the calcination of precursors, where the transportation of raw materials to the production plant, the precipitation and separation of solids from the solution, the grinding, packaging and shipping of reactive MgO samples are not included in our calculations since these processes are needed regardless of the production routes and these would not contribute significantly to the overall calulations. Reject brine is the waste water produced at the end in the desalination plant, thus, the energy consumption of the production of reject brine is assumed to be zero.

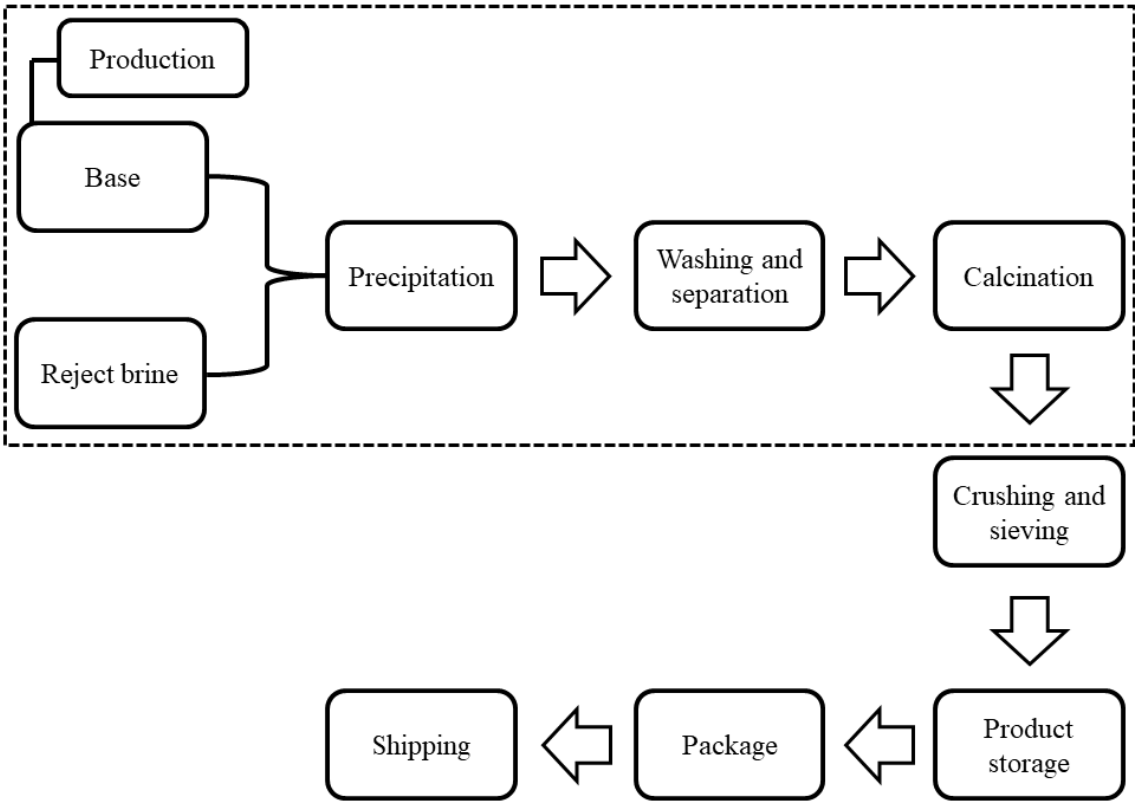

Figure 8.1 Scope of comparative LCA showing the production process of reactive MgO

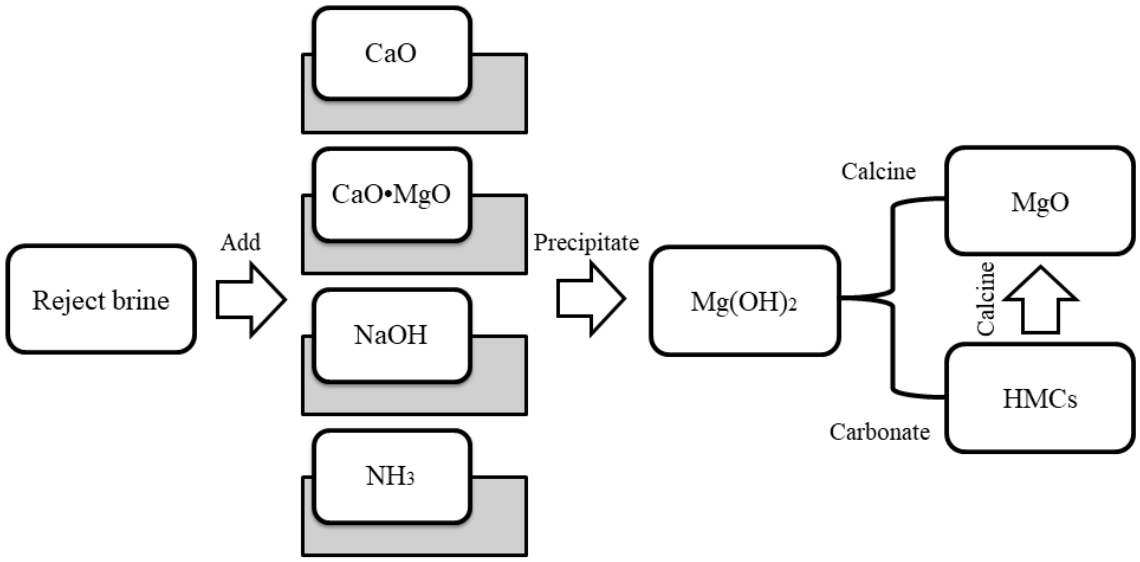

Figure 8.2 Material flow diagram for the production of reactive MgO from reject brine

8.2.2. Inventory

The production of reactive MgO from reject brine followed two steps, the synthesis of precursors from reject brine followed by the thermal decomposition into MgO. The raw materials used for this research mainly included reject brine and various chemicals. Since the inventory of the production of 1 tonne of reactive MgO is not available in existing database in SimaPro 7.3, the inputs (i.e. energy consumption and CO_2 emission), e.g. the production of raw materials and the calcination process, were mainly derived from the experiments detailed in previous studies and reported literatures (Dong, Unluer et al. 2017, Dong, Unluer et al. 2018, Dong, Unluer et al. 2018, Dong, Unluer et al. 2018).

8.2.2.1 Reject brine

Reject brine was collected and sampled from a local desalination plant in Singapore, which adopts a reverse osmosis (RO) membrane system to purify saline water and produce drinkable water for human use. These membranes reject more than 99.5% of the dissolved salts and suspended materials in the feedwater, resulting in a highly concentrated reject waste stream which contains suspended constituents and a 2- to 7-fold increased concentration of dissolved salts (Fritzmann, Lowenberg et al. 2007, Greenlee, Lawler et al. 2009, Elimelech and Phillip 2011). Prior to any analysis, reject brine was firstly passed through a 45 μm membrane filter to remove the large suspended solids. The chemical composition of reject brine, obtained via

inductively coupled plasma-optical emission spectroscopy (ICP-OES), is summarized in Table 8.2. Along with Mg^{2+}, which was present at a concentration of 1718 ppm, other impurities such as Na^{+}, Cl^{-}, SO_4^{2-}, K^{+} and Ca^{2+} were also identified in the reject brine.

Table 8.2 Chemical composition of reject brine used in this study.

Element	Cl	Na	SO_4	Mg	K	Ca	Sr	B	Si	Li	P	Al
Concentration (ppm)	55243 ±58.6	13580 ±41.2	4423 ±7.8	1718 ±5.4	845.7 ±4.8	471.3 ±1.2	14.6 ±0.1	3.8 ±0.1	3.7	0.3	0.2	0.1

8.2.2.2 Production of reactive MgO

Reactive MgO can be prepared via the calcination of different Mg compounds, e.g. $Mg(OH)_2$ and HMCs synthesized from reject brine. The synthesis of $Mg(OH)_2$ involves the addition of a base (e.g. CaO, CaO•MgO, sodium hydroxide (NaOH) and ammonia solution (NH_4OH)) into reject brine to precipitate $Mg(OH)_2$, which is then heated to around 500-700 ℃ to produce MgO as shown in Equations 8-2 to 8-4. Compared with the use of NH_4OH and NaOH, if CaO and CaO•MgO are used, an extra step involving the addition of calcium chloride ($CaCl_2$) to de-sulphate the reject brine to avoid the precipitation of gypsum ($CaSO_4$) was included in the pre-treatment since the additionally introduced Ca^{2+} will bond to the SO_4^{2-} in the solution. The precipitates produced from reject brine are in the form of a filter cake which contains ~50% solids depending on the type of precursors, which was calculated based on the mass before and after drying. The calcination process of the filter cake involved the removal of free water and the decomposition of precursors as shown in aforementioned Equation 8-4.

8.2.2.4. Carbonation process

The carbonation of $Mg(OH)_2$ slurries was studied to explore the efficiency of capturing CO_2 gas into $Mg(OH)_2$ slurries in the long time thermal-stable HMCs. Furthermore, the results could be used to indicate the carbonation potential of reactive MgO in concrete products since reactive MgO firstly hydrates to form $Mg(OH)_2$ and then carbonates to form different HMCs to provide strength. The synthesis of HMCs (e.g. nesquehonite, $MgCO_3•3H_2O$) was achieved via passing

CO_2 gas into $Mg(OH)_2$ slurries obtained from reject brine as detailed in (Dong, Unluer et al. 2018). The obtained $MgCO_3 \cdot 3H_2O$ can be used directly or further calcined to produce reactive MgO as shown in Equation 8-6. The source of CO_2 gas can either be from waste gas generated from a power plant or from the CO_2 generated during the thermal decomposition of $MgCO_3 \cdot 3H_2O$, which could be realized through an internal loop. The energy consumption of CO_2 gas in this research was therefore assumed to be zero.

$$Mg(OH)_2 + CO_2 + 3H_2O \rightarrow MgCO_3 \cdot 3H_2O + H_2O \quad (8\text{-}5)$$

$$MgCO_3 \cdot 3H_2O \rightarrow MgO + 3H_2O + CO_2 \quad (8\text{-}6)$$

8.2.2.5. Energy in Singapore

As of 2015, Singapore uses natural gas (95%) and others (4%) for the power generation. The electricity generation industry has over the years shifted from using oil-fired steam turbine plants to combined cycle gas turbine (CCGT) plants as shown in Table 8.3 (EMA 2016). As a result, the energies provided for the production of raw materials and the calcination of filter cake were assumed to be provided via the combustion of natural gas in Singapore.

Table 8.3 Annual fuel mix for electricity generation by energy products (Energy Market Authority (EMA))

Element	2005	2010	2012	2013	2014	2015	2016
Petroleum Products (%)	23.1	20.2	13.0	4.7	0.7	0.7	0.2
Natural gas (%)	74.4	77.2	84.3	91.8	95.4	95.3	95.5
Coal (%)	-	-	-	-	1.1	1.2	1.1
Others (%)	2.5	2.6	2.7	3.5	2.8	2.9	3.2

8.2.3. Impact assessment

In this LCA study, cumulative energy demand (CED) was used to calculate the energy consumption of each route to produce 1 tonne of reactive MgO from reject brine. IPCC 2007 within a timeframe of 100 years was incorporated to investigate the global warming potential of greenhouse gases (GHG) emissions (tonne CO_2-eq.). The results obtained at the end of the study aim to provide comprehensive knowledge for policy makers within the MgO industry on a local and global level.

8.3. Results and discussions

8.3.1 Production of raw materials

As illustrated in aforementioned text, a main contribution of the energy consumption and carbon emission come from the production of chemicals added into reject brine as listed in Table 8.4. The production of CaO is calcined from calcium carbonate ($CaCO_3$) which is mainly found in limestone via a dry route while the feedstock of CaO•MgO is dolomite which is a double carbonate containing 54–58% $CaCO_3$ and 40–44% $MgCO_3$. Calcination process is the most energy intensive in the production of CaO and CaO•MgO and the energy consumptions vary depending on the types of kilns used in the process, which are in a range of 3.50-9.20 GJ/tonne CaO and 6.50-13.0 GJ/tonne CaO•MgO (Ecofys 2009). CO_2 is released both from the chemical decomposition as well as from the combustion of the fuel and therefore, the GHG emissions add up to 1.02-1.40 tonne CO_2/tonne CaO and 1.40-1.84 tonne CO_2/tonne CaO•MgO, respectively. The production of NaOH is mainly from the chlor-alkali process that involves the electrolysis of brine. Chlorine gas is also produced while solid NaOH is obtained via the evaporation of water. The energy consumption of NaOH is reported to be in a range of 7.34-9.54 GJ/tonne NaOH with the lowest GHG emission of 0.49-0.63 tonne CO_2/tonne NaOH (Bureau 2013).

About 85% of world ammonia (NH_3) production is from the Haber Process which combines nitrogen (N_2) from air with hydrogen (H_2) derived mainly from natural gas (methane) into NH_3 based on the steam reforming concept. The production of NH_3 is a very energy demanding process, which requires 27.6-42.0 GJ/tonne NH_3 with the highest GHG emission of 3.13-4.09 tonne CO_2/tonne NH_3 (Commission 2007). However, the use of NH_3 can be advantageous as

NH_3 can be fully recovered from mother liquid and re-used for the same purpose when reacted with alkali, generally milk of lime as shown in Equation 8-9, followed by steam stripping to recover free gaseous NH_3. This technique is mainly applied in the Solvay process to produce soda ash (Na_2CO_3), where the co-generated by-product calcium chloride ($CaCl_2$) could be used to desulfate reject brine in the pre-treatment step. As 1.65 tonne CaO is required to recover 1 tonne NH_3, assuming an average of 10 recycling cycles, the average energy demand of $NH_{3(rec)}$ as the source would decrease to 7.76-17.6 GJ/tonne $NH_{3(rec)}$. If unlimited cycles applied, the average energy consumption would tend to be 5.78-15.2 GJ/tonne $NH_{3(rec)}$ with the GHG emission of 1.68-2.31 tonne CO_2/tonne $NH_{3(rec)}$. Thereby a closed-loop process can be formed with very low net environmental impacts.

Lime: $CaCO_3 \rightarrow CaO + CO_2$ (quarrying) (8-5)

Dolime: $MgCO_3 \bullet CaCO_3 \rightarrow MgO \bullet CaO + 2CO_2$ (quarrying) (8-6)

Sodium hydroxide: $NaCl_{(aq)} + H_2O_{(l)} \rightarrow NaOH_{(aq)} + ½H_{2(g)} + ½Cl_{2(g)}$ (electrolysis) (8-7)

Ammonia: $N_2 + 3H_2 \leftrightarrow 2NH_3$ (Haber Process) (8-8)

Ammonia recovery: $2NH_4Cl + CaO + H_2O \rightarrow CaCl_2 + 2NH_3 + 2H_2O$ (8-9)

Table 8.4 Inventory for the energy consumption of the production of raw materials (unit GJ/tonne) (Neelis, Worrell et al. 2009).

Input/emissions	CaO	CaO•MgO	NaOH	NH_3	$NH_{3(rec)}$
Energy (GJ/tonne)	3.50-9.20	6.50-13.0	7.34-9.54	27.6-42.0	5.78-15.2
CO_2-eq (tonne/tonne)	1.02-1.40	1.40-1.84	0.49-0.63	3.13-4.09	1.68-2.31

8.3.2 Calcination of $Mg(OH)_2$ from reject brine

The energy demand for the calcination of $Mg(OH)_2$ into reactive MgO was calculated based on the previous study on the synthesis of reactive MgO from reject brine via the addition of NH_4OH (Dong, Unluer et al. 2017). 773 K (500 ℃) was chosen as the calcination temperature in the case study. After the addition of NH_4OH into reject brine to precipitate $Mg(OH)_2$, $Mg(OH)_2$ was in

the form of filter cake which was composed of 55.2% solids. The energy consumption in the calcination of $Mg(OH)_2$ filter cake is derived by considering two steps: (i) the energy consumed to increase the temperature from room temperature (298 K, 25 ℃) to the decomposition temperature of $Mg(OH)_2$ (773K, 500 ℃), (ii) the enthalpy in the decomposition process of $Mg(OH)_2$ as shown in Table 8.5 (Shand 2006).

Table 8.5 Energy consumption of the calcination process to produce 1 tonne of reactive MgO via the decomposition of $Mg(OH)_2$.

	Filter cake (tonne)	Mass percentage (%)	Mass (tonne)	Heat energy (GJ)	Decomposition energy (GJ)	Total (GJ)
$Mg(OH)_2$	2.63	55.2	1.45	1.15	1.77	2.92
Free water	2.63	44.8	1.18	0.37	2.69	3.06
Water vapour	2.63	44.8	1.18	0.88	0	0.88
Total (GJ)						6.85

A production yield of 1 tonne of MgO requires decomposing 1.45 tonne of pure $Mg(OH)_2$ and the decomposition temperature of $Mg(OH)_2$ under one atmosphere CO_2 pressure is in the range between 773 K and 973 K (500 and 700 ℃). Firstly the energy required to raise the temperature from ambient air (298 K) to the decomposition temperature (773 K) is calculated using the formula: $C_p \times$ increase in temperature (K). The specific heat capacity (C_p) of $Mg(OH)_2$ at 773 K is 1.78 kJ/kg K, which results in the energy demand of 1.15 GJ in consideration of the purity of the synthesized $Mg(OH)_2$ of ~94%. The energy required for the decomposition of $Mg(OH)_2$ is calculated based on the enthalpy of decomposition (1304 kJ/kg), which brought in 1.77 GJ. As for the free water, the energy required to raise the room temperature (298 K) to boiling point (373 K) is calculated based on the specific heat capacity of water (4.18 kJ/kg K) and the percentage of water in the filter cake (44.8%), resulting in 0.37 GJ. This is followed by the

enthalpy of the vaporization of water (2283 kJ/kg), resulting in 2.69 GJ. Finally the energy required to heat up the resultant steam to 773 K is calculated via the heat capacity of water vapour (1.86 kJ/kg K), bringing in 0.88 GJ. The total energy required for the calcination process is the summation of the energy required for each individual step, resulting in a total of 6.85 GJ for the production of 1 tonne reactive MgO. The energy demand for the calcination of the synthesized $Mg(OH)_2$ from reject brine was assumed to be same for the use of other bases.

8.3.3 CED and GHG emission of MgO calcined from $Mg(OH)_2$

The energy consumptions of the production of 1 tonne of reactive MgO from reject brine via different routes are compared via the calculations of CED of each route as shown in Figure 8.3 and Table 8.6. The energy demands for the calcination process via different routes remain same as 8.0 GJ/tonne MgO, therefore the total energy consumptions of each route are dependent on the energy requests of the production of raw materials. The use of NH_3 without recycling as the base source requests the highest energy demand of 35.6-49.9 GJ/tonne MgO, being responsible for the highest GHG emission of 2.02-2.83 tonne CO_2-eq/tonne MgO, which was obtained by using an IPCC climate change factor with a timeframe of 100 years. However, if NH_3 is recycled unlimitedly through the addition of CaO milk, the final energy consumption can significantly decrease to 13.9-23.2 GJ/tonne MgO with the GHG emission of 1.89-2.42 tonne CO_2-eq/tonne MgO, which is at the same level of using CaO purely as the base. On the other hand, the application of CaO requires the least energy demand of 13.9-23.2 GJ/tonne MgO while if CaO•MgO applied, a slightly higher energy of 18.4-27.6 GJ/tonne MgO is needed. However, the use of CaO•MgO releases the highest the GHG emissions of 2.14-2.66 tonne CO_2-eq/tonne MgO since the decomposition of dolomite and limestone releases significant amount of CO_2 gas. Even though the use of NaOH requests the second highest energy demand of 25.2-30.4 GJ/tonne MgO next to NH_3, the least GHG emission of 1.43-1.72 tonne CO_2-eq/tonne MgO is observed as the GHG emission is only coming from the fuels burning for the power generation. It must be noted that reactive MgO cement can fully carbonate and achieve a carbonation degree of 100% in concrete products. Thus, when this carbonation capability of MgO (1.10 tonne CO_2-eq/tonne MgO) is integrated in the calculation of its overall GHG emission, the GHG emission would

decrease to as low as 0.33-0.62 tonne CO_2-eq/tonne MgO after fully carbonation, which enables a stable and permanent storage of CO_2 within construction products while gaining strength.

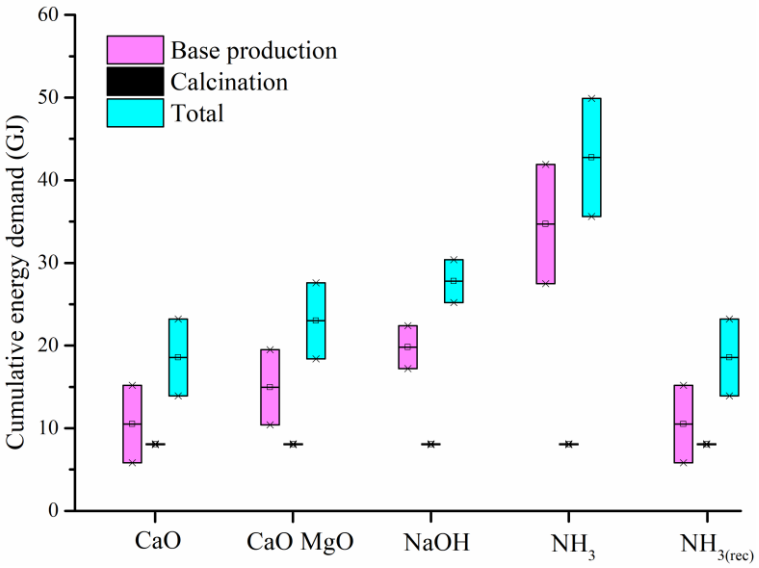

Figure 8.3 CED of the production of 1 tonne of reactive MgO calcined from $Mg(OH)_2$ obtained from reject brine via different routes

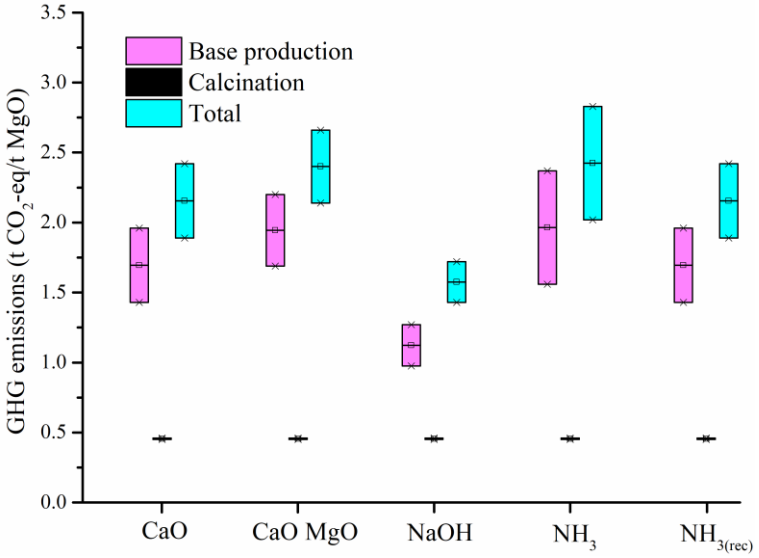

Figure 8.4 GHG emission of the production of 1 tonne of reactive MgO calcined from $Mg(OH)_2$ obtained from reject brine via different routes

Table 8.6 Global warming potential of the production of 1 tonne of reactive MgO via the decomposition of $Mg(OH)_2$ obtained from reject brine via different routes.

Input/emissions	CaO	CaO•MgO	NaOH	NH_3	$NH_{3(rec)}$
CED (GJ)	13.9-23.2	18.4-27.6	25.2-30.4	35.6-49.9	13.9-23.2
CO_2-eq (tonne)	1.89-2.42	2.14-2.66	1.43-1.72	2.02-2.83	1.89-2.42

8.3.4 Carbonation of $Mg(OH)_2$ from reject brine

Table 8.7 Global warming potential of the production of 1 tonne of $MgCO_3•3H_2O$ via the direct carbonation of $Mg(OH)_2$ slurries obtained from reject brine via different routes.

Input/emissions	CaO	CaO•MgO	NaOH	NH_3	$NH_{3(rec)}$
CED (GJ)	2.22-5.79	3.96-7.45	6.57-8.53	10.5-16	2.22-5.79
CO_2-eq (tonne)	0.23-0.43	0.32-0.52	0.05-0.17	0.28-0.59	0.23-0.43

The efficiency of the sequestration of CO_2 into $Mg(OH)_2$ slurries synthesized from reject brine in the form of $MgCO_3•3H_2O$ via the addition of NaOH was achieved at 82.6% (Dong, Unluer et al. 2018), which is assumed to achieve the same level if other bases are used in this study. Since the precipitation and carbonation are not included in the calculation of the energy consumption and GHG emission, the CED of the production of 1 tonne of $MgCO_3•3H_2O$ would be solely coming from the production of raw materials as shown in

Table 8.7. However, the carbonation of $Mg(OH)_2$ slurries could sequestrate CO_2 gas and store into $MgCO_3•3H_2O$, leading to the reduction in the GHG emission. The use of NH_3 without recycling reveals the highest CED of 10.5-16.0 GJ/tonne MgO with the GHG emission of 0.28-0.59 tonne CO_2-eq/tonne MgO. However, if NH_3 is recycled unlimitedly, the CED would go

down to the same level of use of CaO at 2.22-5.79 GJ/tonne MgO with the GHG emission of 0.23-0.43 tonne CO_2-eq/tonne MgO. While if NaOH is used, a GHG emission as low as 0.05-0.17 tonne CO_2-eq/tonne MgO could be achieved. As a result, when reactive MgO hydrates to $Mg(OH)_2$ and further carbonates to HMCs in the construction products, the GHG emission would significantly decrease to a nearly zero carbon footprint.

8.3.5 Calcination of $MgCO_3•3H_2O$ from reject brine

Table 8.8 Energy consumption of the calcination process to produce 1 tonne of reactive MgO via the decomposition of $MgCO_3•3H_2O$.

	Filter cake (tonne)	Weight percentage (%)	Content weight (tonne)	Heat energy (GJ)	Decomposition energy (GJ)	Total (GJ)
$MgCO_3•3H_2O$	7.36	41.5	2.84	3.21	4.98	8.18
$Mg(OH)_2$	7.36	41.5	0.11	0.14	0.15	0.28
Free water	7.36	58.5	4.31	1.35	9.83	11.2
Water vapour	7.36	58.5	4.31	4.81	0	4.81
Total (GJ)						24.2

The energy demand for the calcination of $MgCO_3•3H_2O$ into MgO was calculated following the same methodology as detailed in the aforementioned section 3.2. 700 ℃ was chosen as the calcination temperature in the case study to ensure the fully decomposition of $MgCO_3•3H_2O$ into reactive MgO. The precipitated $MgCO_3•3H_2O$ was also in the form of filter cake which was composed of 41.5% solids and the energy consumption was calculated to be 24.2 GJ/tonne MgO as shown in Table 8.8, which is significantly higher than the energy demand for the calcination of $Mg(OH)_2$. This is mainly due to a much more raw material needed to obtain the 1 tonne of

reactive MgO and a higher calcination temperature of 700 ℃ compared to 500 ℃ in $Mg(OH)_2$. The energy demand for the calcination of $MgCO_3•3H_2O$ obtained from reject brine is assumed to be same for the use of other bases.

The energy consumptions of the production of 1 tonne of reactive MgO calcined from $MgCO_3•3H_2O$ obtained from reject brine via different routes are compared via the calculation of CED of each route as shown in Figure 8.5 and Table 8.9. Due to the high energy demand of the calcination process, a doubled CED of each route of production 1 tonne of reactive MgO is observed compared with reactive MgO calcined from $Mg(OH)_2$. The use of NH_3 if not recycled requests the highest energy demand of 60.4-77.1 GJ/tonne MgO with the highest GHG emission of 2.45-3.39 tonne CO_2-eq/tonne MgO. While if NH_3 is fully recycled unlimitedly, CED would significant decease to the same level of use of CaO as the base source of 35.1-46.4 GJ/tonne MgO. However, the GHG emission still remain high as 2.3-2.92 tonne CO_2-eq/tonne MgO since the decomposition of 1 tonne of limestone to produce 0.56 tonne of CaO would release 0.44 tonne of CO_2. The use of NaOH requests the second highest CED of 48.4-54.4 GJ/tonne MgO with the lowest GHG emission of 1.77-2.11 tonne CO_2-eq/tonne MgO. Overall, the production of 1 tonne of reactive MgO calcined from $MgCO_3•3H_2O$ stays uncompetitive compared with reactive MgO calcined from $Mg(OH)_2$ due to the doubled CED and ~20% more GHG emission.

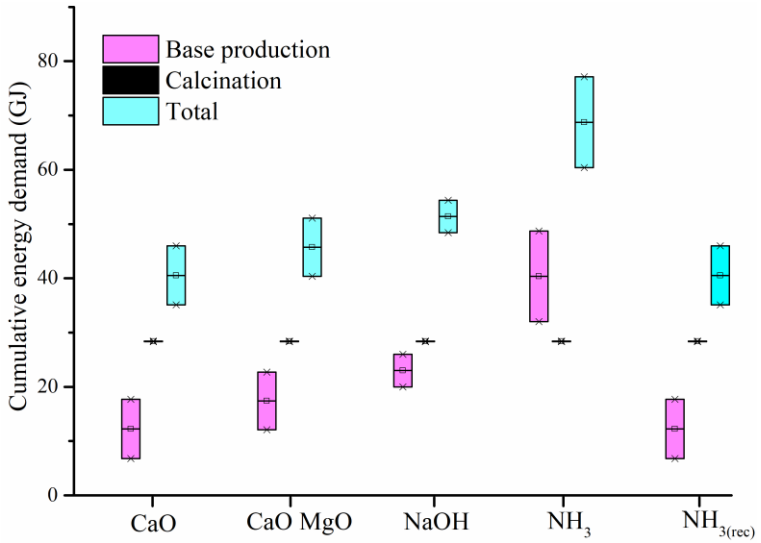

Figure 8.5 CED of the production of 1 tonne of reactive MgO calcined from $MgCO_3•3H_2O$ obtained from reject brine via different routes

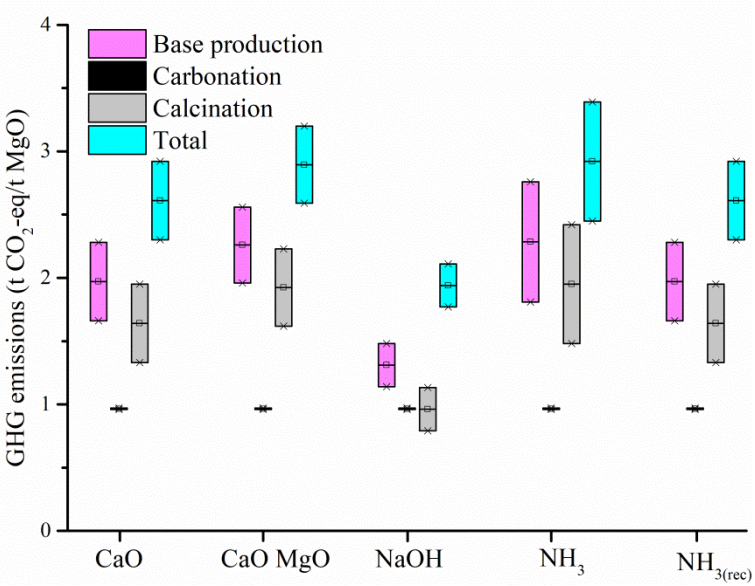

Figure 8.6 GHG emission of the production of 1 tonne of MgO calcined from $MgCO_3 \cdot 3H_2O$ obtained from reject brine via different route

Table 8.9 Global warming potential of the production of 1 tonne of reactive MgO via the decomposition of $MgCO_3 \cdot 3H_2O$ obtained from reject brine via different routes.

Input/emissions	CaO	CaO•MgO	NaOH	NH_3	$NH_{3(rec)}$
CED (GJ)	35.1-46.4	40.4-51.1	48.4-54.4	60.4-77.1	35.1-46.4
CO_2-eq (tonne)	2.30-2.92	2.59-3.2	1.77-2.11	2.45-3.39	2.30-2.92

8.4. Conclusions

This study mainly evaluates the CED and GHG emission of the production of reactive MgO calcined from $Mg(OH)_2$ and $MgCO_3 \cdot 3H_2O$ obtained from reject brine via different routes. A cradle-to-gate LCA of the production of reactive MgO from reject brine has been performed. The effects of key parameters, which are identified as the production of raw materials and calcination

process, are studied and compared on the CED and GHG emission of the production of reactive MgO from reject brine via different routes. Generally the production of 1 tonne of reactive MgO calcined from $MgCO_3 \cdot 3H_2O$ requests a doubled CED and ~20% more GHG emission compared with reactive MgO calcined from $Mg(OH)_2$ in every route. When reactive MgO is calcined from $Mg(OH)_2$, the use of NH_3 without recycling requests the highest energy demand of 35.6-49.9 GJ/tonne MgO with the highest GHG emission of 2.02-2.83 tonne CO_2-eq/tonne MgO. While if NH_3 is recycled unlimitedly through the addition of CaO milk, the final energy consumption can significantly decrease to the same level of use of CaO, being responsible for 13.9-23.2 GJ/tonne MgO with the GHG emission of 1.89-2.42 tonne CO_2-eq/tonne MgO. The use of NaOH requests the second highest energy demand of 25.2-30.4 GJ/tonne MgO next to NH_3, however, the least GHG emission of 1.43-1.72 tonne CO_2-eq/tonne MgO is observed.

The carbonation of $Mg(OH)_2$ slurries was also studied to explore the CCS potential of $Mg(OH)_2$ slurries in the carbonates, which could be used to indicate the carbonation potential of reactive MgO in concrete products. When NaOH is used as the base source, an as low as GHG emission of 0.05-0.17 tonne CO_2-eq/tonne MgO could be achieved. As a result, a nearly zero carbon footprint could be achieved when reactive MgO hydrates to $Mg(OH)_2$ and further carbonates to HMCs in the construction products.

Chapter 9 Conclusions and recommendations for future research

9.1. Conclusions

This research develops different routes to synthesize and characterize the precursors, i.e. $Mg(OH)_2$, hydrated magnesium carbonates (HMCs) and $MgC_2O_4•2H_2O$ from reject brine, which have been calcined to produce reactive MgO. The economic feasibility, energy consumption and carbon footprint of the production of reactive MgO from reject brine via different routes have been calculated and evaluated by means of life cycle assessment (LCA). Research activities are planned and conducted accordingly, and significant findings and accomplishments in this thesis are summarized in the following sections.

The synthesis of the precursor $Mg(OH)_2$ from reject brine has been realized via the addition of NH_4OH and NaOH as illustrated in Chapter 3, 4 and 5. The influence of the molar ratios of Mg:NH_4OH and Mg:NaOH was investigated with the goal of optimizing the yield and the purity of the precipitates. An optimum NH_4OH to Mg^{2+} ratio of 6 and NaOH to Mg^{2+} ratio of 2, which resulted in a high Mg content while minimizing Ca-based impurities, was determined and achieving a high purity of ~94%. Type of alkali source used during the synthesis of $Mg(OH)_2$ had a notable influence on the properties of $Mg(OH)_2$, as the use of NaOH generated a densely packed granular morphology with relatively clear boundaries while a flake-like morphology with a more porous structure was observed via the use of NH_4OH.

A correlation between the calcination conditions and the reactivity, SSA of MgO was established. While a certain minimum temperature was required for the complete decomposition of $Mg(OH)_2$ into MgO, an increase in the calcination temperature and duration lowered the SSA and reactivity of MgO regardless of bases used. However, the use of NH_4OH generated MgO samples with porous structures, which enabled higher SSA and reactivities than those observed in NaOH-based samples calcined under lower temperatures. The SSA and reactivity of NH_4OH-based MgO were more vulnerable to the changes in the calcination conditions and therefore indicated a sharper decline at higher calcination temperatures and durations, which was associated with its relatively more porous structure in comparison to NaOH-based MgO. Out of

all MgO samples, calcination of $Mg(OH)_2$ at 500 ℃ for 2 hours resulted in the most reactive MgO, which generated NH_4OH-based MgO with a SSA of 78.8 m^2/g compared with NaOH-based MgO with a SSA of 51.4 m^2/g.

The production of HMCs via the sequestration of CO_2 through sparging CO_2 gas directly into $Mg(OH)_2$ slurries generated from reject brine was presented in Chapter 6. The carbonation of $Mg(OH)_2$ slurries under the elevated $Mg(OH)_2$:CO_2 ratio led to the generation of nesquehonite compared to dypingite precipitated at lower $Mg(OH)_2$:CO_2 ratios of 1:1. A specific "house of cards" texture, involving the formation of rosette-like dypingite flakes on the surface of nesquehonite needles, was discovered under elevated pH and $Mg(OH)_2$:CO_2 ratios conditions. The carbonation of $Mg(OH)_2$ slurry prepared from reject brine led to a high yield of nesquehonite with a higher purity than the dypingite obtained from the carbonation of commercial $Mg(OH)_2$ slurry. The higher degree of carbonation revealed by reject brine $Mg(OH)_2$ than commercial $Mg(OH)_2$ slurry (82.6 vs. 43.7%) demonstrated its high potential to be used in the capture and long-term storage of CO_2 in the form of HMCs.

A comprehensive investigation on a two-step synthesis of MgC_2O_4•$2H_2O$ from reject brine via the use of $H_2C_2O_4$•$2H_2O$, which was further calcined to produce reactive MgO with ultra-high purity, was reported in Chapter 7. The addition of $H_2C_2O_4$•$2H_2O$ into reject brine proved to be a successful method to selectively precipitate out CaC_2O_4•H_2O and MgC_2O_4•$2H_2O$ under a controlled pH. The effects of Ca^{2+}:$H_2C_2O_4$•$2H_2O$, Mg^{2+}:$H_2C_2O_4$•$2H_2O$ and pH on the final yield and purity was investigated with the goal of optimizing the yield and purity of the synthesized MgC_2O_4•$2H_2O$. MgC_2O_4•$2H_2O$ with a ultra-high purity of 99.5% was obtained, achieving a high recovery rate of Mg^{2+} of 94.9%. An increase in the calcination temperatures and durations lowered the SSA values of MgO. Out of all samples, calcination of MgC_2O_4•$2H_2O$ at 700 ℃ for 2 hours resulted in the most reactive MgO samples, with a SSA of 30.2 m^2/g.

Finally a local life cycle inventory (LCI) and a comprehensive life cycle assessment (LCA) on the economic feasibility, energy consumption and carbon footprint of the production of reactive MgO from reject brine via different routes were revealed in Chapter 4 and 8. Generally the

production of 1 tonne of reactive MgO calcined from $MgCO_3•3H_2O$ requests a doubled CED and ~20% more GHG emission compared with reactive MgO calcined from $Mg(OH)_2$ in every route. The use of recycled NH_3 or CaO can achieve the lowest CED of 13.9-23.2 GJ/tonne MgO if reactive MgO is calcined from $Mg(OH)_2$ obtained from reject brine. However, the least GHG emissions of 1.43-1.72 tonne CO_2-eq/tonne MgO are observed when NaOH is used as the base source since the CO_2 emissions are only generated from the fuels burning. The economic feasibility of producing reactive MgO from reject brine via different bases has been calcuated and a cheaper base alternative would make the production of reactive MgO from reject brine more economically feasible. The overall cost was calculated as S$622/tonne MgO if CaO is used, which matches the market price of MgO via a dry route of S$617/tonne MgO.

9.2. Recommendations for future research

In this study, the presence of Ca in the reject brine remains a main challenge to produce reactive MgO with high purity. Efforts have been made through the optimization of the ratios of $Mg:NH_4OH$ and Mg:NaOH to minimize the co-precipitation of $CaCO_3$ to enhance the purity of MgO. A two-step synthesis of $MgC_2O_4•2H_2O$ from reject brine via the use of $H_2C_2O_4•2H_2O$ to separate Mg and Ca has also been developed. It is suggested that future efforts can be made to identify and study the key parameters, e.g. pH, temperature, foreign ions added and etc., on the ion competitions between Ca and Mg in the reject brine to generate numeric models to better describe the ion behaviours, which can provide future support and guidance on the production of reactive MgO from reject brine.

In this study, reactive MgO is produced from reject brine in small-scale. Scaling up the production of reactive MgO from reject brine is suggested to be studied in the future and compared with the properties of reactive MgO produced in this research. Furthermore, the application of the reactive MgO produced from reject brine in the construction materials is encouraged to explore and compare the performance of reactive MgO synthesized from reject brine as an alternative binder with commercial MgO and PC products.

With regard of the direct carbonation of $Mg(OH)_2$ slurries generated from reject brine in the form of dypingite or nesquehonite, it is suggested to further study the thermal and structural

stability of HMCs in the long run to ensure the safety of CO_2 stable storage. Further efforts are suggested to make on the study of the mechanism of the formation of the "house of cards" texture and the application of this special texture.

Finally, the LCA study reveals that a cheaper and cleaner base source could make the production of reactive MgO from reject brine more economic feasible and environmentally friendly. Thus, it is suggested to explore the feasibility of the use of waste bases to produce reactive MgO from reject brine and compare with NH_4OH and NaOH.

References

Adham, S., A. Hussain, J. M. Matar, R. Dores and A. Janson (2013). "Application of Membrane Distillation for desalting brines from thermal desalination plants." Desalination **314**: 101-108.

Agency, I. E. and I. E. Agency (2007). Tracking industrial energy efficiency and CO2 emissions, Organisation for Economic Co-operation and Development.

Ahmaruzzaman, M. (2010). "A review on the utilization of fly ash." Progress in Energy and Combustion Science **36**(3): 327-363.

Ahmed, M., A. Arakel, D. Hoey, M. R. Thumarukudy, M. F. A. Goosen, M. Al-Haddabi and A. Al-Belushi (2003). "Feasibility of salt production from inland RO desalination plant reject brine: a case study." Desalination **158**(1-3): 109-117.

Al-Tabbaa, A. (2013). Eco-Efficient Concrete: Reactive magnesia cement. F. PachecoTorgal, S. Jalali, J. Labrincha and V. M. John**:** 523-543.

Al-Zahrani, A. and M. Abdel-Majeed (2007). "Production of magnesia from local dolomite ores and rejected brines from local desalination plants." Saudi Engineering Conference.

Al Bazedi, G., R. S. Ettouney, S. R. Tewfik, M. H. Sorour and M. A. El-Rifai (2014). "Salt recovery from brine generated by large-scale seawater desalination plants." Desalination and Water Treatment **52**(25-27): 4689-4697.

Alberti, F., N. Mosto and C. Sommariva (2012). "Salt production from brine of desalination plant discharge." Desalination and Water Treatment **10**(1-3): 128-133.

Almutaz, I. S. and K. M. Wagialia (1990). "Production of magnesium from desalination brines." Resources Conservation and Recycling **3**(4): 231-239.

Alvarado, E., L. M. Torres-Martinez, A. F. Fuentes and P. Quintana (2000). "Preparation and characterization of MgO powders obtained from different magnesium salts and the mineral dolomite." Polyhedron **19**(22-23): 2345-2351.

Aphane, M. E. (2009). The hydration of magnesium oxide with different reactivities by water and magnesium acetate.

Arakawa, H., M. Aresta, J. N. Armor, M. A. Barteau, E. J. Beckman, A. T. Bell, J. E. Bercaw, C. Creutz, E. Dinjus, D. A. Dixon, K. Domen, D. L. DuBois, J. Eckert, E. Fujita, D. H. Gibson, W. A. Goddard, D. W. Goodman, J. Keller, G. J. Kubas, H. H. Kung, J. E. Lyons, L. E. Manzer, T. J. Marks, K. Morokuma, K. M. Nicholas, R. Periana, L. Que, J. Rostrup-Nielson, W. M. H. Sachtler, L. D. Schmidt, A. Sen, G. A. Somorjai, P. C. Stair, B. R. Stults and W. Tumas (2001). "Catalysis research of relevance to carbon management: Progress, challenges, and opportunities." Chemical Reviews **101**(4): 953-996.

Arnal, J. M., M. Sancho, I. Iborra, J. M. Gozalvez, A. Santafe and J. Lora (2005). "Concentration of brines from RO desalination plants by natural evaporation." Desalination **182**(1-3): 435-439.

Baglioni, P., G. Ferraro, S.-H. Chen, E. Fratini, F. Ridi, U. S. Jeng, W.-S. Chiang and Y.-Q. Yeh (2014). "Multiscale structure of calcium- and magnesium-silicate-hydrate gels." Journal of Materials Chemistry A.

Balkevich, V. and V. Lemeshev (1968). "Super-refractory grain-structured materials from fused MgO." Refractories and Industrial Ceramics **9**(5): 313-316.

Ballirano, P., C. De Vito, V. Ferrini and S. Mignardi (2010). "The thermal behaviour and structural stability of nesquehonite, MgCO3.3H2O, evaluated by in situ laboratory parallel-beam X-ray powder diffraction: New constraints on CO2 sequestration within minerals." Journal of Hazardous Materials **178**(1-3): 522-528.

Ballirano, P., C. De Vito, S. Mignardi and V. Ferrini (2013). "Phase transitions in the Mg-CO2-H2O system and the thermal decomposition of dypingite, Mg5(CO3)4(OH)2 5H2O: Implications for geosequestration of carbon dioxide." Chemical Geology **340**: 59-67.
Bartley, J. K., C. L. Xu, R. Lloyd, D. I. Enache, D. W. Knight and G. J. Hutchings (2012). "Simple method to synthesize high surface area magnesium oxide and its use as a heterogeneous base catalyst." Applied Catalysis B-Environmental **128**: 31-38.
Behij, S., H. Hammi, H. Hamzaoui and A. M'nif (2013). "Magnesium salts as compounds of the preparation of magnesium oxide from Tunisian natural brines." Chemical Industry and Chemical Engineering Quarterly **19**(2): 263-271.
Berner, R. A. (1975). "The role of magnesium in the crystal growth of calcite and aragonite from sea water." Geochimica et Cosmochimica Acta **39**(4): 489-504.
Bhatti, A. S., D. Dollimore and A. Dyer (1984). "Magnesia from seawater - a review." Clay Minerals **19**(5): 865-875.
Bogner, S. (2015). "MGX minerals plans to enter the magnesium market in 2016." Rockstone Reserach Ltd.
Botha, A. and C. A. Strydom (2001). "Preparation of a magnesium hydroxy carbonate from magnesium hydroxide." Hydrometallurgy **62**(3): 175-183.
Boyd, C. E. (2015). Water Quality: An Introduction, Springer International Publishing.
Boynton, R. S. (1980). Chemistry and technology of lime and limestone, John wiley.
Bureau, E. I. (2013). Best available techniques reference document for the production of chlor - alkali, final draft, European IPPC Bureau.
Caraballo, M. A., T. S. Rotting, F. Macias, J. M. Nieto and C. Ayora (2009). "Field multi-step limestone and MgO passive system to treat acid mine drainage with high metal concentrations." Applied Geochemistry **24**(12): 2301-2311.
Casas, S., C. Aladjem, E. Larrotcha, O. Gibert, C. Valderrama and J. L. Cortina (2014). "Valorisation of Ca and Mg by-products from mining and seawater desalination brines for water treatment applications." Journal of Chemical Technology and Biotechnology **89**(6): 872-883.
Choudhary, V. R., V. H. Rane and R. V. Gadre (1994). "Influence of Precursors Used in Preparation of MgO on Its Surface Properties and Catalytic Activity in Oxidative Coupling of Methane." Journal of Catalysis **145**(2): 300-311.
Christ, C. and P. Hostetler (1970). "Studies in the system MgO-SiO2-CO2-H2O (II); the activity-product constant of magnesite." American Journal of Science **268**(5): 439-453.
Cipollina, A., A. Misseri, G. D. A. Staiti, A. Galia, G. Micale and O. Scialdone (2012). "Integrated production of fresh water, sea salt and magnesium from sea water." Desalination and Water Treatment **49**(1-3): 390-403.
Commission, E. (2007). Reference document on best available techniques for the manufacture of large volume inorganic chemicals - ammonia, acids and fertilisers, European Commission.
commission, E. (2010). Cement, Lime and Magnesium Oxide Manufacturing Industries.
Crawford, J. T., W. A. Hustrulid, M. American Institute of Mining and P. Engineers (1979). Open pit mine planning and design, Society of Mining Engineers of the American Institute of Mining, Metallurgical, and Petroleum Engineers.
Dave, R. H. and P. K. Ghosh (2005). "Enrichment of bromine in sea-bittern with recovery of other marine chemicals." Industrial & Engineering Chemistry Research **44**(9): 2903-2907.
Dell, R. and S. Weller (1959). "The thermal decomposition of nesquehonite MgCO3 ·3H2O and magnesium ammonium carbonate MgCO3 (NH4)2CO3 · 4H2O." Transactions of the Faraday Society **55**: 2203-2220.

Dlugokencky, E. and P. Tans. (2017). from www.esrl.noaa.gov/gmd/ccgg/trends/.
Dong, H., C. Unluer, E.-H. Yang and A. Al-Tabbaa (2018). "Production of Mg-carbonates via the sequestration of CO2 in Mg(OH)2 slurries generated from reject brine (unpublished)."
Dong, H. L., C. Unluer, E. H. Yang and A. Al-Tabbaa (2017). "Synthesis of reactive MgO from reject brine via the addition of NH4OH." Hydrometallurgy **169**: 165-172.
Dong, H. L., C. Unluer, E. H. Yang and A. Al-Tabbaa (2018). "Recovery of reactive MgO from reject brine via the addition of NaOH." Desalination **429**: 88-95.
Dong, H. L., C. Unluer, E. H. Yang, F. Jin and A. Al-Tabbaa (2018). "Investigation of the properties of MgO recovered from reject brine obtained from desalination plants." Journal of Cleaner Production **196**: 100-108.
Drom;, A. and K. Loveland (1998). "Saltcrete: a partnership in treatment and disposal. ." Waste Management Symposia.
Druckenmiller, M. L. and M. M. Maroto-Valer (2005). "Carbon sequestration using brine of adjusted pH to form mineral carbonates." Fuel Processing Technology **86**(14-15): 1599-1614.
Dung, N. and C. Unluer (2017). "Sequestration of CO 2 in reactive MgO cement-based mixes with enhanced hydration mechanisms." Construction and Building Materials **143**: 71-82.
Dyer, O. (2003). A rock and a hard place, eco-cement yet to cover ground in the building industry. The guardian.
Ecofys (2009). Methodology for the free allocation of emission allowances in the EU ETS post 2012: Sector report for the lime industry, Fraunhofer Institute for Systems and Innovation Research.
EIPPCB (2007). Reference document on best available techniques for the manufacture of large volume inorganic chemicals - solids and others industry. Brussels, Belgium, European commission.
El-Naas, M. H. (2011). Reject brine management. Desalination, trends and technologies, InTech**:** 237-252.
El-Naas, M. H., A. H. Al-Marzouqi and O. Chaalal (2010). "A combined approach for the management of desalination reject brine and capture of CO2." Desalination **251**(1): 70-74.
Elimelech, M. and W. A. Phillip (2011). "The future of seawater desalination: Energy, technology, and the environment." Science **333**(6043): 712-717.
Elving, P. J. and E. R. Caley (1937). "Separation of magnesium as oxalate." Industrial & Engineering Chemistry Analytical Edition **9**(12): 558-562.
EMA (2016). "Singapore energy statistics 2016." Energy Market Authority.
Eubank, W. R. (1951). "Calcination studies of magnesium oxides." Journal of the American Ceramic Society **34**(8): 225-229.
Fellner, P., J. Híveš, V. Khandl, M. Králik, J. Jurišová, T. Liptaj and L. Pach (2011). "Preparation of magnesium hydroxide from nitrate aqueous solution." Chemical Papers **65**(4).
Ferrini, V., C. De Vito and S. Mignardi (2009). "Synthesis of nesquehonite by reaction of gaseous CO2 with Mg chloride solution: Its potential role in the sequestration of carbon dioxide." Journal of Hazardous Materials **168**(2-3): 832-837.
Figueroa, J. D., T. Fout, S. Plasynski, H. McIlvried and R. D. Srivastava (2008). "Advancesn in CO2 capture technology - the US department of energy's carbon sequestration program." International Journal of Greenhouse Gas Control **2**(1): 9-20.
Forster, P., V. Ramaswamy, P. Artaxo, T. Berntsen, R. Betts, D. W. Fahey, J. Haywood, J. Lean, D. C. Lowe and G. Myhre (2007). Changes in atmospheric constituents and in radiative forcing. Chapter 2. Climate Change 2007. The Physical Science Basis.

Friedrich, R., H. Robinson and R. Spencer (1946). Magnesium hydroxide from sea water, Google Patents.
Fritzmann, C., J. Lowenberg, T. Wintgens and T. Melin (2007). "State-of-the-art of reverse osmosis desalination." Desalination **216**(1-3): 1-76.
Fukushima, Y. (2016). "Caustic soda prices on upward trend in Asian markets."
Gao, P., X. Lu, F. Geng, X. Li, J. Hou, H. Lin and N. Shi (2008). "Production of MgO-type expansive agent in dam concrete by use of industrial by-products." Building and Environment **43**(4): 453-457.
Gerdemann, S. J., W. K. O'Connor, D. C. Dahlin, L. R. Penner and H. Rush (2007). "Ex situ aqueous mineral carbonation." Environmental Science & Technology **41**(7): 2587-2593.
Gibbins, J. and H. Chalmers (2008). "Carbon capture and storage." Energy Policy **36**(12): 4317-4322.
Giwa, A., V. Dufour, F. Al Marzooqi, M. Al Kaabi and S. Hasan (2017). "Brine management methods: Recent innovations and current status." Desalination **407**: 1-23.
Greenlee, L. F., D. F. Lawler, B. D. Freeman, B. Marrot and P. Moulin (2009). "Reverse osmosis desalination: Water sources, technology, and today's challenges." Water Research **43**(9): 2317-2348.
Guo, H., Y. Pei, Z. Wang, Y. Yang, K. Wang, J. Xie and Y. Liu (2015). "Preparation of Mg(OH)2 with caustic calcined magnesia through ammonium acetate circulation." Hydrometallurgy **152**: 13-19.
Hanchen, M., V. Prigiobbe, R. Baciocchi and M. Mazzotti (2008). "Precipitation in the Mg-carbonate system - effects of temperature and CO2 pressure." Chemical Engineering Science **63**(4): 1012-1028.
Hanlon, J. M., L. B. Diaz, G. Balducci, B. A. Stobbs, M. Bielewski, P. Chung, I. MacLaren and D. H. Gregory (2015). "Rapid surfactant-free synthesis of Mg(OH)(2) nanoplates and pseudomorphic dehydration to MgO." Crystengcomm **17**(30): 5672-5679.
Hao, R. (2017). Investigation into the production of carbonates and oxides from synthetic brine through carbon sequestration. Ph.D., University of Cambridge.
Hao, Z. H. and F. L. Du (2009). "Synthesis of basic magnesium carbonate microrods with a "house of cards" surface structure using rod-like particle template." Journal of Physics and Chemistry of Solids **70**(2): 401-404.
Harrison, A. J. W. (2008). "Reactive magnesium oxide cements."
Harrison, J. (2004b). "TecEco Cement Concretes – Abatement, Sequestration and Waste utilization in the built environment."
Harrison, J. (2001a). TecEco cements. [online].
Hasanbeigi, A., L. Price and E. Lin (2012). "Emerging energy-efficiency and CO2 emission-reduction technologies for cement and concrete production: A technical review." Renewable & Sustainable Energy Reviews **16**(8): 6220-6238.
Hassan, D. (2013). Environmental Sustainability Assessment & Associated Experimental Investigatations of Magnesia Production Routes. Ph.D., University of Cambridge.
Haszeldine, R. S. (2009). "Carbon capture and storage: How green can black be?" Science **325**(5948): 1647-1652.
Henrist, C., J.-P. Mathieu, C. Vogels, A. Rulmont and R. Cloots (2003). "Morphological study of magnesium hydroxide nanoparticles precipitated in dilute aqueous solution." Journal of Crystal Growth **249**(1): 321-330.

Herzog, H. J. (1998). CO2 capture, reuse, and sequestration technologies for mitigating global climate change, USDOE Federal Energy Technology Center, Morgantown, WV (United States).
Holth, T. (1949). "Separation of Calcium from Magnesium by Oxalate Method." Analytical Chemistry **21**(10): 1221-1226.
Hopkinson, L., P. Kristova, K. Rutt and G. Cressey (2012). "Phase transitions in the system MgO-CO2-H2O during CO2 degassing of Mg-bearing solutions." Geochimica Et Cosmochimica Acta **76**: 1-13.
Huijgen, W. J. J., G. J. Witkamp and R. N. J. Comans (2005). "Mineral CO2 sequestration by steel slag carbonation." Environmental Science & Technology **39**(24): 9676-9682.
Huntzinger, D. N. and T. D. Eatmon (2009). "A life-cycle assessment of Portland cement manufacturing: comparing the traditional process with alternative technologies." Journal of Cleaner Production **17**(7): 668-675.
Hyflux (2011). Pollution control study for Tuas desalination and power plant project, TuasSpring Pte Ltd.
IDA. (2015). "The current state of desalination." Retrieved June 30.
IPCC (2007). "The fourth assessment report of the Intergovernmental Panel on Climate Change."
IPCC (2013). "Climate change 2013_the physical science basis."
Irving, L. (1926). "The Precipitation of Calcium and Magnesium from Sea Water." Journal of the Marine Biological Association
Itatani, K., A. Itoh, F. S. Howell, A. Kishioka and M. Kinoshita (1993). "Densification and microstructure development during the sintering of submicrometer magnesium-oxide particles prepared by a vapor-phase oxidation process." Journal of Materials Science **28**(3): 719-728.
Itatani, K., K. Koizumi, F. S. Howell, A. Kishioka and M. Kinoshita (1988). "Agglomeration of magnesium oxide particles formed by the decomposition of magnesium hydroxide .1. Agglomeration at increasing temperature." Journal of Materials Science **23**(9): 3405-3412.
Itatani, K., M. Nomura, A. Kishioka and M. Kinoshita (1986). "Sinterability of various high-purity magnesium-oxide powders." Journal of Materials Science **21**(4): 1429-1435.
Jin, F. and A. Al-Tabbaa (2014). "Characterisation of different commercial reactive magnesia." Advances in Cement Research **26**(2): 101-113.
Johnson, D. A. (2002). Metals and chemical change, Royal Society of Chemistry.
Johnston, J. (1915). "The solubility-product constant of calcium and magnesium carbonates." Journal of the American Chemical Society **37**: 2001-2020.
Jones, A. (2016). "Why do ammonia prices keep falling?".
Jones, G. G. and L. Bouamane (2012). ""Power from Sunshine": A Business History of Solar Energy."
Khuyen Thi, T., K. S. Han, S. J. Kim, M. J. Kim and T. Tam (2016). "Recovery of magnesium from Uyuni salar brine as hydrated magnesium carbonate." Hydrometallurgy **160**: 106-114.
Kim, D. H. (2011). "A review of desalting process techniques and economic analysis of the recovery of salts from retentates." Desalination **270**(1-3): 1-8.
Kittrick, J. and F. Peryea (1986). "Determination of the Gibbs free energy of formation of magnesite by solubility methods." Soil Science Society of America Journal **50**(1): 243-247.
Kloprogge, J. T., W. N. Martens, L. Nothdurft, L. V. Duong and G. E. Webb (2003). "Low temperature synthesis and characterization of nesquehonite." Journal of Materials Science Letters **22**(11): 825-829.
Knibbs, N. V. S. (1924). "Lime and magnesia."

Kontoyannis, C. G. and N. V. Vagenas (2000). "Calcium carbonate phase analysis using XRD and FT-Raman spectroscopy." The Analyst **125**(2): 251-255.
Kotsupalo, N. P., A. D. Ryabtsev, V. N. Zyryanova, G. I. Berdov and V. I. Vereshchagin (2010). "Magnesia binders from natural highly mineralized multicomponent brines." Theoretical Foundations of Chemical Engineering **44**(5): 762-768.
Kramer, D. A. "Magnesium Minerals and Compounds."
Lal, R. (2004). "Soil carbon sequestration impacts on global climate change and food security." Science **304**(5677): 1623-1627.
Lanas, J. and J. I. Alvarez (2004). "Dolomitic lime: thermal decomposition of nesquehonite." Thermochimica Acta **421**(1): 123-132.
Lea, F. M. and P. C. Hewlett (1998). Lea's chemistry of cement and concrete, Arnold.
Lee, E. K., K. D. Jung, O. S. Joo and Y. G. Shul (2004). "Magnesium oxide as an effective catalyst in catalytic wet oxidation of H2S to sulfur." Reaction Kinetics and Catalysis Letters **82**(2): 241-246.
Li, X. (2012). Mechanical properties and durability performance of reactive magnesia cement concrete, University of Cambridge.
Liska, M. and A. Al-Tabbaa (2009) "Ultra-green construction: reactive magnesia masonry products." Proceedings of the ICE - Waste and Resource Management **162**, 185-196.
Liska, M., A. Al-Tabbaa, K. Carter and J. Fifield (2012a). "Scaled-up commercial production of reactive magnesium cement pressed masonry units. Part I: Production." Proceedings of the Institution of Civil Engineers-Construction Materials **165**(4): 211-223.
Liska, M., A. Al-Tabbaa, K. Carter and J. Fifield (2012b). "Scaled-up commercial production of reactive magnesia cement pressed masonry units. Part II: Performance." Proceedings of the Institution of Civil Engineers-Construction Materials **165**(4): 225-243.
Liska, M., L. J. Vandeperre and A. Al-Tabbaa (2008). "Influence of carbonation on the properties of reactive magnesia cement-based pressed masonry units." Advances in Cement Research **20**(2): 53-64.
Luo, R., Y. B. Cai, C. Y. Wang and X. M. Huang (2003). "Study of chloride binding and diffusion in GGBS concrete." Cement and Concrete Research **33**(1): 1-7.
Markov, I. V. (2016). Crystal growth for beginners: Fundamentals of nucleation, crystal growth and epitaxy, World Scientific Publishing Company.
Maroto-Valer, M. M., D. J. Fauth, M. E. Kuchta, Y. Zhang and J. M. Andrésen (2005). "Activation of magnesium rich minerals as carbonation feedstock materials for CO2 sequestration." Fuel Processing Technology **86**(14-15): 1627-1645.
Mehta, P. (1978). "History and status of performance tests for evaluation of soundness of cements." Cement Standards-Evaluation and Trends, ASTM STP **663**: 35.
Mignardi, S., C. De Vito, V. Ferrini and R. F. Martin (2011). "The efficiency of CO2 sequestration via carbonate mineralization with simulated wastewaters of high salinity." Journal of Hazardous Materials **191**(1-3): 49-55.
Mironyuk, I. F., V. M. Gun'ko, M. O. Povazhnyak, V. I. Zarko, V. M. Chelyadin, R. Leboda, J. Skubiszewska-Zięba and W. Janusz (2006). "Magnesia formed on calcination of Mg(OH)2 prepared from natural bischofite." Applied Surface Science **252**(12): 4071-4082.
Mo, L. W., M. Deng and M. S. Tang (2010). "Effects of calcination condition on expansion property of MgO-type expansive agent used in cement-based materials." Cement and Concrete Research **40**(3): 437-446.

Mo, L. W., M. Deng, M. S. Tang and A. Al-Tabbaa (2014). "MgO expansive cement and concrete in China: Past, present and future." Cement and Concrete Research **57**: 1-12.
Mohamed, A. M. O., M. Maraqa and J. Al Handhaly (2005). "Impact of land disposal of reject brine from desalination plants on soil and groundwater." Desalination **182**(1-3): 411-433.
Morita, T., J. Robinson, A. Adegbulugbe, J. Alcamo, D. Herbert, E. L. La Rovere, N. Nakicenovic, H. Pitcher, P. Raskin and K. Riahi (2001). "Greenhouse gas emission mitigation scenarios and implications." Climate change: 115-166.
Moussavi, G. and M. Mahmoudi (2009). "Removal of azo and anthraquinone reactive dyes from industrial wastewaters using MgO nanoparticles." Journal of Hazardous Materials **168**(2-3): 806-812.
Nassar, M. K. K., R. M. El-Damak and A. H. M. Ghanem (2007). "Impact of desalination plants brine injection wells on coastal aquifers." Environmental Geology **54**(3): 445-454.
Neelis, M., E. Worrell, N. Mueller, T. Angelini, C. Cremer, J. Schleich and W. Eichhammer (2009). "Developing benchmarking criteria for CO2 emissions." Ecofys Netherlands und Fraunhofer Institut für System und Innovationsforschung im Auftrag der Europäischen Kommission–DG Environment.
O'Connor, W. K., D. C. Dahlin, G. E. Rush, C. L. Dahlin and W. K. Collins (2002). "Carbon dioxide sequestration by direct mineral carbonation: process mineralogy of feed and products." Minerals & Metallurgical Processing **19**(2): 95-101.
Oelkers, E. H., S. R. Gislason and J. Matter (2008). "Mineral carbonation of co2." Elements **4**(5): 333-337.
Olivier, J. G. J.-M. and J. A. H. W. P. Marilena Muntean (2014). Trends in global CO2 emissions: 2014 report.
Oner, A. and S. Akyuz (2007). "An experimental study on optimum usage of GGBS for the compressive strength of concrete." Cement & Concrete Composites **29**(6): 505-514.
Oss;, V. (2015). Mineral commudity summaries 2015, USGS & U.S. Department of the Interior (USDI).
Pal, S. and A. K. Bandyopadhyay (2008). "Suitability of different grades of fused magnesia for magnesia-carbon refractories for critical applications." Transactions of the Indian Ceramic Society **66**(2): 103-105.
Palomo, A., M. W. Grutzeck and M. T. Blanco (1999). "Alkali-activated fly ashes - A cement for the future." Cement and Concrete Research **29**(8): 1323-1329.
Pankratz, T. (2004). "An overview of seawater intake facilities for seawater desalination." The Future of Desalination in Texas **2**.
Patterson, A. L. (1939). "The Scherrer formula for X-ray particle size determination." Physical Review **56**(10): 978-982.
Pearce, F. (2002). Green foundation. New Scientist. **175:** 39-41.
Petric, N., V. Martinac and M. Labor (1997). "The effect of mannitol and pH of the solution on the properties of sintered magnesium oxide obtained from sea water." Chemical Engineering & Technology **20**(1): 36-39.
Pieter Tans, R. K. (2014). NOAA/ESRL, Scripps Institution of Oceanography.
Pilarska, A. A., Ł. Klapiszewski and T. Jesionowski (2017). "Recent developments in the synthesis, modification and application of Mg (OH) 2 and MgO: A review." Powder Technology.
Pita, I. S. (2011). Seawater intake structures International Symposium on Outfall Systems. Mar del Plata, Argentina.
PUB. (2015). "The Singapore water story."

RAM (2015). Global magnesium oxide industry report 2015 - Forecasts to 2020, Research and Markets.
Rao, A. B. and E. S. Rubin (2002). "A technical, economic, and environmental assessment of amine-based CO2 capture technology for power plant greenhouse gas control." Environmental Science & Technology **36**(20): 4467-4475.
Rendek, E., G. Ducom and P. Germain (2006). "Carbon dioxide sequestration in municipal solid waste incinerator (MSWI) bottom ash." Journal of Hazardous Materials **128**(1): 73-79.
Root, T. L., J. T. Price, K. R. Hall, S. H. Schneider, C. Rosenzweig and J. A. Pounds (2003). "Fingerprints of global warming on wild animals and plants." Nature **421**(6918): 57-60.
Ruan, S. and C. Unluer (2016). "Comparative life cycle assessment of reactive MgO and Portland cement production." Journal of Cleaner Production **137**: 258-273.
Sanna, A., M. Uibu, G. Caramanna, R. Kuusik and M. M. Maroto-Valer (2014). "A review of mineral carbonation technologies to sequester CO2." Chemical Society Reviews **43**(23): 8049-8080.
Schneider, M., M. Romer, M. Tschudin and H. Bolio (2011). "Sustainable cement production—present and future." Cement and Concrete Research **41**(7): 642-650.
Shand, M. A. (2006). The Chemistry and Technology of Magnesia, Wiley.
Sillén, L. G., A. E. Martell and J. Bjerrum (1964). Stability constants of metal-ion complexes, Chemical Society.
Simons, H. J. and N. Vlasopoulos (2012). Integrated process for producing compositions containing magnesium, Google Patents.
Sodaye, H., S. Nisan, C. Poletiko, S. Prabhakar and P. K. Tewari (2009). "Extraction of uranium from the concentrated brine rejected by integrated nuclear desalination plants." Desalination **235**(1-3): 9-32.
Soong, Y., D. L. Fauth, B. H. Howard, J. R. Jones, D. K. Harrison, A. L. Goodman, M. L. Gray and E. A. Frommell (2006). "CO2 sequestration with brine solution and fly ashes." Energy Conversion and Management **47**(13-14): 1676-1685.
Soong, Y., A. L. Goodman, J. R. McCarthy-Jones and J. P. Baltrus (2004). "Experimental and simulation studies on mineral trapping of CO2 with brine." Energy Conversion and Management **45**(11-12): 1845-1859.
ST. (2016). "Fifth Singapore desalination plant in the pipeline."
Teir, S., S. Eloneva, C.-J. Fogelholm and R. Zevenhoven (2009). "Fixation of carbon dioxide by producing hydromagnesite from serpentinite." Applied Energy **86**(2): 214-218.
Teir, S., R. Kuusik, C. J. Fogelhohn and R. Zevenhoven (2007). "Production of magnesium carbonates from serpentinite for long-term storage of CO2." International Journal of Mineral Processing **85**(1-3): 1-15.
Tran, K. T., T. Van Luong, J. W. An, D. J. Kang, M. J. Kim and T. Tran (2013). "Recovery of magnesium from Uyuni salar brine as high purity magnesium oxalate." Hydrometallurgy **138**: 93-99.
Turek, M. and W. Gnot (1995). "Precipitation of magnesium hydroxide from brine." Industrial & Engineering Chemistry Research **34**(1): 244-250.
Unluer, C. and A. Al-Tabbaa (2011). Green Construction with Carbonating Reactive Magnesia Porous Blocks: Effect of Cement and Water Contents. International Conference on Future Concrete, Dubai, UAE.
Unluer, C. and A. Al-Tabbaa (2013). "Impact of hydrated magnesium carbonate additives on the carbonation of reactive MgO cements." Cement and Concrete Research **54**: 87-97.

Unluer, C. and A. Al-Tabbaa (2014). "Characterization of light and heavy hydrated magnesium carbonates using thermal analysis." Journal of Thermal Analysis and Calorimetry **115**(1): 595-607.
Unluer, C. and A. Al-Tabbaa (2014). "Enhancing the carbonation of MgO cement porous blocks through improved curing conditions." Cement and Concrete Research **59**: 55-65.
USGS (2012). Minerals Information Yearbook: Cement Statistics and Information.
USGS (2012). "Minerals yearbook-lime 2012."
Venkatesha, T. G., R. Viswanatha, Y. A. Nayaka and B. K. Chethana (2012). "Kinetics and thermodynamics of reactive and vat dyes adsorption on MgO nanoparticles." Chemical Engineering Journal **198**: 1-10.
Wang, F., F. Jin, Z. T. Shen and A. Al-Tabbaa (2016). "Three-year performance of in-situ mass stabilised contaminated site soils using MgO-bearing binders." Journal of Hazardous Materials **318**: 302-307.
Wang, Y., Z. Li and G. P. Demopoulos (2008). "Controlled precipitation of nesquehonite (MgCO3 3H2O) by the reaction of MgCl2 with (NH4)2CO3." Journal of Crystal Growth **310**(6): 1220-1227.
Wang, Z., N. H. Wang, T. Li and Y. Cao (2012). "3D numerical analysis of the arc plasma behavior in a submerged DC electric arc furnace for the production of fused MgO." Plasma Science & Technology **14**(4): 321-326.
Wolery, T. J. (1992). A software package for geochemical modeling of aqueous systems: package overview and installation guide (version 7.0), Lawrence Livermore National Laboratory Livermore, CA.
Wright, J. M. and A. Colling (1995). Seawater: Its Composition, Properties and Behaviour, Elsevier Science.
Wu, D., B. J. Luo, W. Liu, L. C. Wang, Y. Yao and X. P. Huang (2014). Study on the process optimization for intermediate Magnesium Carbonate Tri-hydrate. Advanced Materials Research, Trans Tech Publ.
Yan, C., D. Xue, L. Zou, X. Yan and W. Wang (2005). "Preparation of magnesium hydroxide nanoflowers." Journal of Crystal Growth **282**(3): 448-454.
Yi, Y., M. Liska and A. Al-Tabbaa (2012). "Initial investigation into the use of GGBS-MgO in soil stabilisation." Grouting and Deep Mixing 2012: 444-453.
Zachos, J., M. Pagani, L. Sloan, E. Thomas and K. Billups (2001). "Trends, rhythms, and aberrations in global climate 65 Ma to present." Science **292**(5517): 686-693.
Zhang, Z., Y. Zheng, Y. Ni, Z. Liu, J. Chen and X. Liang (2006). "Temperature-and pH-dependent morphology and FT-IR analysis of magnesium carbonate hydrates." The Journal of Physical Chemistry B **110**(26): 12969-12973.